Impact of Propeller Gyroscopic Effect on the Handling Qualities of Multi-Engine Light Aircraft

W. Hu

TU Delft

Impact of Propeller Gyroscopic Effect on the Handling Qualities of Multi-Engine Light Aircraft

by

W. Hu

in partial fulfillment of the requirements for the degree of

Master of Science
in Aerospace Engineering

at the Delft University of Technology,
to be defended publicly on Friday September 22nd, 2023 at 1:00 PM.

Student number:	5239613	
Project duration:	June, 2022 – September, 2023	
Supervisor:	Dr. ir. C. Varriale,	TU Delft
Thesis committee:	Prof. dr. L. L. M. Veldhuis,	TU Delft, Chair
	Ir. P. C. Roling,	TU Delft, Examiner
	Dr. ir. A. C. in ’t Veld,	TU Delft, Additional Assessor

An electronic version of this thesis is available at `http://repository.tudelft.nl/`.

Preface

The completion of this thesis project concludes my three-year journey as a TU Delft Master of Aerospace student. Even though flight simulation has always been my passion, I had no idea how much I would be involved in this field throughout my study and beyond. Whilst this learning process came with quite a lot of twists and turns both in academics and life, I'm still grateful for this unique opportunity of building up physical simulations from the ground up from first principles while also being able to draw my own experience and passion as a flight simulation enthusiast and a student pilot.

Of course, I couldn't have survived without people around me: thank you, mom and dad, for giving your strongest support, both financially and emotionally, as well as for not letting me off the hook when I lose focus; thank you, Nancy, my lovely girlfriend, who had to sometime embrace my emotions but always believed in me; thank you, Yuchen and Tommy, for keeping me company throughout these years; thank you, to everyone who's supported me in the past. Most importantly, I'd like to thank Carmine, my supervisor, for giving me this fantastic and interesting topic, as well as being supportive and understanding throughout the time.

W. Hu
Leiden, September 2023

Contents

Executive Summary ix

Nomenclature xiii

List of Figures xv

List of Tables xvii

I Introduction 1

1 Introduction 3

1.1 State of Art Review . . . 3
1.2 Research Objective and Questions . . . 4
1.3 Report Outline . . . 4

II Academic Paper 5

III Literature Study Report (Previously Graded) 35

2 Introduction 37

2.1 Background and Motivation . . . 37
2.2 State-of-Art . . . 38
2.3 Research Gap . . . 38
2.4 Research Statement . . . 38
2.5 Reference Aircraft . . . 39
2.6 Report Outline . . . 40

3 Flight Dynamics Modelling 41

3.1 Introduction . . . 41
3.2 Equations of Motion for Flight Dynamics . . . 41
3.3 Modelling of Gyroscopic Effects . . . 41
3.4 Modelling of Powertrain . . . 42
  3.4.1 Propeller Inertia Model . . . 42
  3.4.2 Electric . . . 43
  3.4.3 Piston . . . 43
  3.4.4 Turboprop . . . 44
3.5 Modelling of Inertia and Moments of Inertia . . . 45
3.6 Implementation . . . 45

4 **Aerodynamic Modelling** **47**
4.1 Introduction 47
4.2 Aircraft Aerodynamic Modelling 47
4.2.1 Overview of Approaches 47
4.2.2 NASA Full-Scale Windtunnel Investigation 49
4.2.3 Athena Vortex Lattice(AVL) 50
4.2.4 Selection: OpenVSP and FlightStream 50
4.3 Propeller Performance Modelling 52
4.3.1 Empirical Method 53
4.3.2 Wind Tunnel Experiments 53
4.3.3 Computational Tools 53
4.4 Propeller-Airframe Interaction Effects Modelling 54
4.5 Validation and Verification 55

5 **Handling Qualities and Stability** **57**
5.1 Introduction 57
5.2 Classic Handling Quality Analysis 57
5.3 Time-domain Handling Quality Analysis 57
5.3.1 Certification Standards and Test Flight Maneuvers 57
5.3.2 Other Representative Maneuvers 59
5.4 Modelling of Pilot 59

6 **Methodology** **63**
6.1 Introduction 63
6.2 Experiment Setup Overview 63
6.3 Aerodynamic, Propulsion, and Inertia Model Generation 63
6.4 Baseline Configuration 63
6.5 Validation and Verification Studies 64
6.5.1 Flight Dynamics Model Validation 64
6.5.2 Aerodynamic and Propulsion Model Validation 64
6.6 Main Test 65
6.7 Comparison Studies 65

7 **Conclusion** **67**

IV **Conclusions, Recommendations and Appendices** **69**

8 **Conclusions and Recommendations** **71**
8.1 Conclusion 71
8.2 Future Recommendations 72

Bibliography **73**

A Appendix 77

A.1 Flight Mechanics Model 77

A.2 Simulink Models 79

A.3 Static Windtunnel data 83

A.4 Complete Time Simulation Summarized Results 87

A.4.1 Result Summary for All-Engine-Operative Open-Loop Maneuvers 87

A.4.2 Result Summary for One-Engine-Inoperative Open-Loop Maneuvers. 88

A.4.3 Result Summary for All-Engine-Operative Closed-Loop Maneuvers. 89

Executive Summary

Flying characteristics of a multi-engined light general aviation (GA) aircraft during and after an engine failure is often a major safety consideration when both designing and operating the aircraft. In the meantime, the propellers, being large rotating masses, can exert considerable gyroscopic effect on the aircraft during flight, itself contributing to a coupling between the pitch and yaw axis, thus affecting flight dynamics. This study presents an investigation on the impact of propeller gyroscopic effects on the flying motion of a representative twin-engine GA aircraft. This is done using a modular flight mechanics toolbox that performs analyses in both frequency domain and time domain. A steady-state windtunnel aerodynamic and control surface model with empirically estimated unsteady aerodynamic coefficients, along with a propeller-governor-engine system simulation, complements the gyroscopic inertia model in the simulation setup.

Firstly, a modal analysis showed that all modes aside the spiral mode does not get discernibly affected by the rotating inertia typical to the reference aircraft's propellers. Then, time-domain simulations of various rapid maneuvers show that gyroscopic effect does cause significant change in the angular response of the coupled axis, e.g. sideslip angle response during a pitch-input-only maneuver, whilst its impact on long-term phugoid motion remained inconclusive due to undesired and uncontrolled roll motion. To compensate for this, maneuvers were performed again with a manually tuned simple wing leveler and results showed that pitch-input maneuvers does not show much deviation in phugoid motion, whereas yaw-input maneuvers such as sudden left engine failure shows discernible difference in airspeed and altitude responses, though the difference in magnitude is still small. Next, comparisons made with different powertrain responsiveness showed that in a power-reducing case such as sudden one-engine-failure, the effect of the powertrain time delay is independent from the influence of gyroscopic effects, whereas for a power-increase case, such as going around, the impact of the two is simultaneous and intertwined. Finally, a sensitivity study on unsteady aerodynamic coefficients showed that their effects on flying motion are generally independent from the gyroscopic effect.

Nomenclature

Abbreviations

AFM	Aircraft Flight Manual
AMM	Aircraft Maintenance Manual
BLDC	Brushless Direct-Current
CFD	Computational Fluid Dynamics
CoG	Center of Gravity
DAE	Differential-Algebraic Equation
EoM	Equation(s) of Motion
GA	General Aviation
HALE	High-Altitude Long-Endurance
IAS	Indicated Airspeed
MoI	Mass Moment of Inertia
NTSB	National Transportation Safety Board
OEI	One Engine Inoperative
PMSM	Permanent-Magnet Synchronous Motor
TAS	True Airspeed
VLM	Vortex Lattice Method

Math Symbols

α	angle of attack, °
β	Sideslip Angle
β	angle of sideslip, °
β_{p}	propeller blade pitch angle °
ω	angular velocity vector
$\delta_{\mathrm{e}}, \delta_{\mathrm{a}}, \delta_{\mathrm{r}}$	elevator, aileron, rudder deflection, °
η	propeller efficiency
γ	flight path angle, °
$\mathbf{M}_{\mathrm{Gyro}}$	gyroscopic moment vector, N m
ω	angular velocity magnitude, rad s^{-1}
ω_{p}	Angular velocity of the propeller
ϕ, θ, ψ	body-axis roll, pitch, yaw angles, °

$\boldsymbol{L}$	Angular Momentum(Vector)
ρ	local air density, $\mathrm{kg\,m^{-3}}$
τ_{eng}	time constant for engine response delay, s
b_{ref}	reference span, m
c_{ref}	mean aerodynamic chord, m
C_L, C_D	lift and drag coefficients
c_p	propeller coefficient of power
C_{Mx}, C_{My}, C_{Mz}	moment coefficients around x, y, z body-axis, NED
C_x, C_y, C_z	force coefficients along x, y, z body-axis, NED
D_{p}	Propeller diameter, m
g	gravitational acceleration, $\mathrm{m\,s^{-2}}$
h	altitude, m
$I_{xx,\mathrm{A}}, I_{yy,\mathrm{A}}, I_{zz,\mathrm{A}}, I_{xz,\mathrm{A}}$	aircraft mass moments of inertia, $\mathrm{kg\,m^2}$
I_{xx}	propeller mass moment of inertia, $\mathrm{kg\,m^2}$
J	Advance Ratio
J	propeller advance ratio
$L, \mathbf{L}$	magnitude and vector of angular momentum, $\mathrm{kg\,m^2\,s^{-1}}$
L, M, N	Angular Moments
n_{p}	propeller revolution per second (RPS)
P	power, kW
p, q, r	roll, pitch, yaw rate, $\mathrm{rad\,s^{-1}}$
Q	torque, N m
Q_{p}	Propeller torque
S_{ref}	reference area, $\mathrm{m^2}$
T	thrust, N
T_{p}	Propeller thrust
V_∞	Freestream velocity
V_∞	true airspeed, $\mathrm{m\,s^{-1}}$
x, y	longitudinal and lateral position, m
X, Y, Z	Translational forces
$x_{\mathrm{a}}, x_{\mathrm{b}}, x_{\mathrm{p}}$	Pilot roll, pitch, yaw inputs
$x_{\mathrm{c,L}}, x_{\mathrm{c,R}}, x_{\mathrm{c}}$	Left, right, combined throttle control

Sub-/Superscript

0	Value of the reference aircraft

A	Aircraft
eng	Engine
L	Left
p	Propeller
p	propeller
R	Right

List of Figures

1.1 Illustration for Gyroscopic Effect 3

2.1 A picture of Diamond DA42 [1] 39

3.1 Picture and Specification of the EMRAX 348[20] (Note that the 208 instead of 348 is an typo in the specsheet) 44

4.1 A table for estimating the drag of various empennage shapes[35] 48
4.2 Classification of (unsteady) CFD methods based on computational cost and model influence, adapted from Saguat et al. [43] 48
4.3 Comparison of various stability derivatives as generated by methods of different fidelity[6] 49
4.4 Picture of a Piper PA-30 Twin Comanche in a wind tunnel test[50] 50
4.5 The lift coefficient vs α curve of the PA-30 with propellers removed and at several flap deflections as obtained from full-scale wind tunnel tests[50] 51
4.6 Screen Captures of the DA-42 aircraft geometry in OpenVSP(Left) and FlightStream(Right) 52
4.7 Lift vs α curve of the DA-42(propeller off) generated by FlightStream 52
4.8 An example of propeller thrust-coefficient vs advance ratio curve for a 2-bladed propeller[56] 53

5.1 MIL-F-8785C[68] Short-period frequency requirement for Category B(left) and C(right) flight phases 58
5.2 A block diagram of pilot-vehicle system under manual control[69] 60
5.3 A block diagram overview of the quasi-linear pilot model[72], as adapted from Lone and Cooke[69] 61

6.1 Tentative Flowchart of the Experimental Setup, with colored blocks indicating the origins of each components 64

A.1 Overview of the PHALANX toolbox [74] 77
A.2 Illustration of body(b), wind(w), and aerodynamic(a) axis definition used in PHALANX [74] 78
A.3 Simulink Diagram of the overall view of the PHALANX simulation 79
A.4 Simulink Diagram of the components of the aircraft 80
A.5 Simulink Diagram of the flight control system model 80
A.6 Simulink Diagram of the Engine model 81
A.7 Simulink Diagram of the Ideal Powertrain 81
A.8 Simulink Diagram of the table-based aerodynamicsforce and moment interpolation model 82
A.9 Simulink Diagram of one of the table-based CS force and moment interpolation model . 82

List of Tables

5.1 Level 1 Flying Quality Requirements for Class I Aircraft, as Summarized from MIL-8785-C[68] . . . 58

6.1 Summary of Flight Performance Validation from the AFM[10] . . . 65

A.1 Wind Tunnel Testing Parameters . . . 83
A.2 Percentage Difference in α excursion between cases with and without GE for all-engine-operating scenario . . . 87
A.3 Difference in β excursion between cases with and without GE for all-engine-operating scenario . . . 87
A.4 Max difference in airspeed between cases with and without GE for all-engine-operating scenario . . . 87
A.5 Max difference in altitude between cases with and without GE for all-engine-operating scenario . . . 87
A.6 Difference in initial α excursion between cases with and without GE for one engine inoperative scenario . . . 88
A.7 Difference in initial β excursion between cases with and without GE for one engine inoperative scenario . . . 88
A.8 Max difference in airspeed between cases with and without GE for one engine inoperative scenario . . . 88
A.9 Max difference in altitude between cases with and without GE for one engine inoperative scenario . . . 88
A.10 Percentage Difference in α excursion between cases with and without GE for all-engine-operating scenario with wing leveler enabled . . . 89
A.11 Difference in β excursion between cases with and without GE for all-engine-operating scenario with wing leveler enabled . . . 89
A.12 Max difference in airspeed between cases with and without GE for all-engine-operating scenario with wing leveler enabled . . . 89
A.13 Max difference in altitude between cases with and without GE for all-engine-operating scenario with wing leveler enabled . . . 89

I

Introduction

1

Introduction

Safety is the priority focus when designing an aircraft. A National Transportation Safety Board (NTSB) study [1] found in 1979 that the change of a fatal crash is four times more likely for a twin-engine general aviation(GA) aircraft than that of a single-engine aircraft when an engine failure occurs. Despite the redundancy of an extra engine, this higher fatality rate is a result of pilots being unable to bring the aircraft under control due to the presence of asymmetric thrust. As a result, controllability during and after a engine failure situation is a dominant factor in the sizing of the aircraft control surfaces, especially that of vertical tails and rudders. However, larger vertical tails and rudders would lead to higher weight and parasitic drag, causing detriment to the fuel efficiency and environmental friendliness of the aircraft.

With that in mind, one effect that could impact to the controllability of an aircraft is the gyroscopic precession effect. This refers to the tendency of a rotating object to maintain its orientation and exert a reacting moment when its orientation is being changed by an external moment. This coupled moment is in the direction perpendicular to both the exerted moment and the rotation axis. For propeller-driven aircraft, the propellers, with their relatively high rotation mass and rate, are a primary source of gyroscopic precession moment. As propeller rotation axes are often close to parallel to the longitudinal axis, a rotation rate in the aircraft's pitch axis would result in a corresponding pitching moment being exerted on the propeller by the airframe. This then causes a reacting moment on the Z-axis, leading to a coupled yaw motion. The converse could also happen as a rotation in yaw axis would result in a reacting pitching moment. This effect is best visualized in figure 1.1.

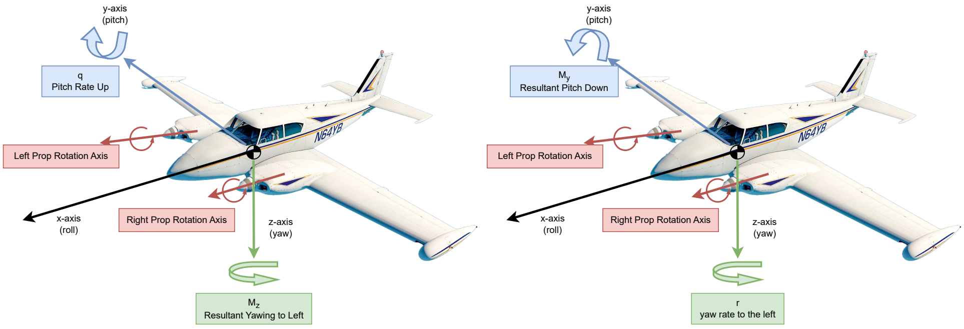
y-axis (pitch)
q Pitch Rate Up
N64YB
Left Prop Rotation Axis
x-axis (roll)
Right Prop Rotation Axis
z-axis (yaw)
M_z Resultant Yawing to Left
y-axis (pitch)
M_y Resultant Pitch Down
N64YB
Left Prop Rotation Axis
x-axis (roll)
Right Prop Rotation Axis
z-axis (yaw)
r yaw rate to the left

Figure 1.1: Gyroscopic yaw moment due to pitch rate (left) and pitch moment due to yaw rate[1]

1.1. State of Art Review

Some previous research was done to attempt to quantify the impact of gyroscopic moments produced by propeller on the aircraft, though most of those are concerning the structural or local aerodynamics effect. Scanlan and Truman [2], for example, analyzed the impact that gyroscopic effects have on engine on-wing vibration modes. Using an analytical approach, Liu's study on propeller whirl-flutter [3] also found that the presence of propeller gyroscopic effect leads to a change in the free-vibration modes. Meanwhile, Teixeira and Cesnik [4] demonstrated that the inclusion of the simulation of propeller gyroscopic effects in the aero-elastic simulations of high-altitude long-endurance (HALE) aircraft affects the wing twist distribution.

---

[1] Image source: https://www.key.aero/article/twin-comanche-pa-30-flight-adventure

On the area of flight dynamics, Smith's 1958 experiment [5] using a flywheel in a scaled jet-powered VTOL model showed that, when the flywheel is enabled to simulate powertrain gyroscopic effect, the scaled model becomes difficult to control without added stabilization. For conventional airplanes, Goraj and Chichoka [6] performed a more detailed study on the impact of weak and strong gyroscopic effects on the flying motion of a single-engine turboprop aircraft. In this case, weak gyroscopic effects refer to those that can be investigated using the traditional method of modal analysis, whereas strong gyroscopic effects refers to those that are more pronounced during a dynamic maneuver, such that it can only be analyzed from the time domain. The research shows that while the presence of weak gyroscopic effect does modify the aircraft's dynamic modes, the change is not of large significance. On the other hand, the impact of strong gyroscopic effect is more pronounced in the time-domain simulation of rapid maneuvers such as step deflections of elevator and rudders as well as gust encounter.

With that in mind, one of the *research gap* currently present is the impact of the gyroscopic effect produced by multiple engines/propellers on the flight dynamics of light airplanes. For twin-engine light aircraft, a sudden engine failure can lead to the excitation similar to a rapid maneuver, which may in turn improve or worsen the ease of recovery maneuver. Moreover, the effect of different transient powertrain response characteristics on the flying motions, especially in combination with the presence of gyroscopic effect, has yet to be investigated.

1.2. Research Objective and Questions

In consideration of the current gaps, the main research question aimed to be answered by the study is:

> How can one quantify the impact of propeller gyroscopic procession effect on the flight dynamic behaviors of light multi-engine aircraft through flight simulation, especially during the event of a powertrain failure?

To help with answering the question, the following research sub-questions were formed:

- What are the relevant parameters that can be used to quantify the impact of the gyroscopic effect on the flying qualities?
- During which maneuvers is the effect of propeller gyroscopic procession more prominent?
- How do different powertrain torque responses impact the results?
- How sensitive is the result of this study to the unsteady aerodynamic derivatives?

The main contribution of this research aims to grant an insight on the effect of propeller gyroscopic procession on light multi-engine aircraft especially during rapid maneuvers similar to those encountered during the event of engine failure. It would also help to add an additional layer of fidelity to flight dynamics simulation, which could help with the preliminary design and sizing of the aircraft flight control systems.

1.3. Report Outline

The content of this thesis report is organized into four parts. Part I (this part) is the introduction. Part II presents the research done in this thesis study in an academic paper format. Part III presents the *previously graded* literature study report for this research. Part IV presents the conclusion to the research and a list of recommendations for future research. Appendices with supplemental information on the experimental setup and results are also provided in this section.

II

Academic Paper

Impact of Propeller Gyroscopic Effect on the Handling Qualities of Multi-Engine Light Aircraft

Wei Hu*
Delft University of Technology, Delft, 2629 HS, The Netherlands

Flying characteristics of a multi-engined light general aviation (GA) aircraft during and after an engine failure is often a major safety consideration when both designing and operating the aircraft. In the meantime, the propellers, being large rotating masses, can exert considerable gyroscopic effect on the aircraft during flight, itself contributing to a coupling between the pitch and yaw axis, thus affecting flight dynamics. This study presents an investigation on the impact of propeller gyroscopic effects on the flying motion of a representative twin-engine GA aircraft. This is done using a modular flight mechanics toolbox that performs analyses in both frequency domain and time domain. A steady-state windtunnel aerodynamic and control surface model with empirically estimated unsteady aerodynamic coefficients, along with a propeller-governor-engine system simulation, complements the gyroscopic inertia model in the simulation setup. Firstly, a modal analysis showed that all modes aside the spiral mode does not get discernibly affected by the rotating inertia typical to the reference aircraft's propellers. Then, time-domain simulations of various rapid maneuvers show that gyroscopic effect does cause significant change in the angular response of the coupled axis, e.g. sideslip angle response during a pitch-input-only maneuver, whilst its impact on long-term phugoid motion remained inconclusive. Finally, comparisons made with different powertrain responsiveness along with a sensitivity study on unsteady aerodynamic coefficients showed that their effects on flying motion are generally independent from the gyroscopic effect.

List of symbols

α	angle of attack, deg	C_L, C_D	lift and drag coefficients
β	angle of sideslip, deg	C_{Mx}, C_{My}, C_{Mz}	moment coefficients around x, y, z body-axis, NED
β_p	propeller blade pitch angle deg	C_x, C_y, C_z	force coefficients along x, y, z body-axis, NED
γ	flight path angle, deg	D_p	Propeller diameter, m
$\delta_\mathrm{e}, \delta_\mathrm{a}, \delta_\mathrm{r}$	elevator, aileron, rudder deflection, deg	$I_{xx,\mathrm{A}}, I_{yy,\mathrm{A}}, I_{zz,\mathrm{A}}, I_{xz,\mathrm{A}}$	aircraft mass moments of inertia, $\mathrm{kg\,m^2}$
η	propeller efficiency	I_{xx}	propeller mass moment of inertia, $\mathrm{kg\,m^2}$
ϕ, θ, ψ	body-axis roll, pitch, yaw angles, deg	J	propeller advance ratio
ρ	local air density, $\mathrm{kg\,m^{-3}}$	$L, \mathbf{L}$	magnitude and vector of angular momentum, $\mathrm{kg\,m^2\,s^{-1}}$
τ_eng	time constant for engine response delay, s	$\mathbf{M}_\mathrm{Gyro}$	Gyroscopic moment vector, N m
ω	angular velocity magnitude, $\mathrm{rad\,s^{-1}}$	P	power, kW
$\boldsymbol{\omega}$	angular velocity vector	Q	torque, N m
b_ref	reference span, m	S_ref	reference area, $\mathrm{m^2}$
c_ref	mean aerodynamic chord, m	T	thrust, N
c_p	propeller coefficient of power	V_∞	true airspeed, $\mathrm{m\,s^{-1}}$
g	gravitational acceleration, $\mathrm{m\,s^{-2}}$	*Subscripts and superscripts*	
h	altitude, m	A	Aircraft
n_p	propeller revolution per second (RPS)	eng	Engine
p, q, r	roll, pitch, yaw rate, $\mathrm{rad\,s^{-1}}$	p	propeller
x, y	longitudinal and lateral position, m	0	Value of the reference aircraft
$x_\mathrm{a}, x_\mathrm{b}, x_\mathrm{p}$	Pilot roll, pitch, yaw inputs	L	Left
$x_{\mathrm{c,L}}, x_{\mathrm{c,R}}, x_\mathrm{c}$	Left, right, combined throttle control	R	Right

---

*MSc. Candidate, Flight Performance Profile, Faculty of Aerospace

I. Introduction

Safety is the priority focus when designing an aircraft. A National Transportation Safety Board (NTSB) study [1] found in 1979 that the change of a fatal crash is four times more likely for a twin-engine general aviation(GA) aircraft than that of a single-engine aircraft when an engine failure occurs. Despite the redundancy of an extra engine, this higher fatality rate is a result of pilots being unable to bring the aircraft under control due to the presence of asymmetric thrust. As a result, controllability during and after a engine failure situation is a dominant factor in the sizing of the aircraft control surfaces, especially that of vertical tails and rudders. However, larger vertical tails and rudders would lead to higher weight and parasitic drag, causing detriment to the fuel efficiency and environmental friendliness of the aircraft.

With that in mind, one effect that could impact to the controllability of an aircraft is the gyroscopic precession effect. This refers to the tendency of a rotating object to maintain its orientation and exert a reacting moment when its orientation is being changed by an external moment. This coupled moment is in the direction perpendicular to both the exerted force and the rotation axis. For propeller-driven aircraft, the propellers, with their relatively high rotation mass and rate, are a primary source of gyroscopic precession moment. As propeller rotation axes are often close to parallel to the longitudinal axis, a rotation rate in the aircraft's pitch axis would result in a corresponding pitching moment being exerted on the propeller by the airframe. This then causes a reacting moment on the Z-axis, leading to a coupled yaw motion. The converse could also happen as a rotation in yaw axis would result in a reacting pitching moment.

Some previous research was done to attempt to quantify the impact of gyroscopic moments produced by propeller on the aircraft, though most of those are concerning the structural or local aerodynamics effect. Scanlan and Truman [2], for example, analyzed the impact that gyroscopic effects have on engine on-wing vibration modes. Using an analytical approach, Liu's study on propeller whirl-flutter [3] also found that the presence of propeller gyroscopic effect leads to a change in the free-vibration modes. Meanwhile, Teixeira and Cesnik [4] demonstrated that the inclusion of the simulation of propeller gyroscopic effects in the aero-elastic simulations of high-altitude long-endurance (HALE) aircraft affects the wing twist distribution.

On the area of flight dynamics, Smith's 1958 experiment [5] using a flywheel in a scaled jet-powered VTOL model showed that, when the flywheel is enabled to simulate powertrain gyroscopic effect, the scaled model becomes difficult to control without added stabilization. For conventional airplanes, Goraj and Chichoka [6] performed a more detailed study on the impact of weak and strong gyroscopic effects on the flying motion of a single-engine turboprop aircraft. In this case, weak gyroscopic effects refer to those that can be investigated using the traditional method of modal analysis, whereas strong gyroscopic effects refers to those that are more pronounced during a dynamic maneuver, such that it can only be analyzed from the time domain. The research shows that while the presence of weak gyroscopic effect does modify the aircraft's dynamic modes, the change is not of large significance. On the other hand, the impact of strong gyroscopic effect is more pronounced in the time-domain simulation of rapid maneuvers such as step deflections of elevator and rudders as well as gust encounter.

With that in mind, one of the research gap currently present is the impact of the gyroscopic effect produced by multiple engines/propellers on the flight dynamics of light airplanes. For twin-engine light aircraft, a sudden engine failure can lead to the excitation similar to a rapid maneuver, which may in turn improve or worsen the ease of recovery maneuver. Moreover, the effect of different transient powertrain response characteristics on the flying motions, especially in combination with the presence of gyroscopic effect, has yet to be investigated.

In this paper, the development of a physics-based gyroscopic effect model and powertrain transient response model as a part of flight dynamics simulation suite is presented. The model is then used to investigate the impact of propeller gyroscopic effects on the flight dynamics of a twin-engine general aviation aircraft through frequency-domain analysis as well as time-domain simulation of various types of rapid maneuvers. It therefore aims to contribute by assessing the impact of propeller gyroscopic effects on aircraft handling qualities and to add an additional layer of fidelity to flight dynamics simulation, which could help with the preliminary design and sizing of the aircraft flight control systems.

The content of this paper is divided into five sections. Whilst Section I is the introduction, Section II provides a description of the flight dynamics simulation model, with the focus being on the features and limitations of each components. Section III presents the methodology used for performing both the frequency-domain and time-domain simulations, including an outline of the way specified maneuvers are performed. Section IV provides some validations and verifications done to the simulation setup. Section V then shows and discusses the results generated from the flight simulations. Last but not least, section VI provides a conclusion by summarizing the results as well as highlighting future works to be done.

II. Flight Dynamics Model Setup

This section intends to present the setup of the simulation model for this study. The simulation model used in this experiment is built based upon the in-house built Performance, Handling Qualities and Load Analysis Toolbox (PHALANX) suite, which has been used for 6-Degree of Freedom (DoF) flying and handling quality assessments in researches such as [7–9]. The PHALANX suite is written using MATLAB/Simulink and is modular, which is especially beneficial as modules particular to this study can be added to the existing PHALANX architecture whilst also avoiding the need to spend time on implementing existing parts. The overview of the particular PHALANX setup for this study is shown in figure 1, with the blue parts denoting original contributions.

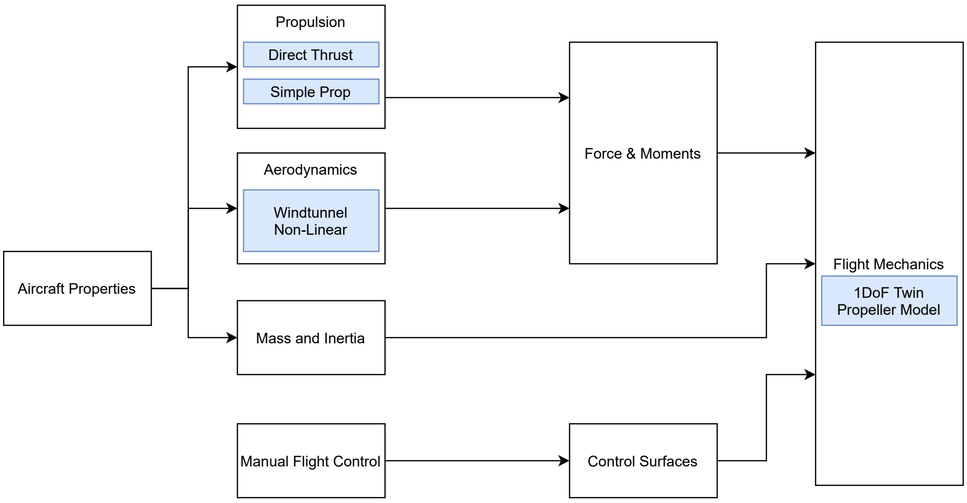

Fig. 1 A summary of the flight simulation setup

A. Reference Aircraft

The Piper PA-30 Twin Comanche is chosen as the reference aircraft because it is a representative general aviation twin-piston-engine light aircraft and its static wind tunnel aerodynamics data [10] as well as pilot's operating handbooks (POH) are readily available. The three-view drawing of the reference aircraft as well as some measurements of the aircraft is shown in figure 2. The basic mass and inertia, geometry parameters, as well as the engine-propeller system of the reference aircraft are shown in table 1.

The aircraft is of conventional layout with an all-moving tail serving as both stabilizer and elevator. The rudder is a single-piece on the vertical tailplane and a pair of ailerons are placed along the wing's outer span and trailing edge. The pair of piston engines are located in pods above the wing and drive a couple of constant-speed two-bladed propellers.

Table 1 Basic specifications of the reference aircraft

PA-30 Twin Commanche			
Mass and Inertia[11]		Geometry	
mass	1633 kg	Wing Area (S_{ref})	16.5 m^2
$I_{xx,A}$	3796 $kg \cdot m^2$	Wing Span (b_{ref})	10.97 m
$I_{yy,A}$	2576 $kg \cdot m^2$	Mean Aerodynamic Chord (c_{ref})	1.53 m
$I_{zz,A}$	6101 $kg \cdot m^2$		
$I_{xz,A}$	108 $kg \cdot m^2$		
Longitudinal CoG	2.16m behind reference plane		
Engine		Propeller	
Max RPM		2700	
Rated Power	119.3 kW	Diameter	1.92 m
Maximum Torque	422 $N \cdot m$	Mass	26.6 kg
		No. Blade	2
Prop Hub Location (Relative to CoG)		1.535m Forward, 1.675m to the side, 0.242m above	

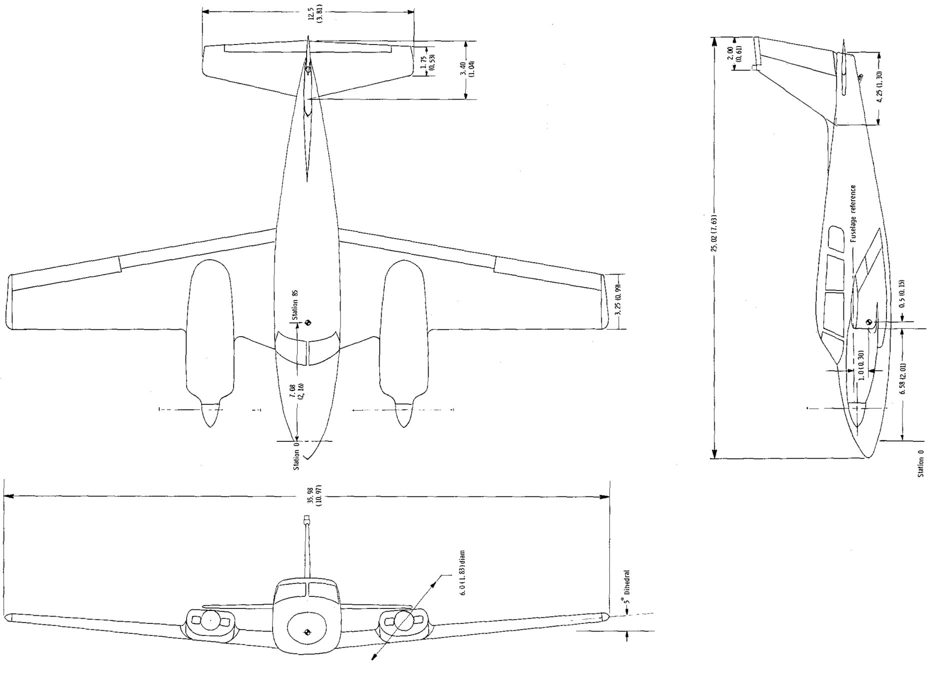
Station 85
Station 0
Fuselage reference
5° Dihedral

Fig. 2 Three-view drawing of the PA-30

B. Gyroscopic

The equation for the gyroscopic moment is:

$$\mathbf{M}_{Gyro} = \begin{bmatrix} M_x \\ M_y \\ M_Z \end{bmatrix} = \frac{\mathrm{d}\mathbf{L}_p}{\mathrm{d}t} + \omega_a \times \mathbf{L}_p \tag{1}$$

Where $\mathbf{L}_p = I \times \omega_p$ is the angular momentum of the propeller.

Assuming that the propeller's rotational axis is parallel to the longitudinal axis of the aircraft, the propeller angular momentum can be further simplified into:

$$\mathbf{L}_p = I_{xx}\omega_p \begin{bmatrix} 1 & 0 & 0 \end{bmatrix}^T \tag{2}$$

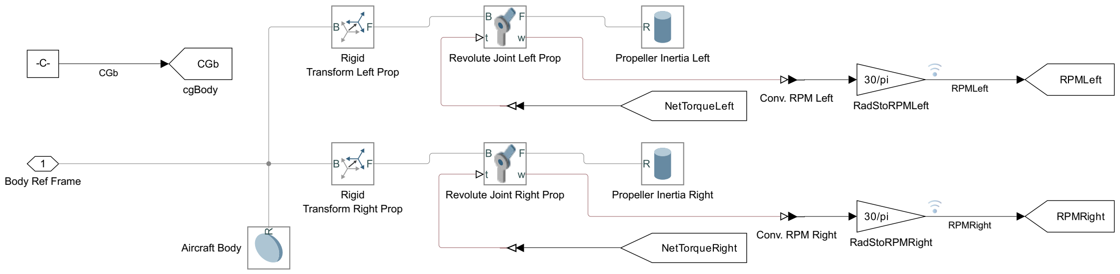
-C-
CGb
CGb
cgBody
1
Body Ref Frame
Aircraft Body
B
F
Rigid Transform Left Prop
B
F
Rigid Transform Right Prop
B
F
t
w
Revolute Joint Left Prop
B
F
t
w
Revolute Joint Right Prop
R
Propeller Inertia Left
R
Propeller Inertia Right
NetTorqueLeft
NetTorqueRight
Conv. RPM Left
Conv. RPM Right
30/pi
RadStoRPMLeft
30/pi
RadStoRPMRight
RPMLeft
RPMRight
RPMLeft
RPMRight

Fig. 3 The Simulink diagram of the aircraft-propeller multi-body model

In this study, the SimScape multi-body physical simulation was employed to simulate the effect of the two propeller rotational masses. The airframe itself is modelled as a single lump mass with the same mass and mass moments of inertia as the aircraft, as listed in table 1. The propellers are then also modelled as individual cylinders with equivalent mass and mass moments of inertia as the real propellers. The propellers confined to 1 degree of freedom by a rotational joint around its rotating axis, which takes in the net torque input from the propulsion model as the sum of the produced engine torque and the aerodynamic "drag" torque of the propeller. The propeller masses are then rotated and translated using a rigid transformation joint to align with the orientation and location of the propellers.

As the exact mass composition of the propeller is not given, considering that the reference aircraft uses two-bladed propellers, the MoI of the propellers are estimated by assuming them to be the same of a uniform long rod around its center of mass, such that:

$$I_{xx} = \frac{m_p D_P^2}{12} \tag{3}$$

Where m_p is the mass of the propeller and D_P is the diameter of the propeller. In the model setup stage, the mass and moment arm contribution of the propellers are deducted from the aircraft mass and CG as quoted in table 1.

C. Aerodynamics

The aerodynamic model is split into three parts: steady-state airframe coefficients ($C_{f,b}$), steady-state (incremental) control surface (CS) coefficients ($dC_{f,\delta_{\{e,a,r\}}}$), as well as unsteady airframe coefficients due to body rotation rates ($C_{f,\{p,q,r\}}$). The coefficients are functions of angle of attack (AoA, α), sideslip angle (β), angular rates (p, q, r), and control surface deflections (elevator δ_e, aileron δ_a, and rudder δ_r), and take the general form shown in Equation 4. As the flight envelope of the aircraft is not expected to exceed Mach 0.3, compressibility is not considered and therefore the aerodynamic model is not dependent on Mach number.

$$C_f(\alpha, \beta, p, q, r, \delta_{\mathrm{CS}}) = C_{f,b}(\alpha, \beta) + \sum_{i=\{p,q,r\}} C_{f,i}(\alpha, \beta, i) + \sum_{j=\{\delta_\mathrm{e}, \delta_a, \delta_r\}} dC_{f,j}(\alpha, \beta, j) \tag{4}$$

Where $f = \{fx, fy, fz, Mx, My, Mz\}$ represents the 6 body-axis forces and moments corresponding to the 6 DoF.

The steady-state aerodynamics and control surface coefficients are obtained from the static windtunnel data by Fink and Freeman[10] (Figures 6, 16, 25, and 31). Specifically, the dataset is obtained with the propeller *net* thrust manually set to zero by setting the blade pitch angle and advance ratio corresponding to the zero net thrust and the (tunnel) airspeed of $28.35 m/s$. As such, propeller whirl and slipstream effect is present to a degree. For the scope of this research, only the clean configuration of the aircraft, i.e. flaps and gear up, is used. The data points are collected from the chart then placed in a multi-dimensional look-up table where the coefficients are linearly interpolated. As the windtunnel data was in terms of coefficient of lift and drag, the data needs to be transformed into the body-axis NED coordinate system used by PHALANX using Equation 5.

$$\begin{cases} C_X = -C_D \cos\alpha + C_L \sin\alpha \\ C_Z = -C_D \sin\alpha - C_L \cos\alpha \end{cases} \tag{5}$$

Due to the limitation of the windtunnel data, the longitudinal force and moment coefficients, C_x, C_z, and C_{My}, as well as the forces and moment increment caused by longitudinal control surface δ_e are symmetrical and therefore does not depend on β. In the meantime, lateral forces and moments are not affected by the elevator deflections. Table 2 gives a summary of the dependency of each steady-state aero and CS coefficients on α, β, and CS deflections. It is also worth noting that no control interaction effects is presented in the wind tunnel data, and therefore the force and moment contributions of each control surfaces are simply superimposed.

Table 2 Steady Aerodynamic & Control Surface Coefficients Dependency Chart

	α	β	δ_e	δ_a	δ_r
C_x	✓		✓		
C_z	✓		✓		
C_{My}	✓		✓		
C_y	✓	✓		✓	✓
C_{Mx}	✓	✓		✓	✓
C_{Mz}	✓	✓		✓	✓

The shape of the steady-state airframe aerodynamic coefficients are shown in figure 4 and a selection of steady-state CS aerodynamics coefficients vs α or β at every deflection are shown in figure 5 and 6. One can observe that the aerodynamics data, especially the lateral force and moments, are quite nonlinear when plotted against AoA.

Due to the lack of windtunnel data, the *unsteady aerodynamic coefficients* due to rotation rates are estimated empirically using the various methods summarized in Smetana et al.[12]. Those unsteady coefficients are constant and independent of α, β, and control surface deflections. Whilst most of those coefficients are deemed insignificant

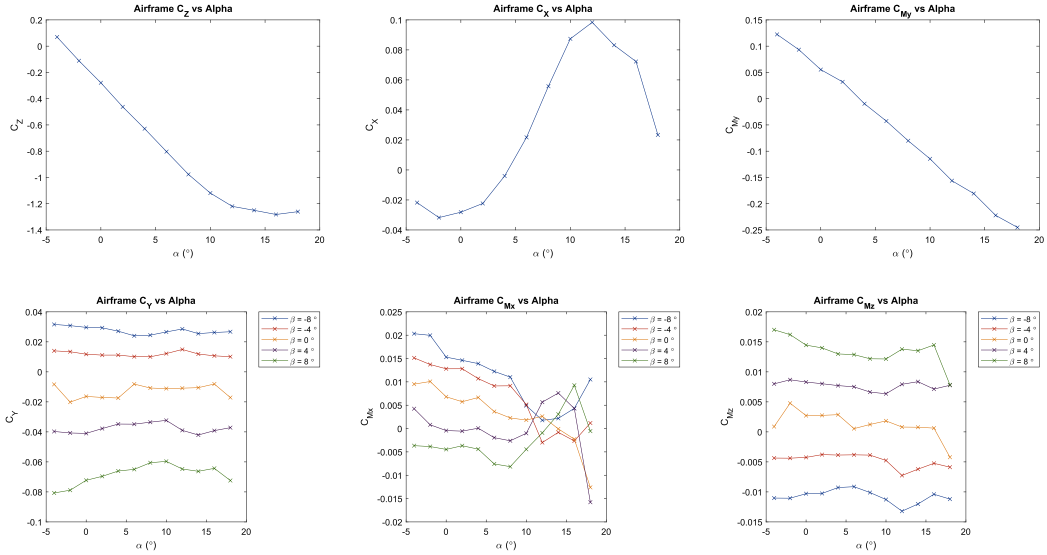

Fig. 4 Steady-State Airframe Aerodynamics Coefficient vs α and β

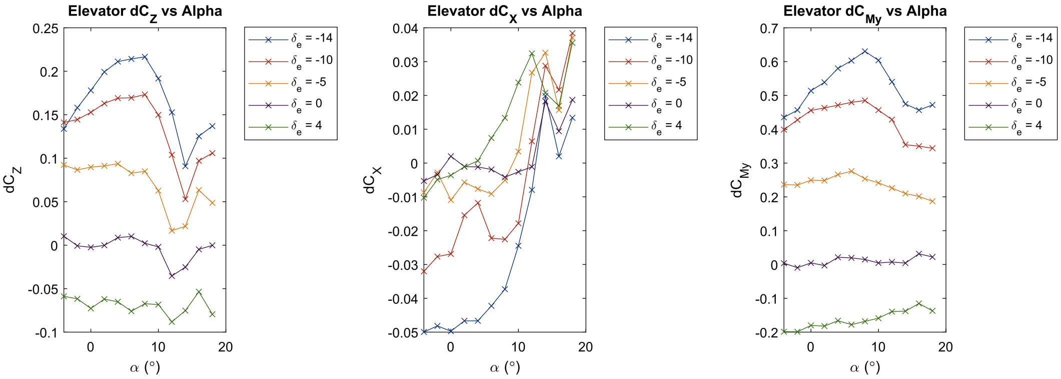

Fig. 5 Steady-State Elevator CS Coefficient vs α

for light aircraft, the value used for the non-zero rate coefficients are listed below in Equation 6:

$$\begin{aligned} C_{Mx,p} &= -0.4 & C_{z,q} &= 3.9 & C_{Mx,r} &= 0.08 \\ C_{Mz,p} &= -0.05 & C_{My,q} &= -12.43 & C_{Mz,r} &= -0.1 \\ & & & & \text{Unit} &: 1/(\text{rad/s}) \end{aligned} \tag{6}$$

D. Propulsion

Two variants of the propulsion sub-systems were implemented for the simulation. *The first one* is a simple `ideal` model where the thrust output from each engine is a function of the percentage throttle control (x_c) and the specified maximum thrust of the engine(T_{max}), as seen in equation 7, regardless of airspeed and other atmospheric conditions. This model is used for two main purposes: to facilitate development of other modules as well as facilitate the modal analysis.

A first-order delay in the form of transfer function $\mathrm{tf}(s) = \frac{(1/\tau_{\text{eng}})}{1+(1/\tau_{\text{eng}})s}$ in the thrust output is also implemented to simulate a delay of engine thrust response to change in throttle input. The delay can be adjusted to investigate the effect of powertrain response characteristics on aircraft flight dynamics. The default value of $\tau_{\text{eng}} = 0.1s$, as suggested in [11], was used as a representative value for the internal combustion engine used by the reference aircraft.

In this variant, the propulsion model also does not contribute to any torque experience by the propeller mass.

$$T = x_c(T_{\text{max}}) \tag{7}$$

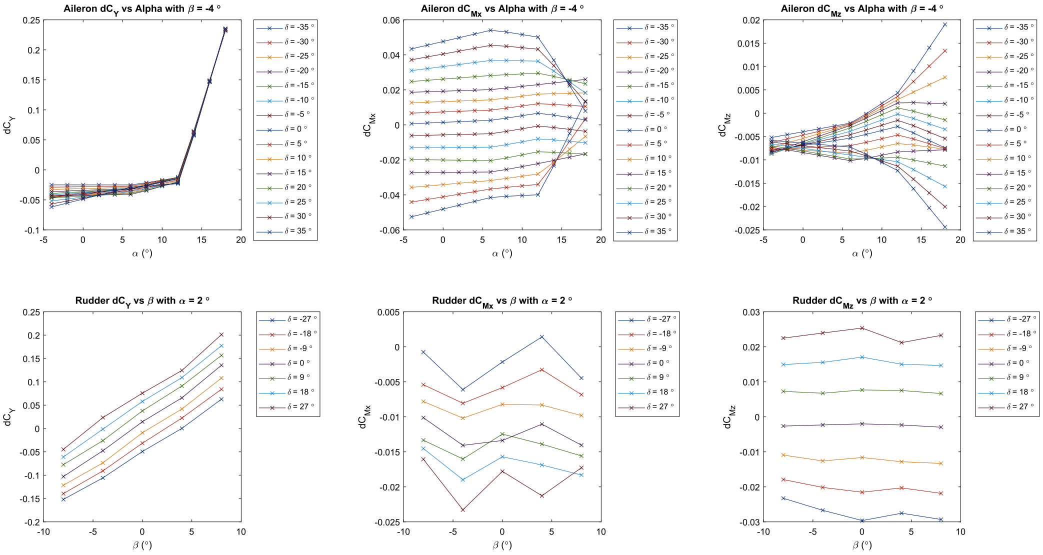

Fig. 6 Steady-State Aileron CS Coefficient vs α and Rudder CS Coefficient vs β

On the other hand, as output characteristics of propeller engines in reality are close to *constant-power* rather than *constant-thrust*, the second propulsion variant functions as a low-medium fidelity model of a propeller-governor-engine system, similar to the constant-speed propeller and piston engine powerplant as used by the PA-30 aircraft. The overview of the Simulink model of propeller-governor-engine system is shown in figure 7.

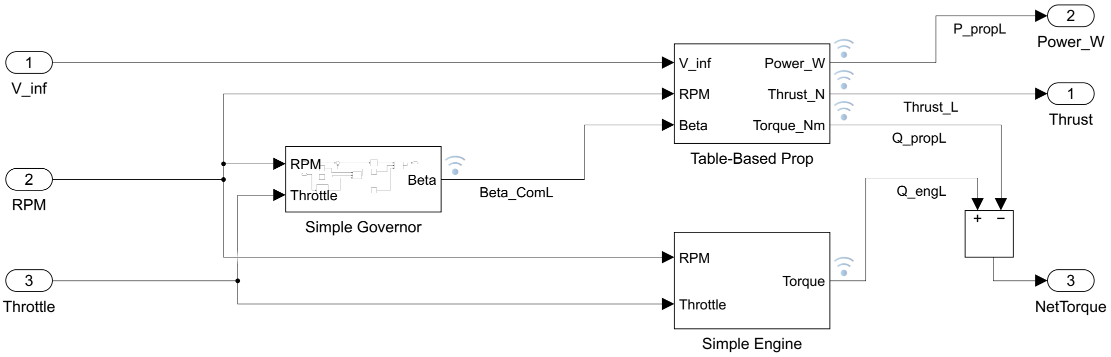
1
V_inf
2
RPM
3
Throttle
RPM
Throttle
Beta
Simple Governor
Beta_ComL
V_inf
RPM
Beta
Power_W
Thrust_N
Torque_Nm
Table-Based Prop
P_propL
2
Power_W
Thrust_L
1
Thrust
Q_propL
Q_engL
+
−
3
NetTorque
RPM
Throttle
Torque
Simple Engine

Fig. 7 The Simulink diagram of the propeller-governor-engine model

The *simple prop* propeller model takes the following input: the freestream airspeed of the aircraft (V_∞), propeller RPS (n_p), propeller diameter (D_p), and propeller blade pitch angle (β_p, defined at $75\%R_\mathrm{p}$ station). It then outputs the power coefficient c_p and efficiency η_p, which in turn can be used to derive thrust:

$$T = \rho n_\mathrm{p}^3 D_\mathrm{p}^5 \eta(\beta_\mathrm{p}, J) c_p(\beta_\mathrm{p}, J) \tag{8}$$

Where $J = V_\infty / n_\mathrm{p} D_\mathrm{p}$ is the advance ratio.

The aerodynamic resistance torque of the propeller can also be derived:

$$Q_\mathrm{p} = P_\mathrm{p}/\omega_\mathrm{p} = \frac{c_\mathrm{p} \rho n_\mathrm{p}^3 D_\mathrm{p}^5}{n_\mathrm{p}(2\pi)} \tag{9}$$

In the absence of aerodynamic data of the exact two-bladed propeller model used by the reference aircraft, the windtunnel data of a Clark-Y-airfoiled two-bladed propeller was used[13]. The propeller performance is charted in figure 8. Due to the limited propeller performance data, *windmilling* or any other negative thrust condition, as well as *feathering*, are not simulated. As a result, the thrust output would be strictly non-negative. The model also only uses the magnitude of airspeed V_∞ and does not consider inflow angles, thus ignoring the effect α and β could have on the thrust produced.

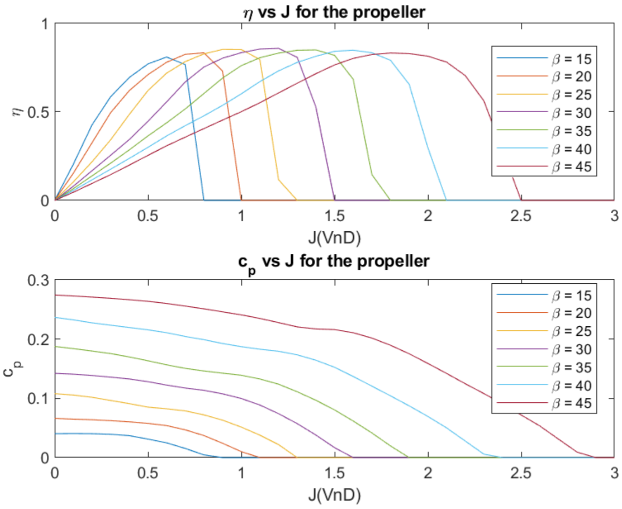

;

Fig. 8 Propeller Performance Chart at various β_p

The simple engine is modelled to be a constant-torque model, where the torque output Q_eng is a function of percentage throttle control and maximum engine torque $Q_\mathrm{eng,max}$, as shown in equation 10. A first-order delay similar to the one introduced above in the ideal variant is also implemented here for the torque output.

$$Q_\mathrm{eng} = x_\mathrm{c}(Q_\mathrm{eng,max}) \tag{10}$$

As mentioned before, the PA-30 is equipped with a constant-speed propeller. Compared with a fixed-pitch propeller, the constant-speed propeller has the ability to vary the pitch angle of the propeller blades to better adapt to the varying flight condition. Specifically, a governor, typically mechanically geared to and driven by the engine whilst hydraulically actuating the blades, is employed to maintain the pilot-commanded propeller RPM by varying the propeller pitch. For example, to absorb the same shaft power at a given RPM, the blade pitch angle β_p needs to become increasingly coarse (large) as airspeed increases. Similarly, at a given airspeed, a reduction in engine torque would mean that a finer (smaller) β_p would be required to maintain a given RPM. To simulate this behaviour, the propeller governor in the simulation is modelled as a PID controller that takes the reference and current RPM as input, and outputs a β_p command to the propeller. The gains of the controller are tuned manually to ensure convergence while limiting rise time to 5 seconds and steady state error to below 20 RPM, both of which are educated guesses that intend to replicate the performance of the real governor system.

This propulsion model is interconnected with the gyroscopic model as mentioned in Section II.B to simulate the coupling between the gyroscopic effect and the powertrain dynamics. The n_p in this propulsion model is provided by the output of the propeller mass model and the net torque $Q = Q_\mathrm{eng} - Q_\mathrm{p}$ of the assembly is then fed back to the propeller mass model, such that the propeller inertia, and thereby its angular momentum, would accelerate and decelerate according to the throttle control setting and the flight condition at the time.

Due to this setup, a torque gain parameter is also implemented to the torque source. The magnitude of the propulsion model torque output is adjusted when the propeller moment of inertia is changed, so that the angular acceleration of the propeller due to aerodynamic drag and engine torque is always the same as the reference propeller regardless of its MoI, thus isolating the effect of propeller angular momentum from other aerodynamic or propulsion effects .

E. Aero/Propulsion Interaction

Recognizing the significant contribution of propeller slipstream and other aero-propulsive interaction effects to the flying characteristics of a light propeller-drive aircraft, during the study, an attempt was made to include the aero-propulsion interaction effect in the simulation by utilizing the windtunnel test results of the aircraft performed at different thrust coefficients[10]. However, as the simulation currently only controls the deflection of the control surfaces directly without taking into account the control forces and hinge moments, the significant increase in control authority under the presence of power effect at a given deflection can cause massive undamped oscillation in the aircraft motion that are uncontrollable during the open-loop simulations. As a result, whilst acknowledging the potential role of such effect could play in altering the results of the comparison, the aero-propulsion interactions are not included in the simulation due to the lack of time to implement a more advanced control system that can accommodate this effect and is left as a recommendation for the future.

F. Flight Control System

The flight control system is a linear direct-gearing type, which maps pilot stick-and-pedal deflections x_a, x_b, and x_p, to the control surface deflections δ_a, δ_e, and δ_r, respectively. The throttles of left and right engines can be controlled individually through $x_\mathrm{c,L}$ and $x_\mathrm{c,R}$, respectively. When they move in unison, a single x_c is used. In the `direct thrust` propulsion variant, they control the percentage of total thrust of the respective propulsors. In the `simple prop` variant, they control instead the percentage torque output from the corresponding engine.

For closed-loop maneuvers, a simple wing leveler is implemented to limit the roll angle excursion. The wing leveler employs a cascaded loop design as seen in figure 9, with the outer loop a proportional gain K_ϕ for error in roll angle ϕ, and the inner loop a proportional gain $K_{\dot\phi}$ for error in roll rate $\dot\phi$.

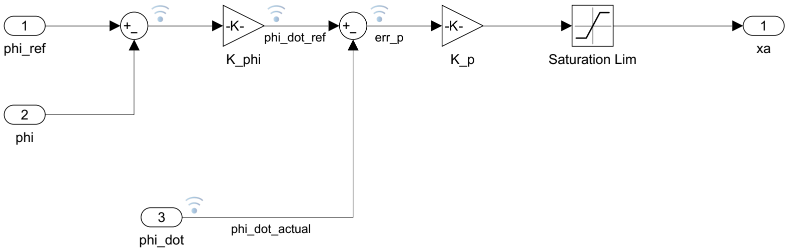

Fig. 9 Block diagram of the wing leveler controller

The controller gains were tuned through a sensitivity study, with the outer loop being tuned for all cases and the inner loop tuned separately for high-speed cruise cases and low-speed climb and approach cases. The criteria used were peak overshoot of 1° and settling time of $5s$.

III. Methodology

This section presents the methodology for the flight dynamics analysis in both time and frequency domains.

A. Trim

In order to perform the flight simulation, the aircraft must first be trimmed to a steady flight condition with no rotation rate or acceleration. Based on the existing PHALANX trimming algorithm, the trimming process is treated as an optimization problem where the objective is zero acceleration and rotation rate. The target sideslip value is also set to zero. The optimization variables are the flight controls (elevator x_b, aileron x_a, rudder x_p, and throttle x_c) as well as the euler angles ϕ, θ, ψ. The optimization itself is solved using a gradient descent technique.

In order to facilitate a faster solution, the degrees of freedom were restricted by ganging the two individual throttle controls using a ganging gain, with such gain set at:

$$K_{[thr.gang]} = \begin{bmatrix} K_{[thr.gang,L]} & K_{[thr.gang,R]} \end{bmatrix}^T = \begin{cases} \begin{bmatrix} 1 & 1 \end{bmatrix}^T & \text{all engine operating} \\ \begin{bmatrix} 1 & 0 \end{bmatrix}^T & \text{right engine inoperative} \\ \begin{bmatrix} 0 & 1 \end{bmatrix}^T & \text{left engine inoperative} \end{cases} \tag{11}$$

When the `simple prop` propulsion model is employed, an additional step is required to reconcile the thrust required to trim the aircraft and the throttle as well as blade pitch angle setting that would produce the said thrust. As such, in this case, the aircraft is first trimmed with the direct thrust model, which yields the trimmed thrust. This trimmed thrust figure is then inputted into the propeller trim algorithm, which first attempts to find the value of β_p that satisfies the equation below with the commanded n_p setting, which is set at $2700RPM$.

$$T = \rho n_\text{p}^3 D_\text{p}^5 \eta(\beta_\text{p}, \frac{V_\infty}{n_\text{p} D_\text{p}}) c_\text{p}(\beta_\text{p}, \frac{V_\infty}{n_\text{p} D_\text{p}}) \tag{12}$$

If a solution cannot be achieved at the desired RPM, it is then assumed that the trimmed thrust is so low that it cannot be achieved through the finest possible blade pitch angle at the commanded RPM. The trimming function then changes to assume the finest possible blade pitch and then starts decreasing the RPM until when the thrust produced approximately resembles the trimmed thrust.

In either cases, after finding the β_p and n_p, the trimmed engine torque setting can then be found using the equation:

$$Q = \frac{P_\text{p}}{\omega_\text{p}} = \frac{\rho n_\text{p}^3 D_\text{p}^5 c_\text{p}(\beta_p, \frac{V_\infty}{n_\text{p} D_\text{p}})}{2\pi n_\text{p}} = \frac{\rho n_\text{p}^2 D_\text{p}^5 c_\text{p}(\beta_p, \frac{V_\infty}{n_\text{p} D_\text{p}})}{2\pi} \tag{13}$$

B. General Test Conditions

In this research, all analysis, unless otherwise specified, are done at the altitude of $h = 0m$. Whilst the aircraft quoted stall speed with flaps and gear retracted (V_S1) is $66kt(33m/s)$, due to the low-fidelity aerodynamic model, the aircraft was unable to be trimmed at that speed. Instead, the single engine minimum control speed $V_\text{MCA} = 78kt(39m/s)$ is used as the minimum speed range, as twin-engine aircraft rarely fly below this speed to ensure controllability in anticipation of a sudden engine failure. In the meantime, the normal operating speed / maximum structural cruising speed (V_NO)of the aircraft is $169kt(84.5m/s)$. As a result, the test airspeed range is decided to be between 40 and $84m/s$.

C. Modal Analysis

The handling quality of the aircraft with gyroscopic effect is first evaluated using the traditional modal analysis. Namely, the full non-linear model is first trimmed for straight and level flight at the designated true airspeeds and altitude. The model is then linearized at that particular operating point. After a linearized model is formed, the eigenmodes of the system are then calculated and analyzed. The `ideal` powertrain is used for this analysis since time-domain simulation is not involved.

The modal analysis consists of two comparisons. The first one compares the effect of increasing propeller rotation speed. The propeller rotation speed is set to $RPM = [0, 0.1, 1] \times 2700$, with the 0 RPM case also representing a negligence of gyroscopic effect. The second one compares the effect of increasing propeller mass moment of inertia, with $I_{xx} = [0.1, 1] \times I_{xx,0}$, where $I_{xx,0}$ is the estimated propeller MoI of the reference aircraft. The $0.1\times$ cases are merely chosen to provide contrast between different magnitudes of rotational momentum, and therefore do not represent real-world objects. Due to the limitation of the physics-based multi-body model, the MoI of the propeller cannot be 0 and therefore the negligence of gyroscopic effect was not simulated in this case. It is important to note that the change in propeller MoI in this case is independent of the propeller mass, which remains constant for this entire study.

D. Open-Loop Flight Maneuvers

Simulations of several open-loop flight maneuvers are performed to investigate the impact of gyroscopic effect on the flying motion of the reference aircraft. A total of 5 maneuvers were devised, all of which starts at trimmed condition at $t = 0s$:

1) *Elevator Impulse-Input*: the elevator is commanded a step input of 5° pitch-up at $t = 1s$ and then a step decrease to the original trimmed value at $t = 2s$
2) *Rudder Impulse-Input*: the rudder is commanded a step input of 5° nose-left at $t = 1s$ and then a step decrease to the original trimmed value at $t = 2s$
3) *Sudden Engine Failure*: the port engine, which is the critical engine, is commanded a 0% throttle at $t = 1s$ and the starboard engine remain at the trimmed throttle setting
4) *Engine Step-Increase*: a step increase to full throttles for all available engines is commanded at $t = 1s$
5) *Going around*: a step increase to full throttles for all available engines in combination with a step input of 5° pitch-up elevator command

No control surface deflection nor throttle control, other than those specified in the list above, is moved from the trimmed position during the maneuver. In the meantime, maneuvers are performed under two engine scenarios: all engine operating (AEO) and one engine inoperative (OEI). In the AEO sceneario, all engines are operating and contributes to both trimming calculation and the flight simulation. In the OEI scenario, the port engine is shut down with 0 RPM and 0 thrust, while only the starboard engine is operating and contributing to both trimming calculation and maneuver simulation. All of the tests here are performed using the `simple-prop` powertrain.

Lastly, three initial conditions were used to represent the three flight phases of interest: initial climb, cruise, and approach, with the initial airspeed, altitude, and flight path angle summarized in table 3. While the initial intention is to chose the specific values based on the quoted best-climb, 75% cruise, and approach speeds from the POH, the current simulation model seems to be unable to trim at some of the specified speeds at the desired flight path angle, due to the inaccuracy in the aerodynamic-propulsive models.

Table 3 Initial trimming condition for Flight Phases

Flight Phase	True Airspeed (V_∞)	Altitude	Flight Path Angle (γ)
Initial Climb	$48.5m/s$ (V_y, AEO) $45.5m/s$ (V_y, OEI)	$151.5m$	4°(AEO) / 1°(OEI)
Cruise	$84.5m/s$	$2424.2m$	0°
Approach	$43.5m/s$ ($V_{App,FlapsUp}$)	$151.5m$	−3°

The test matrix is shown in table 4, indicating which maneuvers are performed at which phases and with which engine configurations. Each simulation is performed for a duration of 20 seconds.

Each test is performed with two simulations, with 1× and 0.01× propeller MoI, denoted *With GE* and *W/O GE* respectively. Due to the limitation of the multi-body model, the propeller MoI cannot be set to zero to prevent singularities. On the other hand, due to the coupling between the multi-body inertia model and the propulsion model, the propeller RPM must be set to the same range as the real aircraft to ensure proper functionality and also cannot be 0 when engine is on. As such, there is no way to set propeller angular momentum to 0 thereby removing the gyroscopic effect entirely. Therefore, throughout the context of this study, the comparison cases are performed with 0.01× propeller MoI to represent a *negligible* level of gyroscopic effect in place of one with completely nullified GE.

The time history of each simulation performed is then characterized using the following four metrics to facilitate comparisons:

1) *Initial Angle of Attack Excursion*: the difference between the initial α value and the first peak value of the α oscillation with respect to time
2) *Initial Side Slip Angle Excursion*: the difference between the initial β value and the first peak value of the β oscillation with respect to time
3) *Largest Airspeed Deviation*: the largest difference in magnitude of true airspeed between the cases with and W/O GE

Table 4 Open-Loop flight maneuver test matrix

Maneuver	Initial Climb	Cruise	Approach
Elevator Impulse-Input Rudder Impulse-Input	All Engine Operative (AEO) One Engine Inoperative (OEI)	AEO	AEO OEI
Sudden Engine Failure	AEO		
Engine Step-Increase	N/A	AEO	AEO & OEI
Going Around	N/A	N/A	AEO & OEI

4) *Largest Airspeed Deviation*: the largest difference in magnitude of altitude between the cases with and W/O GE

The first two metrics are chosen to represent the short-term aircraft motion and also grants some insight on the controllability of the aircraft throughout the maneuver. Whilst the aerodynamic model in this study does not have sufficient fidelity to model inflight upset, monitoring the value of those wind axis angles allows a better view on where the aircraft is in its safe flight envelope when observing its dynamic response.

The other two metrics are chosen to reflect the long-term aircraft dynamic and specifically the aircraft's vertical trajectory and energy state.

The difference and percentage difference of these aforementioned metrics between the 1× propeller MoI case and the 0.01× MoI case is then calculated as follows:

$$\begin{aligned} \text{Difference} \quad &: \Delta\mathcal{M} = \mathcal{M}_{1\times MoI} - \mathcal{M}_{0.01\times MoI} \\ \text{Percent Difference} \; &= \frac{\mathcal{M}_{1\times MoI} - \mathcal{M}_{0.1\times MoI}}{\mathcal{M}_{0.01\times MoI}} \times 100\% \end{aligned} \tag{14}$$

Where $\mathcal{M}$ is any of the four metrics.

E. Closed-Loop Maneuvers with Wing Levelers

In response to the undesired roll axis excursion effect which affects the long-term aircraft motion significantly, partially closed-loop maneuvers based on the same test matrices in table 4 are performed with the implementation of a simple wing-leveler, its design and parameter described in subsection II.F.

F. Powertrain Response

To study the effect of powertrain fidelity and torque response characteristics on the flying characteristics of the aircraft, the flying motion of aircraft with the `simple prop` powertrain and its higher torque lag version was made. The comparisons are made for the throttle-related maneuvers, which are No. 5 through 7 in the maneuvers list with all-engine-operative scenario.

G. Sensitivity Study towards Unsteady Aerodynamic Coefficients

Last but not least, due to the low fidelity method used for determining the unsteady coefficients, a sensitivity study on the unsteady aerodynamic coefficients was performed. As literature[6] as well as the modal analysis results in this study already indicate that classic modal analysis does not capture the influence of propeller gyroscopic effect, it was decided that, instead of comparing the change in aircraft modes in response to variations in unsteady aerodynamic coefficients, short time-domain simulations were performed for variations of the four rates coefficients ($C_{Mzp}, C_{Myq}, C_{Mxr}, C_{Mzr}$). The simulations are performed at cruise condition using the elevator impulse and rudder impulse maneuver with all engine operative, so that both the pitch and yaw axis maneuvers are covered. The control deflections occur at the usual timing but the simulation is truncated to a duration of 5 seconds as only the short-term dynamics are of interest.

IV. Validation and Verifications

Due to the lack of real-world flight-test data, especially those of dynamic flight maneuvers, and considering limited fidelity of aerodynamic data, few validation and verification could be done on a wholistic level to demonstrate that simulation model is a faithful representation of the real reference aircraft. Nevertheless, a few validations and verifications were performed to ensure that the models are showing the correct trend.

Firstly, the correct operation of the propeller governor in the `simple prop` propulsion model is verified by the means of a unit test. The simple prop model was isolated from the rest of the simulation model and put onto a "testbench" with the throttle and aircraft airspeed as the input. The commanded RPM is set at the maximum allowed setting of 2700, which is the typical setting for critical flight phases such as takeoff, initial climb, and approach.

In the first scenario, the throttle set at 100% while the airspeed was raised at a constant rate starting at $t = 5s$. The results of this test is shown in the top graph of 10. As expected, the commanded blade pitch angle (β_p) becomes larger as airspeed increases while the commanded RPM is maintained.

In the second scenario, the airspeed remains constant and the throttle setting is changed through two step inputs. The powertrain behaviour is presented in the bottom graph of Figure 10. After the first step rise of throttle input to full throttle, the governor changes β_p to a larger setting and tracks the commanded RPM fairly well after the initial disturbance. Meanwhile, the thrust increase also reflects the power increase. The second throttle step change closes it completely, commanding 0 torque from the engine. In this case of vanishing torque source, the governor attempts to maintain RPM by commanding the finest possible β_p. However, this is not sufficient as the propeller continues to spin down in RPM in order to reach the new equilibrium of zero thrust and zero shaft power. The result of the simulation is again the same as the real world expectation.

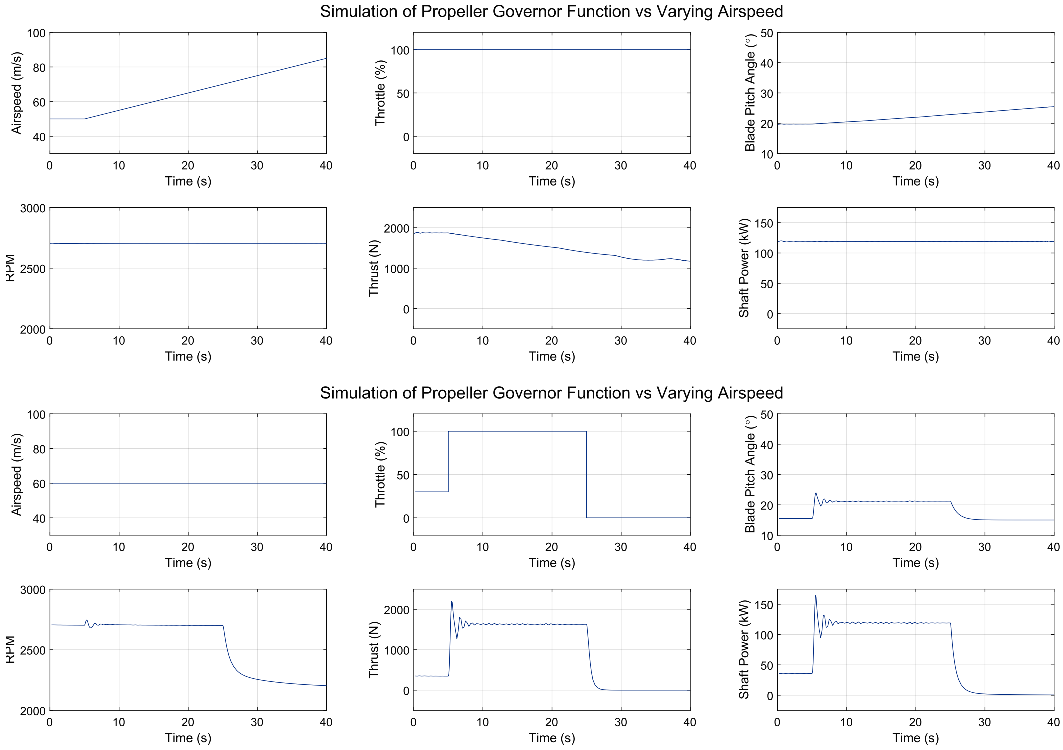

Fig. 10 Response of the propeller-governor model towards increasing airspeed (top) and changing throttle (bottom)

Next, a power-required-curve test was performed to validate the *trimmed* lift to drag curve of the model. The simulation model is trimmed to an unaccelerated straight-and-level flight condition at airspeed from $35m/s$ to $90m/s$ a fixed altitude of $h = 0m$. As only trimming is involved, the `direct thrust` propulsion is utilized. The throttle setting at trimmed condition is then recorded and then converted into thrust and power required to maintain unaccelerated flight.

The result is shown in Figure 11. One can see that the minimum power-required airspeed occurs at around $40m/s$ or around $80kt$. One may recall that the minimum power-required speed is typically the best rate-of-climb speed due to the aircraft having the maximum excess power at that airspeed. Whilst the quoted best rate-of-climb speed of PA-30 is $97kt \approx 47.5m/s$, the result of this test shows that the static aerodynamics performance of the simulation model is still a reasonable resemblance of a typical light general aviation aircraft.

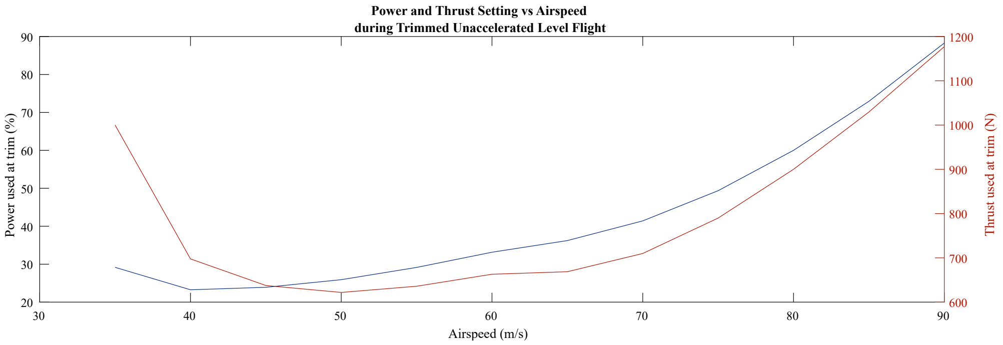

Fig. 11 Thrust and Power vs Airspeed at trimmed condition

V. Results and Discussion

This section presents the results of the simulation performed both in frequency-domain and time-domain. The impact of gyroscopic effects are demonstrated through time-history plots, as well as summarized metrics. After this, the results of the powertrain fidelity and response are also presented, along with the outcome of a sensitivity study on unsteady derivatives.

A. Model Analysis

The change in longitudinal modes of the linearized model for the aircraft due to increasing propeller MoI and increasing RPM is shown in Figure 12 and Figure 13, respectively. One can see that the short-period and phugoid mode frequencies for both the varying propeller RPM and inertia shows similar trend against rising propeller angular momentum L_p. The longitudinal frequencies differ very little in the case of 0×, 0.1×, 1× original propeller angular momentum($L_{p,0}$) Through the airspeed range, there is no case where the change in L_p causes a degradation in frequency or damping criterion levels.

In the meantime, the irregularity around the $50m/s$ to $60m/s$ can be explained the nonlinearity of the longitudinal control surface aerodynamic model. Specifically, the elevator pitching moment incremental coefficients ($dC_{My,\delta_\text{elev}}$) vs α reverses its slope at around $\alpha = 6°$, which is also approximately the trimmed AoA for this speed range.

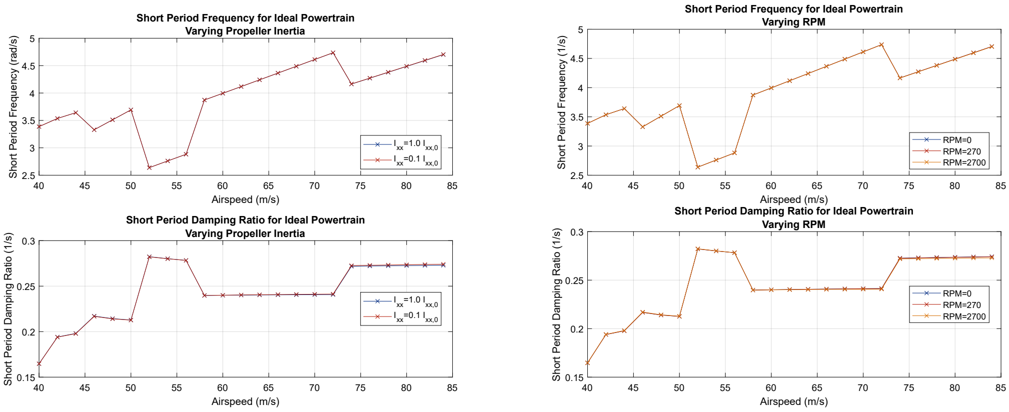

Fig. 12 Effect of increasing propeller moment of inertia (left) and RPM (right) on short-period mode vs airspeed

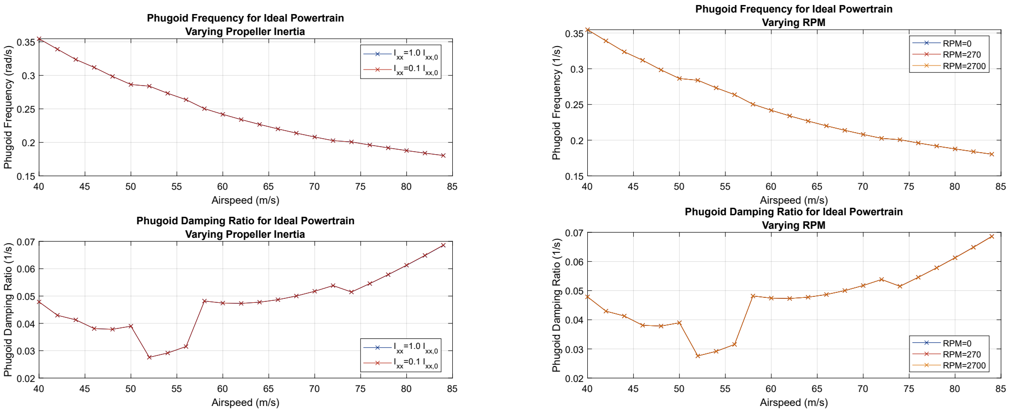

Fig. 13 Effect of increasing propeller moment of inertia (left) and RPM (right) on phugoid mode vs airspeed

The Dutch-roll, roll subsidence, and spiral modes of the aircraft for varying propeller inertia and RPM with respect to increasing airspeed are presented in Figure 14, 15, and 16, respectively. Just as the longitudinal cases, the trends are similar between increasing RPM and increasing inertia.

The frequency and damping ratio for the Dutch Roll mode, presented in Figure 14, shows negligible if any difference between the 0×, 0.1×, 1× $L_{p,0}$ cases. All in all, similar to the longitudinal cases, the handling quality levels do not change with the change in L_p.

The roll subsidence modes are again nearly identical for all cases of propeller RPMs and inertia. This is expected as the roll subsidence mode is mainly dependent on the roll moments and coefficients, whereas the propeller gyroscopic effect mainly concerns the coupled moments between the pitch and the yaw axis.

The spiral modes remain convergent throughout the airspeed range and also for all cases of propeller RPMs and inertia, and therefore are all at handling quality level 1. The spiral frequencies and times to double are also generally overlapping for the the 0×, 0.1×, 1× $L_{p,0}$ cases, as seen from Figure 16. However, the plot of spiral frequency against airspeed does not agree with the usual shape of such curves as seen in literatures such as [14, Fig. 7] and [15, Fig. 11]. This upward inflection after reaching a minimum $Re(\lambda)$ value could not yet be explained without further investigation on the coupling between aerodynamics and inertia model. The said minimum $Re(\lambda)$ approaches zero however does not reach zero. Whilst the deviation from the 0×, 0.1× and $1 \times L_{p,0}$ cases are the most significant, there is also a shift in the airspeed at which minimum spiral frequency occurs.

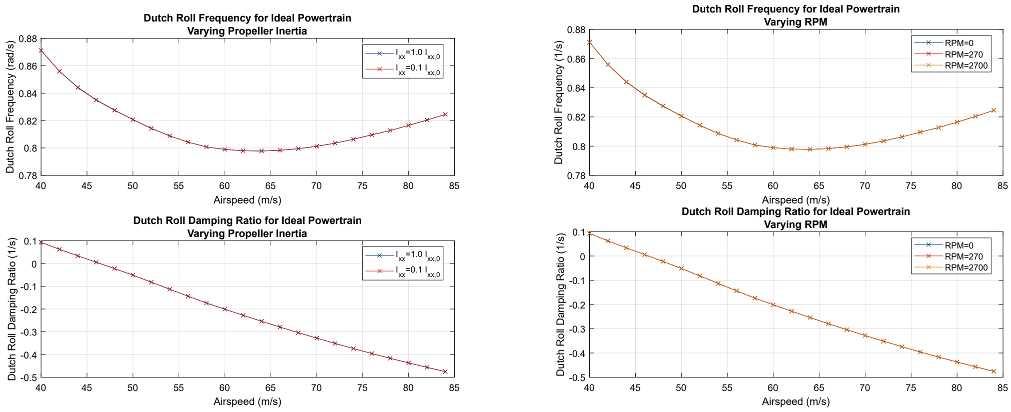

Fig. 14 Effect of increasing propeller moment of inertia (left) and RPM (right) on Dutch-roll mode vs airspeed

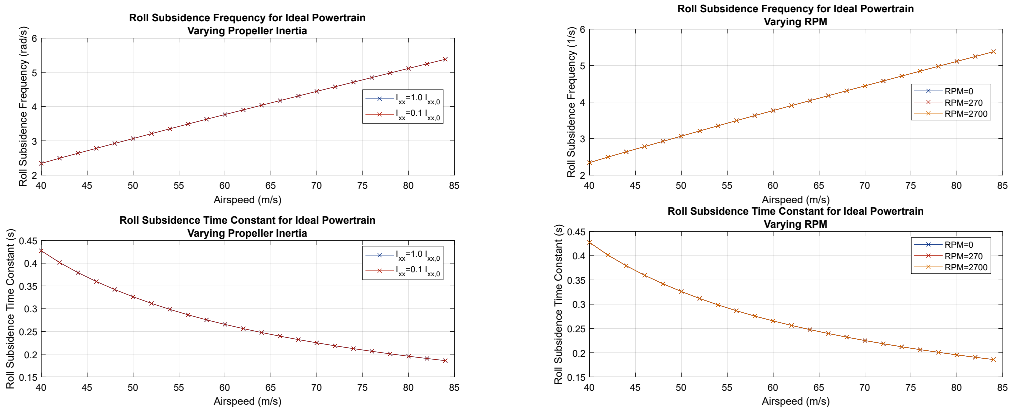

Fig. 15 Effect of increasing propeller moment of inertia (left) and RPM (right) on roll subsidence mode vs airspeed

In summary, while the magnitude of propeller angular momentum does show some effects on the longitudinal and lateral dynamic modes, the differences between the results without or with lower gyroscopic effect are insignificant, except for the spiral mode. The peculiarity of the results, notably short-period and phugoid, are rather due to the aerodynamic models, not the addition of gyroscopic effect. More importantly, changing the magnitude of the propeller angular momentum does not show any downgrade nor upgrade in handling quality levels for all modes. This lack of gyroscopic effect influence on the modal analysis is consistent with existing literature[6] concerning a single-engine aircraft. This can be explained by the fact that small perturbations were used to linearize the model for modal analysis, whereas the gyroscopic effects only manifest themselves at relatively high pitch and/or yaw rates.

B. Open-Loop Flight Response

This subsection intends to present the comparison results of the open-loop flight responses for the two gyroscopic effect (GE) cases (0.01× and 1× propeller MoI) for both all-engine-operating scenario and one-engine-inoperative.

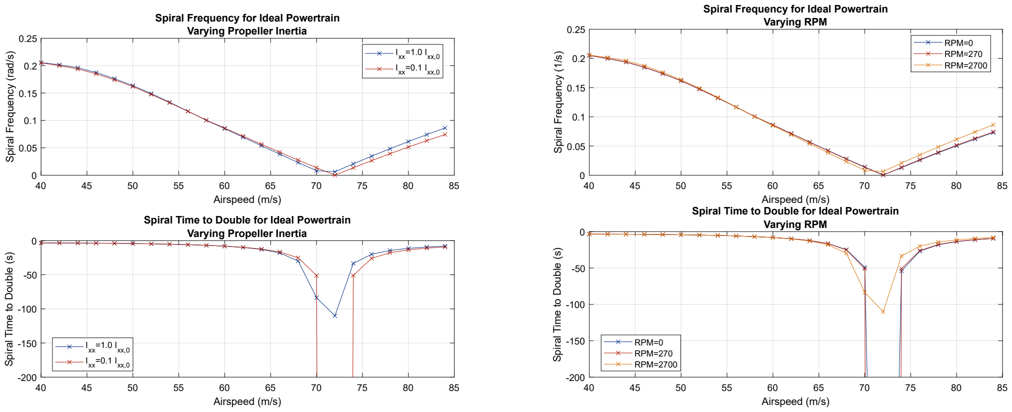

Fig. 16 Effect of increasing propeller moment of inertia (left) and RPM (right) on spiral mode vs airspeed

First, a couple of time history results are shown to demonstrate typical responses for a pitch-input maneuver and a yaw-input maneuver, respectively. Then, a summary of results for all maneuvers in the test matrix using the 5 proposed metrics are shown and discussed. Last but not least, a summarization on the findings from the open-loop maneuver simulations are presented.

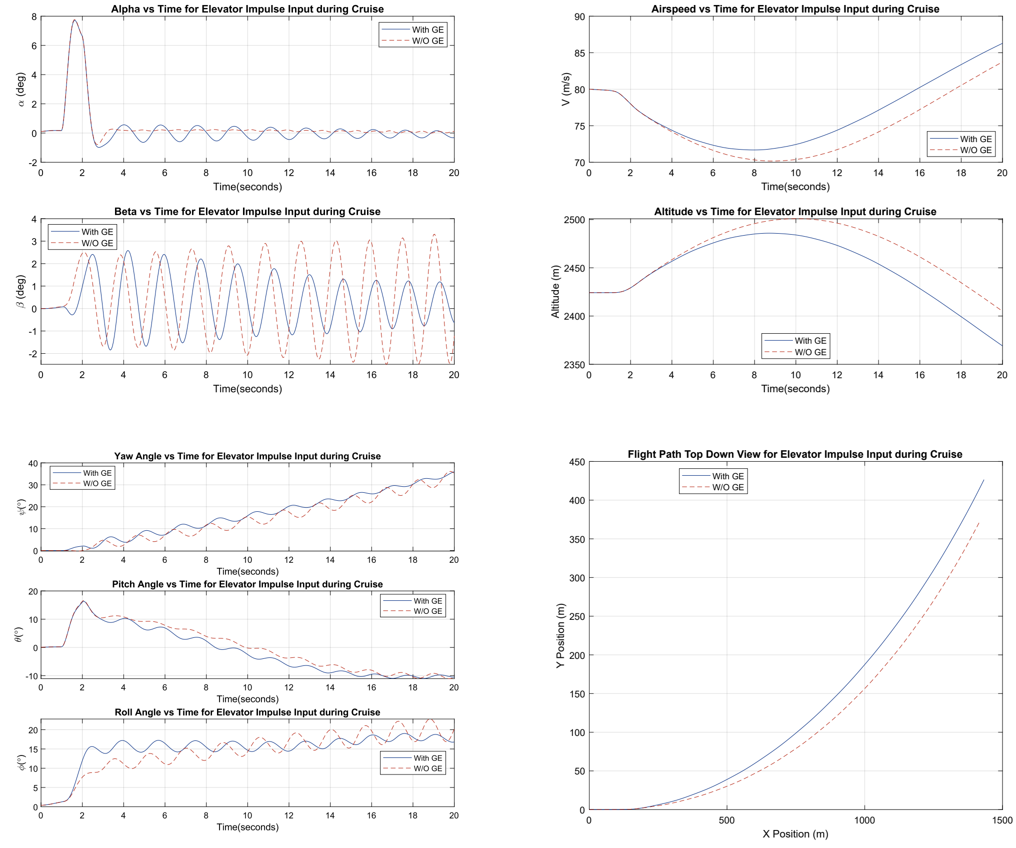

Fig. 17 Time history comparison of the elevator impulse maneuver during cruise condition with all engines operative

Figure 17 shows a time history comparison between the two cases of gyroscopic effect (1× and 0.01× propeller MoI, labeled *With GE* and *W/O* GE respectively) for the elevator impulse-input maneuver with all engines operating at cruise condition ($V_\infty = 169kt$, $h = 8000ft$, and $\gamma = 0°$). This maneuver demonstrates how a input or disturbance in the pitch axis can excite yaw rotation due to the presence of propeller gyroscopic effect. One can observe from the left plot for α and β that the sideslip angle response is significantly different for the two GE cases. For the stronger GE case, a pitch-up moment leads to an almost simultaneous coupled negative rotation in the yaw axis when the step input occurs, which is the expected impact of the propeller gyroscopic effect, whilst the weak GE case shows much less negative rotation before the aerodynamic moments causes a yaw rotation in the positive direction for both cases. This difference leads to not only a much higher initial β but also a noticeable phase offset in β response between the two cases. The β oscillation period is also longer for the stronger GE case, meaning the presence of gyroscopic effect causes a slightly dampening effect on lateral dynamics, which agrees with the increase in Dutch-roll damping for an increasing GE as shown in Figure 14 in the modal analysis. The α response also differs after the initial pull-up, with the stronger GE case having a more noticeable oscillation that corresponds with the β oscillation, signifying a continued gyroscopic influence after the initial disturbance.

The response of the aircraft, in terms of airspeed and altitude, corresponds well with the α and β response. The AoA is consistently lower for the stronger GE case, thus leading to less airspeed loss and more altitude loss. There is also a noticeable shift in phugoid mode, with the stronger GE case having a longer oscillation period However, the top-down view shows that the aircraft has entered a shallow bank and thereafter a divergent spiral mode, despite the fact that the modal analysis suggests spiral modes are convergent throughout the airspeed range. This phenomenon can be explained by three factors of contribution:

- The aileron deflection at trim is non-zero, thus causing additional roll moments as soon as the aircraft departs from trimmed condition due to the elevator deflection.
- The roll moment, yaw moment, as well as side-force coefficients are highly non-linear with respect to both α and β, with $C_{Mx,\alpha}$ flipping sign at medium AoA with $\beta = 4^\circ$, as seen in Figure 4.
- The modal analysis could also have been deficient due to its evident inability to account for strongly non-linear effect such as GE as well as the non-linear nature of the aerodynamic model.

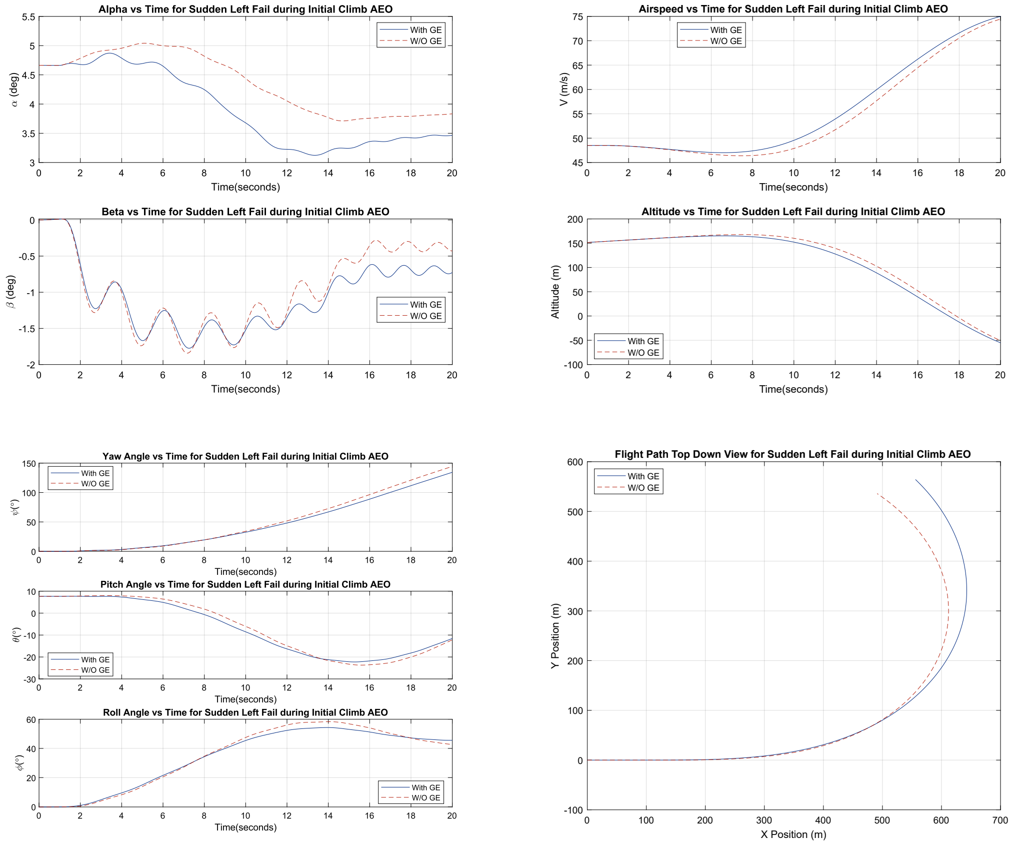

Fig. 18 Time history comparison of the sudden left engine fail maneuver during initial climb condition with all engines operative

Figure 18 shows the time history comparison between cases with and without GE for the sudden left engine failure maneuver during initial climb with all engines operating ($V_\infty = 97kt$, $h = 500ft$, and $\gamma = 4^\circ$) at the start of the simulation. This maneuver is an example of how gyroscopic coupling causes a sudden yaw movement to affect aircraft pitch motions. Similar to the above example, the α and β oscillations are more strongly coupled for the stronger GE case. On the other hand, as the absolute magnitude of AoA and sideslip angle variation remained low, there is noticeably less difference in terms of aircraft phugoid and spiral motion. However, it is worth noting that the propeller system does not model negative thrust conditions, which often is the case when loss of power and oil pressure to the propeller causes the propeller to be windmilled by the incoming airflow, thus causing massive drag and thrust asymmetry before the blades are feathered. As such, a real-world engine failure could incur much higher beta excursion.

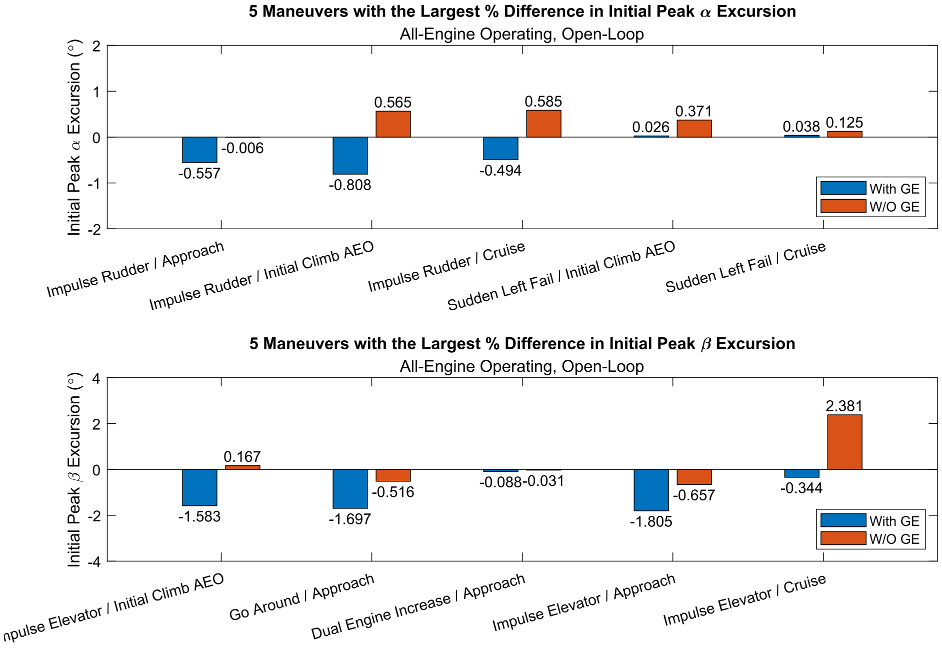

Fig. 19 Maneuvers with the 5 highest percentage difference in α (top) and β (bottom) initial peak excursion between simulation with and without GE, open-loop

The time-simulation results are best summarized by the bar charts in Figure 19, which shows the top 5 maneuvers in terms of percentage difference in initial α (top) and β (bottom) excursions. One can observe from Figure 19 that the top 5 β percentage excursions are dominated pitch-input maneuvers such as elevator impulse pitch-ups, symmetric engine increases as well as go around maneuvers. Accordingly, yaw-input maneuvers such as rudder impulse The negative percentages for the step and impulse elevator during initial climb condition signifies that the initial response of the lesser GE case is in the opposing direction of the stronger GE case. This is due to the fact that the lateral aerodynamic coefficients are also a function of α. As a result, side forces and moments are generated in the direction opposing the gyroscopically coupled moment when aircraft pitches up. In the less GE case, there is not enough gyroscopic moment to counteract such an opposing aerodynamic moments, thus the opposite initial reaction.

For the pure elevator input cases, the magnitude of difference between the initial excursion of the excited axis[*] is significantly higher for the cruise phase compared to the initial climb phases. This is due to the fact that the same angle of control deflection is used for all three flight phases, which means much higher rotation rate was generated at the high-speed cruise phase thanks to the much higher dynamic pressure. This higher rotation rate therefore excites much higher moment in the excited axis for the strong GE cases. However, the low airspeed cases have more difference in excursion in terms of percentages. This is due to the fact that the magnitude of the actual excursions for the no GE cases are rather small due to the low dynamic pressure, leading to less impact on the response by the asymmetric aerodynamic forces, making the GE contributions appear to be much more significant than the aerodynamic contributions. For the dual engine thrust increase cases, the gyroscopic effect is more evident during the approach phase compared to the cruise phase. This is because the trimmed thrust during approach is much farther away from full thrust and power than the cruise case. For pure rudder input cases, the trends between the three flight phases are less clear-cut, with the approach phase presenting the most percentage difference, and the initial climb phase shows the most difference in magnitude of α excursion. This is because rudder effectiveness actually increases with α, which means that the rudders are most powerful for the slow speed phases, thus leading to higher yaw rates and therefore higher pitch rates and excursion. Seeing that the flight conditions and the asymmetric aerodynamics model cause deviations in expected magnitude of gyroscopic-exciting angular rates, further tests are needed to isolate the effect of rotation rates from that of aerodynamics.

---

[*] The excited axis is defined as the axis for which rotation rate is excited by the input axis, e.g. the yaw axis is the excited axis during a pitch maneuver.

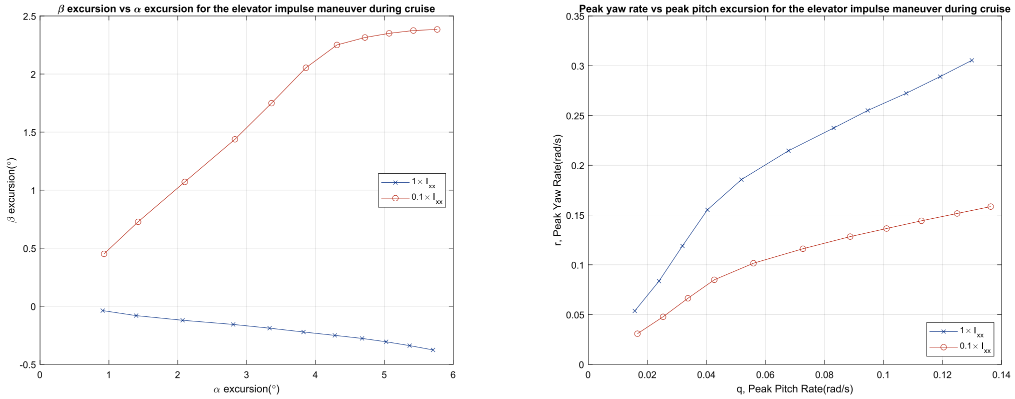

Fig. 20 Angular and rate response of the excursion in excited axis vs the excursion in exciting axis for the elevator impulse maneuvers of various elevator deflection

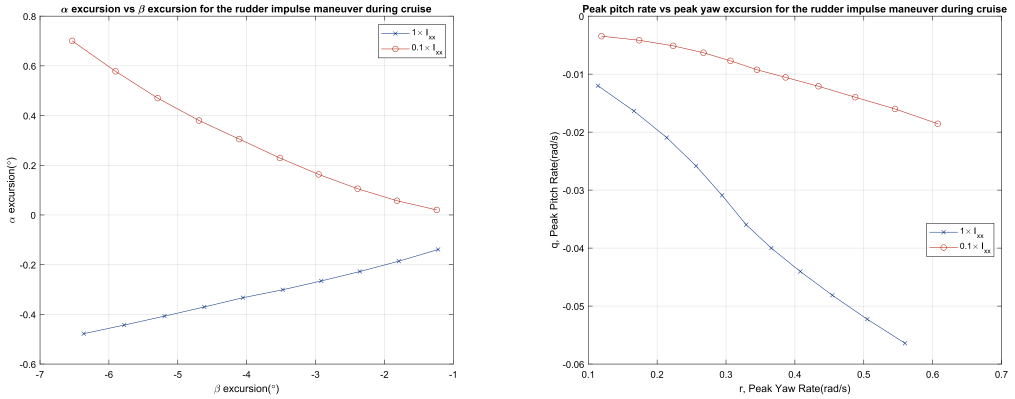

Fig. 21 Angular and rotation rate response of the excursion in excited axis vs the excursion in exciting axis for the rudder impulse maneuvers of various rudder deflection

Therefore, to further investigate the relationship between gyroscopic impact and initial aircraft rotation rates further, the elevator and rudder impulse maneuvers are performed again at cruise condition with a range of increasingly larger elevator and rudder deflections, respectively. The results are presented in Figure 20 and 21 in the form of the excited axis excursion vs exciting axis excursion. For the elevator impulse, the first trend to be noticed is that the peak β excursion becomes increasingly negative as α excursion increases, signifying a positive relation between the rotation rate and the coupled axis excursion. The differences between magnitudes of initial peak β angle excursion of the strong GE cases and the weak GE cases also increase almost linearly with the initial peak α value, further affirming this trend. The rudder impulse response tells a similar story, with the differences in magnitude of the initial peak α angle excursion increasing almost linearly with the initial peak β value. Moreever, one can see that the magnitude of the peak rate of the excited axis is significantly higher for the strong GE cases, again confirming that the impact of gyroscopic effect is strongly related to the rotation of the exciting axis.

On the other hand, due to the presence of significant roll excursion, the characteristics of the phugoid motions are quite varied and no clear trends emerge, as shown in Figure 22, with both pitch and yaw maneuvers during various flight phases among the largest deviations. Further research could instead consider the amplitude, period, and phase lag of the phugoid mode between the weak and strong gyroscopic cases, although the highly nonlinear nature of the influence of the gyroscopic effect may make it hard to determine those values on a large scale.

In general, the results for *one-engine-inoperative scenarios* show similar trends (and lack of trends) in both short-term and long-term aircraft motion, and the results are therefore omitted here.

In summary, time-domain simulations for both all-engine-operating and one engine inoperative scenarios show that:

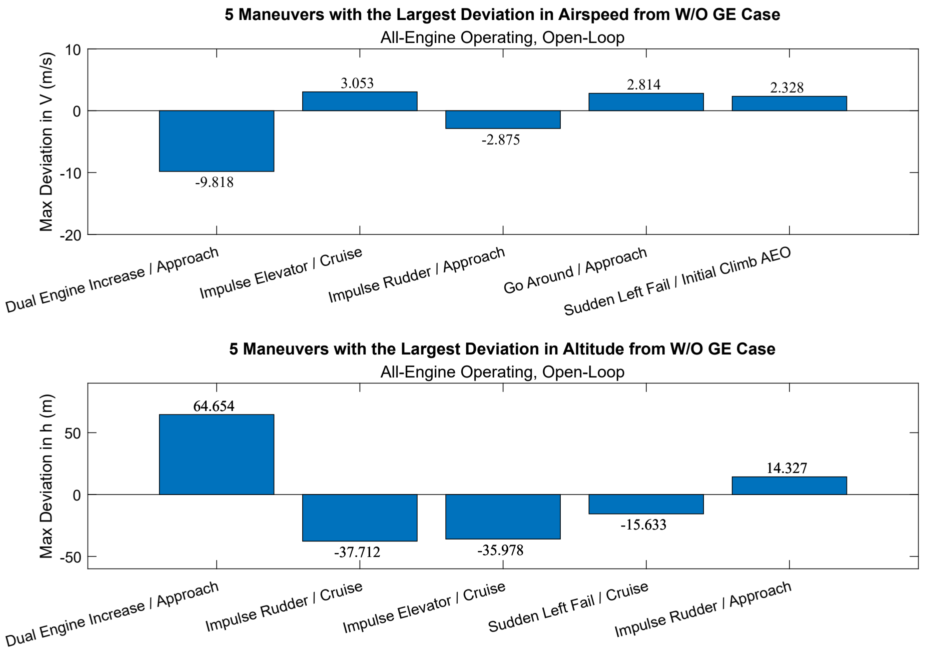

Fig. 22 Maneuvers with the 5 largest deviation in airspeed (top) and altitude (bottom) between simulation with and without GE, open-loop

- The influence by propeller gyroscopic effect on pitch-yaw axis coupling is evident and noticeable, with the difference between the initial excursion of the excited axis of high and low gyroscopic effects in some cases being more than 100%
- It is also evident that by varying the magnitude of the propeller moment of inertia, long-term modes such as phugoid and spiral modes are also modified, despite the outcome of the modal analysis, which only uses small perturbations to linearize the aircraft system.
- The extent to which gyroscopic effects impact short-term aircraft motion, i.e. AoA and sideslip initial response, depends mainly on the angular rate generated by the initial control input.
- The extent to which gyroscopic effects impact the long-term aircraft trajectory (airspeed, altitude, and horizontal paths) is inconclusive and is deemed to be highly dependent on the shape of the steady aerodynamic models, the nature of the maneuver, and the initial condition.

Further targeted study on the effect of long-term aircraft trajectory may require a well-tuned closed-loop flight control system due to the highly nonlinear nature of the aircraft's aerodynamic and control surface model, which, more often than not, led to roll divergence that hinders abilities to draw solid conclusions on the aircraft flight path. A control force-based control system, where control inputs are in terms of stick force rather than simple geared deflection, could also improve the fidelity of the simulation and alleviate the roll divergence in the open-loop simulations.

C. Closed-Loop Flight Responses with Wing Leveler

In order to address some of the adverse effect of roll excursion during the open-loop simulations, flight maneuvers with a closed-loop aileron controller and open-loop elevator and rudder controls were performed to provide additional insight on the impact of gyroscopic effect.

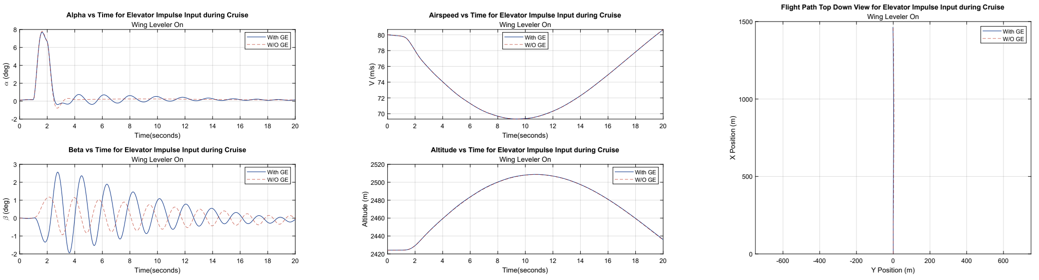

Fig. 23 Time history response for elevator impulse during cruise with all-engine-operative and wing leveler enabled

The time history response for the elevator impulse maneuver during cruise condition with wing leveler enabled is shown in Figure 23. The influence of GE on the short-term angular responses is still evident as seen from the α and β response. In the meantime, the β response shows a much quicker convergence back to symmetric flight for both cases with and without GE, with the strong GE case converging slightly quicker. However, there is no discernible difference in airspeed, altitude, nor ground track trajectory between the with and W/O GE cases, which is in agreement with literature[6] that the long-term flight dynamics does not get affected by the gyroscopic effect.

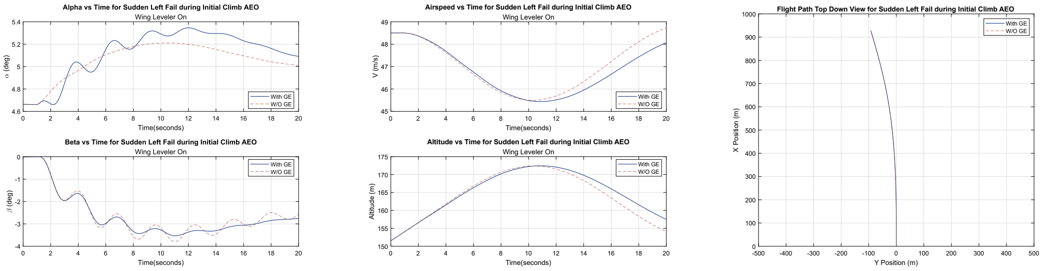

Fig. 24 Time history response for sudden left engine failure during initial climb with all-engine-operative and wing leveler enabled

As shown from the time history response for the sudden left fail maneuver during initial climb condition with wing leveler enabled in Figure 24, the initial response in the excited axis shows again marked difference between cases with and without GE. For the sudden left fail maneuver, instead of settling into a bank into the failed engine and converging to almost no sideslip, the closed-loop cases converge to a non-zero β, which is again within expectation when trying to maintain wing level during engine failure. In contrast to the elevator impulse case, the airspeed and altitude trend does change noticeably. However, the magnitude of changes is still rather small.

The bar graph summary for closed-loop scenarios, shown in Figure 25, shows that the short-term trends shown in the open-loop maneuvers does not change very much with the addition of a wing leveler. Throughout the text matrix, the maneuvers with the largest difference in initial α excursion with wing leveler enabled are still the yaw dominated ones, with similar situation for the initial β excursion observed.

The bar graph summary for the airspeed and altitude shown in Figure 26, however, shows a different trend than that of the open-loop maneuvers. Most of the largest deviations in phugoid motion are yaw-dominant maneuvers. The fact that yaw maneuvers shows more change in phugoid motion than pitch motion is more related to the fact that the longitudinal aerodynamic model is not dependent on lateral dynamics, whereas lateral aerodynamics model does indeed depend on longitudinal dynamics. This dependency, coupled the additional moment generated by the gyroscopic effect, in turn leads to the more noticeable deviation in the phugoid trends.

In the meantime, it is worth noting the caveat that the ailerons also contribute to yaw moment, albeit to a much less degree than rudders. As such, the closed-loop aileron deflections can also contribute to the yaw responses, especially after the initial disturbance.

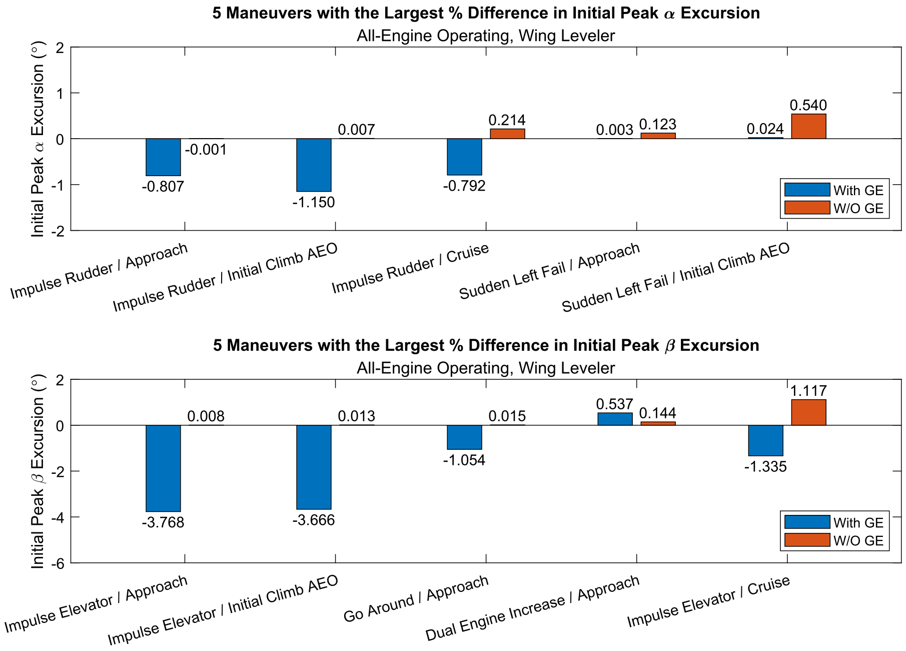

Fig. 25 Maneuvers with the 5 highest percentage difference in α (top) and β (bottom) initial peak excursion between simulation with and without GE, with wing leveler enabled

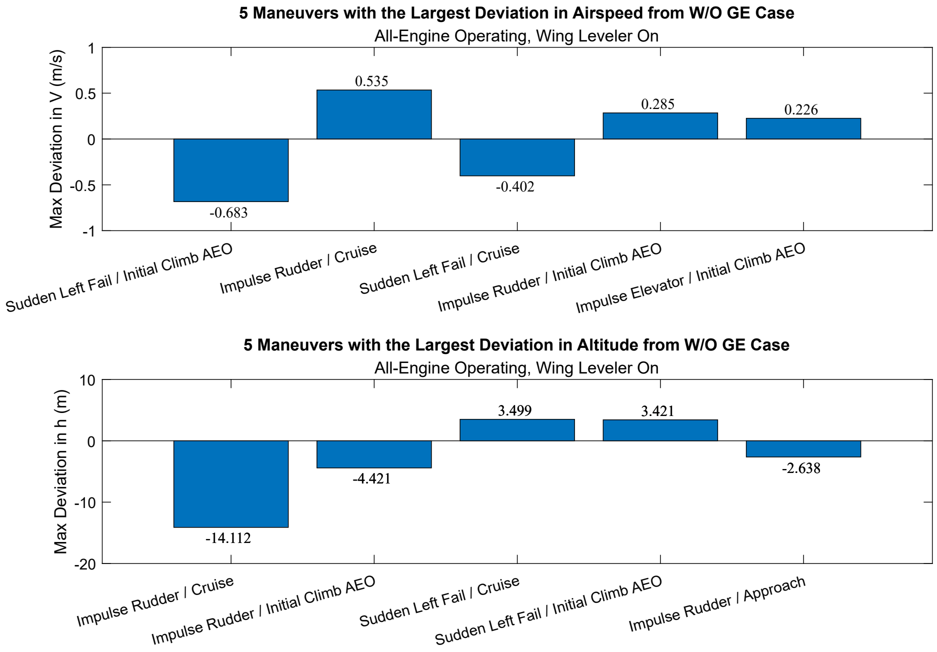

Fig. 26 Maneuvers with the 5 largest deviation in airspeed (top) and altitude (bottom) between simulation with and without GE, with wing leveler enabled

D. Powertrain Response

The *sudden left failure during initial climb* maneuver as well as the *go around during approach* maneuver are the two maneuvers in the test matrices that involves the most changes in engine power setting and therefore are the most suitable ones for exploring the effect of powertrain torque response lag. The four cases presented are the combination of $I_{xx,p} = \{0.1\times, 1\times\} I_{xx,p,0}$ and $\tau_{eng} = \{0.1s, 1s\}$.

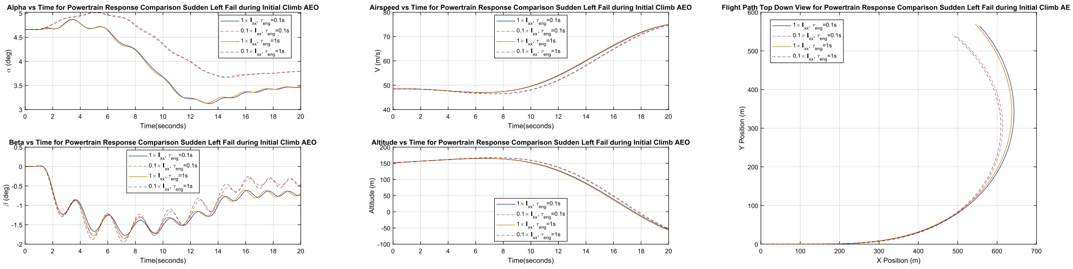

Fig. 27 Time history comparison of the sudden left engine failure maneuver during initial climb condition with all engines operative

The aircraft response for the sudden left failure maneuver is shown in Figure 27. One can observe that the α and β responses, as well as the horizontal motions, are quite similar between cases of identical propeller MoI, whilst the phugoid motions are similar between cases of identical powertrain lag.

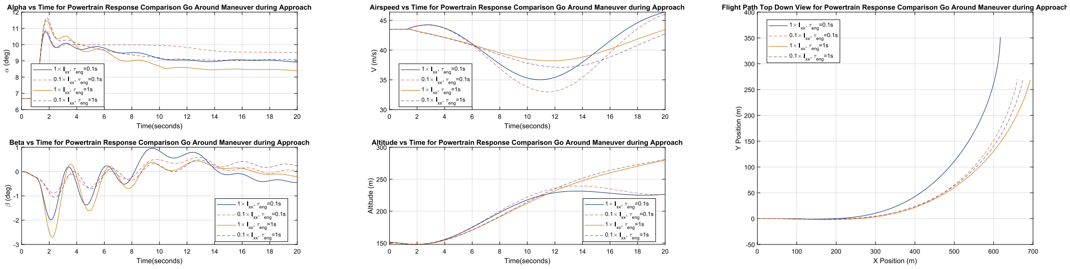

Fig. 28 Time history comparison of the go around maneuver during approach condition with all engines operative

Figure 28 shows the go around maneuver simulation with the four cases. In this case, the initial α response is higher for cases with higher powertrain lag. Because of the higher initial α response, the initial β response is also higher for the higher lag cases. However, the α and β oscillations after the initial peaking are still more dominated by the gyroscopic effect. The phugoid motions are also predominantly affected by the powertrain lag, whilst GE also modifies the phugoid mode by a small extent.

To summarize from the two above cases, the phugoid motion is mainly dominated by powertrain lag, which is within expectation, as the lag in power affects the aircraft's energy state, with is mainly represented by the phugoid motion. When the principal axis of maneuver is the yaw axis, such as during a sudden engine failure, the short-term attitude changes are still dominated by the gyroscopic effect, and the phugoid contribution by the gyroscopic effect is comparatively low. When the principal axis of interest for the maneuver is the pitch axis, the differences in short-term responses are contributed by both the powertrain lag and the gyroscopic effects, with the exact split of influences not quantifiable through the limited test case. The pitching maneuvers also show GE modifying the phugoid motion slightly, though to a much lesser extent than the powertrain lag.

For further investigation, a closed-loop flight control system is again recommended for performing better simulations that more closely replicate real-life situations for evaluating the impact of both the powertrain lag and the gyroscopic effect. This is especially true for the go-around maneuver, which is usually actively performed by the pilot and follows a different routine by following a set airspeed through pitch manipulation, rather than moving the stick to a preset deflection then leaving it there.

E. Unsteady Aerodynamic Coefficient Sensitivity

Figure 29 and Figure 30 show the results of the sensitivity study for elevator and rudder impulse, respectively. For the elevator impulse maneuver, the excitation of yawing motion for the strong GE case is significant for all variations of the unsteady rate derivatives. The variation of C_{Mzp} and C_{Mzr} all sees amplitude reduction with the increased damping, whereas the C_{Myp} variation shows again lower amplitude in yaw when the pitch amplitude itself is lower due to the higher damping. Nevertheless, all strong gyroscopic effect cases are recognizable through the reduced period of β oscillation.

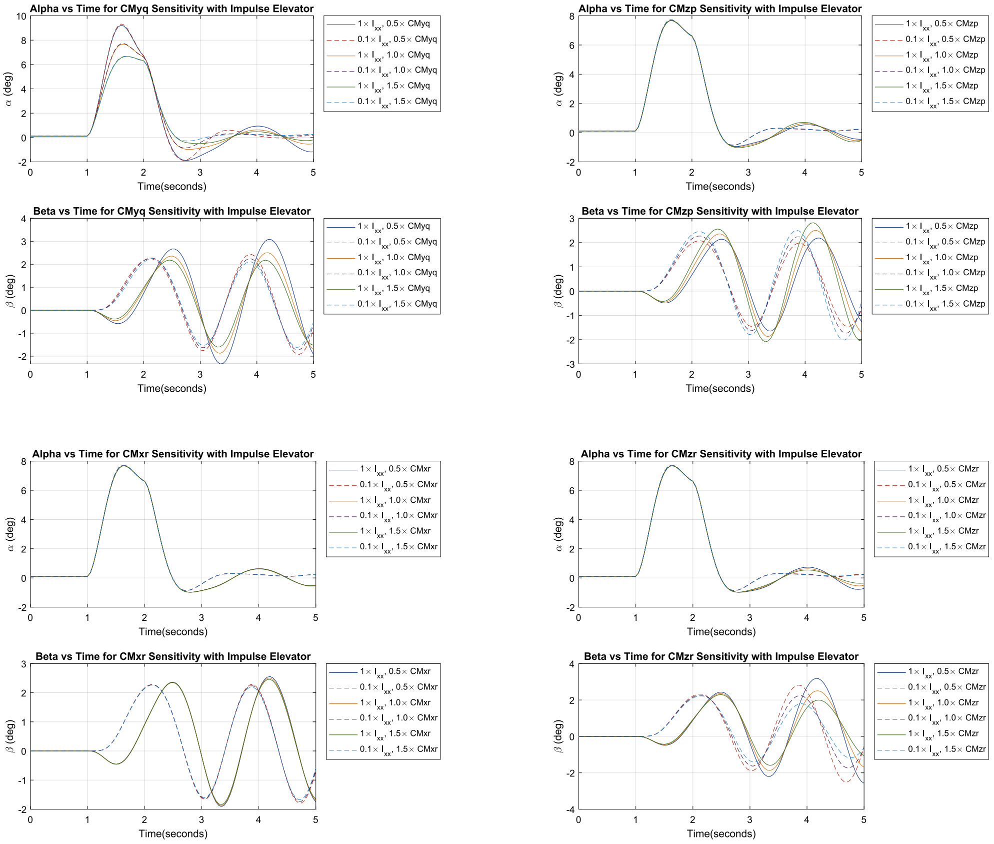

Fig. 29 Aircraft α and β responses for elevator impulse for variations of unsteady aerodynamic coefficients and propeller MoI

For the rudder impulse maneuver, the excitation of the pitching motion for the strong GE case is also evident for all variations of unsteady coefficients. In the case of sensitivity towards the pitch damping coefficient, the peak α amplitude is reduced with the higher C_{Myq} case, which is expected with the increased pitch damping. For the yaw damping coefficient sensitivity, the peak amplitude of the pitch motion is lower for the higher C_{Mzr} because the peak amplitude of the yaw motion itself is more heavily damped, thus leading to lower induced gyroscopic moments. All strong GE cases are detectable by the much higher amplitude and lower frequency of the AoA oscillation.

As such, one can conclude that while the amplitude of the response on the excited axis maybe modified by the variation of some unsteady aerodynamic coefficients, the impact of gyroscopic effect is still very discernible from the impact of those variations.

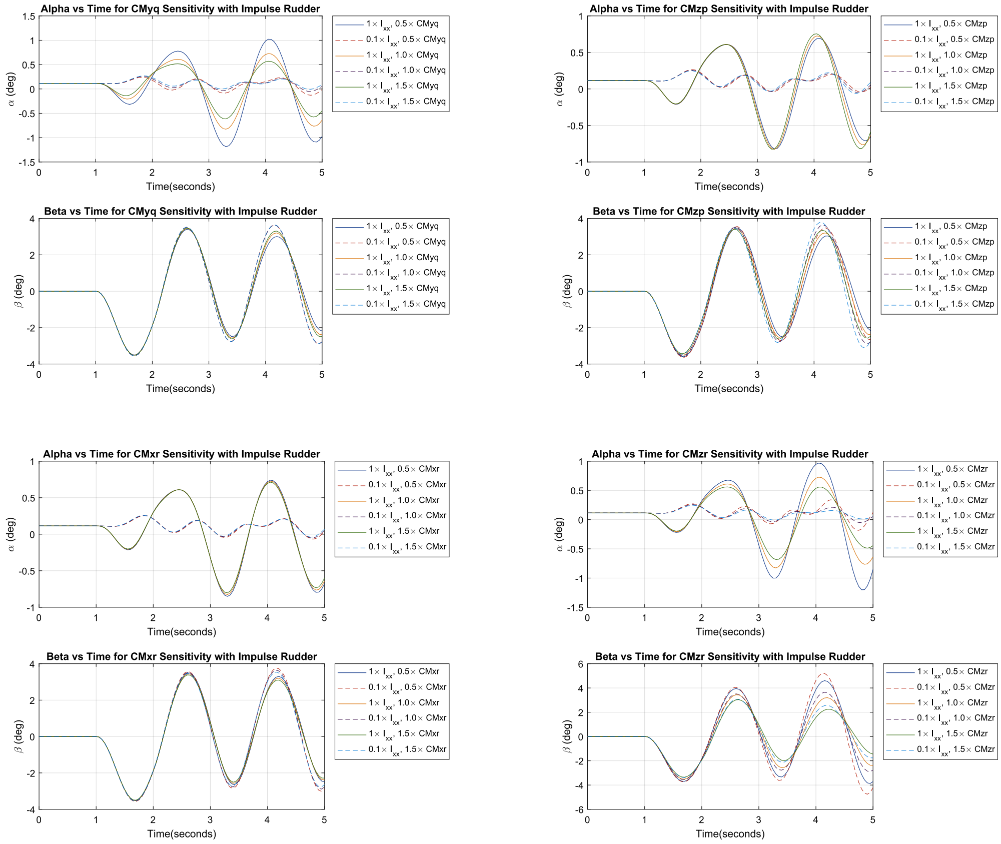
Alpha vs Time for CMyq Sensitivity with Impulse Rudder

Alpha vs Time for CMzp Sensitivity with Impulse Rudder

Beta vs Time for CMyq Sensitivity with Impulse Rudder

Beta vs Time for CMzp Sensitivity with Impulse Rudder

Alpha vs Time for CMxr Sensitivity with Impulse Rudder

Alpha vs Time for CMzr Sensitivity with Impulse Rudder

Beta vs Time for CMxr Sensitivity with Impulse Rudder

Beta vs Time for CMzr Sensitivity with Impulse Rudder

α (deg)
β (deg)
Time(seconds)
1× I_xx, 0.5× CMyq
0.1× I_xx, 0.5× CMyq
1× I_xx, 1.0× CMyq
0.1× I_xx, 1.0× CMyq
1× I_xx, 1.5× CMyq
0.1× I_xx, 1.5× CMyq
1× I_xx, 0.5× CMzp
0.1× I_xx, 0.5× CMzp
1× I_xx, 1.0× CMzp
0.1× I_xx, 1.0× CMzp
1× I_xx, 1.5× CMzp
0.1× I_xx, 1.5× CMzp
1× I_xx, 0.5× CMxr
0.1× I_xx, 0.5× CMxr
1× I_xx, 1.0× CMxr
0.1× I_xx, 1.0× CMxr
1× I_xx, 1.5× CMxr
0.1× I_xx, 1.5× CMxr
1× I_xx, 0.5× CMzr
0.1× I_xx, 0.5× CMzr
1× I_xx, 1.0× CMzr
0.1× I_xx, 1.0× CMzr
1× I_xx, 1.5× CMzr
0.1× I_xx, 1.5× CMzr

Fig. 30 Aircraft α and β responses for rudder impulse for variations of unsteady aerodynamic coefficients and propeller MoI

VI. Conclusion

In conclusion, this paper has presented an investigation on the impact of propeller gyroscopic effects on the handling qualities of a twin-engine light general aviation aircraft. Traditional handling qualities assessments using modal analysis as well as time simulation of rapid maneuvers were performed using an augmented flight mechanics simulation suite which incorporates a multi-body physics based simulation of propeller gyroscopic phenomena, a non-linear wind tunnel aerodynamic model, and propeller-governor-engine dynamics.

Traditional modal analysis shows very little difference between the linearized models with and without the presence of gyroscopic effects. This is because the linearized models are obtained based on small flight parameter perturbations whereas the gyroscopic effect is nonlinear in nature and only manifest itself at considerable rotation rates. Peculiarity in the trend of modes vs airspeed is the same for all amplitudes of propeller angular momentum, and therefore is more likely due to the non-linear aerodynamics model.

Next, open-loop simulations of various flight maneuvers at different flight phases shows that rapid pitch and yaw maneuvers does excite a coupled reaction of the yaw and pitch axis, respectively, as evident from the time history of the angles of attack and sideslip angles. The stronger the angular rate that the maneuver generates, the larger the induced response from the excited axis is. The phugoid motion was also evidently affected by the presence of gyroscopic effect, though the question of which maneuver(s) are more significantly affected by the gyroscopic moments remains inconclusive. The open-loop nature of the simulation and the non-linear aerodynamics model means that undesired roll motion is also introduced, which further restricts the ability to draw more conclusions from the flight trajectory.

To alleviate this roll excursion problem, partially closed-loop maneuvers with a simple wing leveler were also performed. When the roll angle actively controlled, the phugoid motion of the aircraft is more likely to be altered by the presence of gyroscopic effect during yaw-dominant maneuvers rather than pitch-input maneuvers, though overall not much difference was observed between cases with and without gyroscopic effects.

Next, the comparison between different powertrain lag shows that in an sudden one-engine-failure situation, the powertrain lag plays almost no role in the short-term motion of the aircraft and also very little role in the long-term phugoid motion. On the other hand, during a dual engine go around, the powertrain lag plays a major role in changing the phugoid mode as well as the short term dynamics, mainly through reducing the initial peak alpha value.

Last but not least, a sensitivity study on unsteady aerodynamic coefficients shows that whilst the peak amplitude of the gyroscopic moment induced motion changes with the varying damping coefficients on the related axis, the coupling between the pitch and yaw axis is still evident for all cases. One can then reasonably conclude that the relatively low fidelity of the unsteady aerodynamic coefficients do not detract from the comparison between cases with or without the presence of gyroscopic effects.

Nevertheless, further research could consider first enhancing the aerodynamics with higher fidelity model by including the aero-propulsion interaction effects and combine such increase in aerodynamics accuracy by also incorporating force-based controls rather than the existing deflection-based controls. Aerodynamics models for alternative configurations such as flaps down and gear down could also be useful for more accurately studying maneuvers such as engine failure during final approach and missed approach, where twin-engine aircraft are the most vulnerable to the adverse effect of flight upset. The incorporation of a more well-designed three-axis autopilot or human pilot could also be useful for studying how the propeller gyroscopic effect affects closed-loop behavior of the aircraft. Last but not least, the research can be further parameterized to include higher number of propellers/propulsors on the aircraft, similar to the distributed propulsion concerts currently in study for future electric aviation.

References

[1] "Light Twin-Engine Aircraft Accidents Following Engine Failures, 1972-1976," , Dec. 1979.

[2] Scanlan, R. H., and Truman, J. C., "The Gyroscopic Effect of a Rigid Rotating Propeller on Engine and Wing Vibration Modes," *Journal of the Aeronautical Sciences*, Vol. 17, No. 10, 1950, pp. 653–659. https://doi.org/10.2514/8.1758.

[3] Liu, V., "Propeller-Wing Whirl Flutter - An Analytical Study," Master's thesis, Delft University of Technology, 2020.

[4] Teixeira, P. C., and Cesnik, C. E. S., "Propeller Effects on the Response of High-Altitude Long-Endurance Aircraft," *AIAA Journal*, Vol. 57, No. 10, 2019, pp. 4328–4342. https://doi.org/10.2514/1.j057575.

[5] Smith, Jr, C. C., "Hovering and Transition Flight Tests of a 1/5-Scale Model of a Jet-Powered Vertical-Attitude VTOL Research Airplane," techreport, Langley Field, Va., Dec. 1958.

[6] Goraj, Z. J., and Cichocka, E., "Influence of weak and strong gyroscopic effects on light aircraft dynamics," *Aircraft Engineering and Aerospace Technology*, Vol. 88, No. 5, 2016, pp. 613–622. https://doi.org/10.1108/aeat-03-2015-0076.

[7] Voskuijl, M., La Rocca, G., and Dircken, F., "Controllability of blended wing body aircraft," *Proceedings of the 26th International Congress of the Aeronautical Sciences, ICAS 2008, including the 8th AIAA Aviation Technology, Integration and Operations (AIO) Conference, Anchorage, Alaska, September 14-19,(2008)*, Optimage Ltd., 2008.

[8] Varriale, C., Raju Kulkarni, A., La Rocca, G., and Voskuijl, M., "A Hybrid, Configuration-Agnostic Approach to Aircraft Control Surface Sizing," *Proceedings of the 25th International Congress of the Italian Association of Aeronautics and Astronautics (AIDAA), Rome, Italy*, 2019, pp. 9–13.

[9] Varriale, C., Hameeteman, K., Voskuijl, M., and Veldhuis, L. L., "A Thrust-Elevator Interaction Criterion for Aircraft Optimal Longitudinal Control," *AIAA Aviation 2019 Forum*, American Institute of Aeronautics and Astronautics, 2019. https://doi.org/10.2514/6.2019-3001.

[10] Fink, M. P., and Jr, D. C. F., "Full-Scale Wind-Tunnel Investigation of Static Longitudinal and Lateral Characteristics of a Light Twin-Engine Airplane," Tech. rep., Jan. 1969.

[11] Koziol Jr., J. S., "Simulation Model for the Piper PA-30 Light Maneuverable Aircraft in the Final Approach," Tech. rep., Federal Aviation Administration, 1971.

[12] Smetana, F. O., Summery, D., and Johnson, W. D., "Riding and handling qualities of light aircraft: A review and analysis," 1972.

[13] Hartman, E. P., and Biermann, D., "The Aerodynamics Characteristics of Full-Scale Propellers Having 2, 3, and 4 Blades of Clark Y and R. A. F. 6 Airfoil Sections," techreport, 1938.

[14] Goetzendorf-Grabowski, T., and Antoniewski, T., "Three surface aircraft (TSA) configuration – flying qualities evaluation," *Aircraft Engineering and Aerospace Technology*, Vol. 88, No. 2, 2016, pp. 277–284. https://doi.org/10.1108/aeat-02-2015-0055.

[15] Hasan, Y. J., Roeser, M. S., Hepperle, M., Niemann, S., Voß, A., Handojo, V., and Weiser, C., "Flight mechanical analysis of a solar-powered high-altitude platform," *CEAS Aeronautical Journal*, Vol. 14, No. 1, 2022, pp. 201–223. https://doi.org/10.1007/s13272-022-00621-2.

III

Literature Study Report (Previously Graded)

2

Introduction

2.1. Background and Motivation

Safety is of paramount importance in the field of aviation. An NTSB investigation in 1979[1] found that, during the time frame between 1972 and 1976, the likelihood of a fatal crash after an engine failure was four times greater for a twin-engine aircraft than a single-engine aircraft. This is due to the fact that a typical twin-engine General Aviation (GA) aircraft have their engines installed symmetrically on both sides of the airframe. When one of the engine fails and stops producing thrust, the resultant asymmetrical thrust force from the remaining engine would results in a high yaw moment that could cause the aircraft to depart from controlled flight if not handled promptly and correctly by the pilot. In light of this, the sizing of the vertical stabilizer(s) and rudder(s) of multi-engine aircraft is often constrained by the controllability of the aircraft under the one-engine-inoperative (OEI) conditions.

However, whilst larger vertical stabilizers and rudders allow for greater directional controllability, they also lead to higher surface area and mass, both resulting in higher fuel consumption due to increased parasitic drag and lift-induced drag, respectively. As the understanding of aircraft dynamics as well as the capability of modelling the flying motion grows, much of the efforts have been made to take advantage of this new ability in the early phases of the aircraft design cycle in the chase of efficiency. This can be seem from efforts such Soikkeli's study[7] on evaluating the potential reduction of vertical tail sizes through incorporating differential thrust as yaw control device.

With that in mind, the *gyroscopic procession effect* refers the tendency of a rotating mass to resist change in its rotating axis in the form of a restoring moment. Such effect increases with the rotating inertia and rotational speed of the rotating mass. In the context of flight dynamics, aircraft propellers are such major rotating masses in airplanes due to its dimension, mass, and angular velocity. It is therefore interesting to investigate the impact of such effect on the dynamic behavior of an aircraft, which could lead to a significant coupling between axes. Understanding such phenomenon could potentially enable both insights on the handling qualities of aircraft as well as the sizing of the lateral-directional controls. It may also enhance the fidelity of flight training simulations, which would allow pilots to be better trained in dealing with OEI situations.

In the meantime, the advent of electric aircraft also enables the concept of distributed propulsion to be popularized, as the simplicity and compactness of electric motors allows the propulsion devices to be placed more freely than ever before. Whilst distributing propulsive power amongst numerous devices yields tangible benefits in terms of efficiency, it also means that a powertrain failure is more likely to occur and that the number of major rotating masses is also increased. As such, how such a trend in the development of sustainable aviation would affect the contribution of gyroscopic procession to the handling characteristics of light aircraft is also worth investigating.

2.2. State-of-Art

Several researches on the effect of propeller gyroscopic procession in the field of aviation have already be done dating as early as 1940s. However, many of such studies are primarily concerning the structure aspects. The 1941 NACA Technical Memorandum[8] derived the torque and bending moment caused by propellers from a theoretical point of view. Building upon this, Scaland and Truman[2] took an experimental approach to study the effect gyroscopic processions have on engine on-wing vibration modes. Liu's study on propeller whirl-flutter effects[3] from an analytical approach also took gyroscopic procession into account. It was found that when a flexible wing is assumed, the gyroscopic effects of the rotating propellers change the frequencies of the free vibrating modes.

In the meantime, Teixeira and Cesnik provided additional insight on the combination of aerodynamic and gyroscopic effects of the distributed propellers on the highly-elastic wing of a high-altitude long-endurance (HALE) aircraft[4], which showed that gyroscopic effect does affect the wingtip twist of such an wing. Such behavior is expected as gyroscopic precession is only expected to produce a moment but not a translational force.

On the flight dynamics front, early efforts on investigating the impact of gyroscopic procession were made done mainly for rotorcraft and VTOL aircraft due to the relatively large rotating mass of the propulsion devices of those types of aircraft. For example, Smith, Jr.'s experiment in 1958 [5] on the hovering and transition flight of a scaled model of a jet-powered VTOL aircraft uses a air-jet powered flywheel to simulate the gyroscopic forces generated by the rotating masses of the jet engine. It shows that when the simulation of gyroscopic procession is enabled, the scaled model "could not be controlled in hovering flight without artificial stabilization because of the strong gyroscopic coupling of the yawing and pitching motions"[5].

Goraj et al. [6] offered a detailed study into the impact of strong and weak gyroscopic effect on the handling characteristics of a single-engine turboprop light GA aircraft through numerical flight simulation. In this context, *weak gyroscopic effects* was referred to as those that can be investigated using the traditional modal analysis approach of aircraft stability whereas *strong gyroscopic effect* refers to those dynamic ones that are exhibited during time-domain analysis of rapid flight maneuvers. For the weak gyroscopic effects, it was found that the moment of inertia of the propeller does not have an impact on the dynamic modes of the aircraft whereas the rotational speed does. For strong gyroscopic effects, rapid maneuvers such as step deflections of elevator and rudders were performed as well as simulations of gusts. During such maneuvers, the effect of gyroscopic procession is discernible with induced sideslip angle after only longitudinal control excitation.

2.3. Research Gap

As seen from the state-of-art review in section 2.2, the study of gyroscopic procession on aircraft flight dynamics through flight simulation is still rather limited. Notedly, no study has been done on the how gyroscopic effects can impact flight dynamics for multi-engined aircraft. Moreover, as highlighted by Goraj and Chichoka's study[6], propeller gyroscopic procession does have a noticeable effect during rapid maneuvering such as elevator and rudder step inputs as well as gusts. A sudden engine failure for a multi-engine aircraft could also cause the plane to experience sudden attitude change that would induce significant gyroscopic torque, which could potentially contribute to improving or worsening the recovery maneuver.

Furthermore, no study has been performed yet that takes into account of the effect that different powertrain types can have on the behavior of the aircraft when gyroscopic effects are taken into account, as more of the study assumes constant propeller rotational speed. In the meantime, neither was there any sensitivity studies on the sensitivity of such gyroscopic effect on the engine/propeller location relative to the Center of Gravity (CoG).

2.4. Research Statement

With the aforementioned gap in mind, the following research question was then formed:

> How can one quantify the impact of propeller gyroscopic procession effect on the flight dynamic behaviors of light multi-engine aircraft through flight simulation, especially during the event of a powertrain failure?

With that in mind, the sub-research questions are then:

- How sensitive is the result of this study to the fidelity level of aerodynamic modelling?
- During which maneuvers is the effect of propeller gyroscopic procession more prominent?
- What are the relevant parameters that can be used to quantify the impact of the gyroscopic effect on the flying qualities?
- How does different powertrain types (electric, piston, turboprop) impact the results?
- How does the placement of the engines/propulsion devices affect the results?

The main contribution of this research aims to grant an insight on the effect of propeller gyroscopic procession on light multi-engine aircraft especially during rapid maneuvers similar to those encountered during the event of engine failure. With a better understanding of the contribution of such effort on aircraft flight motion, the sizing method of flight controls for meeting controllability constrains could potentially be improved whilst the improved flight dynamics model could also provide the pilots with higher-fidelity flight training simulation. It also serves to give more understanding on the effect of electrification and distributed propulsion on aircraft flight dynamics.

2.5. Reference Aircraft

The base aircraft model chosen for this research is the DA-42 manufactured by Diamond Aircraft Industry, a picture of which is shown in figure 2.1. It is a light four-seater general aviation aircraft powered by two piston engines and constant-speed variable pitch propellers mounted symmetrically on the main wing, which is the conventional layout of a twin-engine GA aeroplane. With initial certification and delivery in 2005 and more than 1000 examples built by March 2019[9], this type of aircraft is chosen for this study due to its ubiquity amongst flight training schools as well as the general flying public. The availability of publicly available technical materials such as the Aircraft Flight Manual (AFM)[10] and the Aircraft Maintenance Manual (AMM)[11] as well as suitable open-source 3D model[12] is also an advantage for the research.

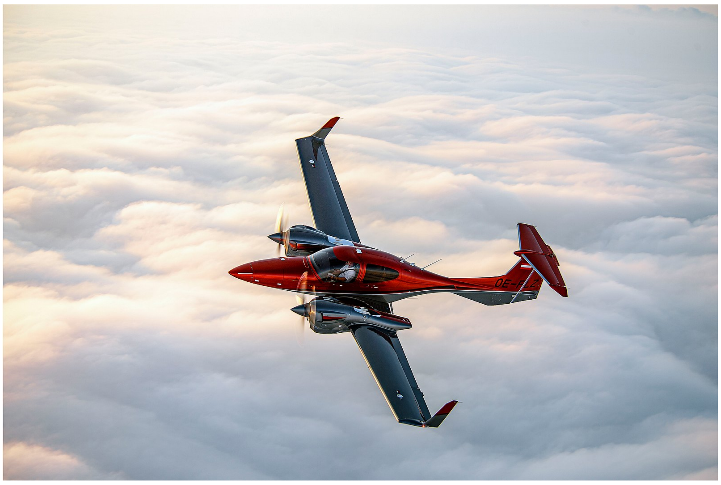

Figure 2.1: A picture of Diamond DA42 [1]

---

[1] Image Source: `https://www.diamondaircraft.com/en/private-owners/aircraft/da42/overview`

2.6. Report Outline

The report is split into three chapters corresponding to the major components of the research. Firstly, *Chapter 3* presents the information on the non-aerodynamic parts of the flight dynamics simulation to be implemented, including the mathematical model for both propeller gyroscopic procession as well as powertrain dynamics. Next, *Chapter 4* reviews the available methods for generating the aerodynamic models for the airframe and the propeller, as well as approaches to account the interaction effects between the airframe and the propeller. Subsequently, *Chapter 5* provides an overview of approaches to assess the impact of propeller gyroscopic effects on the handling qualities and controllability of the simulated aircraft model. Last but not least, *Chapter 6* provides an overview of the methodologies and plans for the research project by outlining the simulations and comparisons to be performed.

3

Flight Dynamics Modelling

3.1. Introduction

This chapter is dedicated to presenting a method of implementing a flight dynamics model for a light multi-engine aircraft that is suitable to simulate the motion of the aircraft for the intended purpose of the study, with the exception of aerodynamics-propulsion model, which would be discussed in detail in Chapter 4. A general unsteady nonlinear equation of motion for aircraft would be reviewed followed by discussions on the appropriate models for the gyroscopic effect. Subsequently, auxiliary components of the flight dynamics simulation such as powertrain response modelling and mass-estimation also being touched upon. Finally, the implementation of such models would also be discussed.

3.2. Equations of Motion for Flight Dynamics

The collective equation of motion for a typical aircraft is given in Etkin's textbook[13]. The model assumes a rigid body aircraft that is symmetric around the XZ plane and have a number of rigid spinning masses attached to it. Such rotating masses would have a fixed direction and a constant angular velocity relative to the body axes.

The translational rigid-body Euler EoM are:

$$\begin{cases} X - mg\sin\theta = m(\dot{u}^E + qw^e - rv^E) \\ Y + mg\cos\theta\sin\phi = m(\dot{v}^E + ru^E - pw^E) \\ Z + mg\cos\theta\cos\phi = m(\dot{w}^E + pv^E - qu^E) \end{cases} \tag{3.1}$$

The angular rigid-body Euler EoM are:

$$\begin{cases} L = I_x\dot{p} - I_{zx}\dot{r} + qr(I_Z - I_y) - I_{zx}pq + qh'_z - rh'_y \\ M = I_y\dot{q} + rp(I_x - Iz) + I_{zx}(p^2 - r^2) + rh'_x - ph'z \\ N = I_z\dot{r} - I_{zx}\dot{o} + pq(I_y - I_x) + (I_{zx}qr) + ph_y - qh'_x \end{cases} \tag{3.2}$$

The $\mathbf{h}'$ vector in Equation 3.2 represents the sum of angular momentum resulting from the rotating masses in the aircraft, which, as stated in the assumptions, are constant in both angular velocity and direction in relation to the body axis of the aircraft. The relevant terms are thus called gyroscopic couples[13].

3.3. Modelling of Gyroscopic Effects

Whilst Equation 3.2 of Etkin's[13] has already included the gyroscopic couples, the assumption used means that it is not suitable for the use of this study, which also concerns varying propeller speed. As such, higher-order gyroscopic effect model would be necessary for the study.

EASA's Certification Standard for Normal Category Aircraft (CS-23)[14] dictates that the aircraft structure, particularly the engine mount, must be able to withstand a certain amount of gyroscopic load due to the rotating propeller. As given in the Accepted Means of Compliance[14], for a three or more bladed propeller, the magnitude of the gyroscopic load acting through the CoG of the propeller can be calculated as:

$$F_{gyro} = I_{\mathrm{p}}\omega_1\omega_2 \tag{3.3}$$

Where I_{p} is the propeller moment of inertia around, ω_1 propeller rotation speed, and ω_2 the pitch or yaw rate of the aircraft.

Teixeira and Cesnik offered a detailed derivation for a blade-by-blade propeller inertia and gyroscopic model in [4]. In this derivation, the propeller is presented by the blades which are rigid massless rods with a concentrated point mass equalling the total blade mass at the CoG of the blade. This culminated in equation 3.4:

$$\mathbf{M}_{\mathrm{rot}} = \sum_{i=1}^{N_{\mathrm{blades}}} -m_i \left[\mathbf{p}_i \times \left(\ddot{\boldsymbol{p}}_i + 2{}^{I}\boldsymbol{\omega}^{B} \times \dot{\boldsymbol{p}}_i + {}^{I}\dot{\boldsymbol{\omega}}^{B} \times \boldsymbol{p}_i + {}^{I}\boldsymbol{\omega}^{B} \times {}^{I}\boldsymbol{\omega}^{B} \times \boldsymbol{p}_i\right)\right] \tag{3.4}$$

Where $\mathbf{p}_i$ is the position vector of the center of mass of the i-th blade, ${}^{I}\boldsymbol{\omega}^{B}$ the angular velocity vector of blade Body frame in relation to the Inertial frame, and m_i the mass of the i-th blade.

However, the goal of Teixeira and Ceinik's study[4] involves the study of gyroscopic effects on the structure of the slender, elastic, high-aspect-ratio wing of HALE aircraft. For a typical light GA aircraft, the wings are typically rigid enough such that the direction of the rotating propeller can be assumed to be *constant* relative to the aircraft frame. As such, a simpler model that only takes into account of the varying rotational velocity can be used.

For this purpose, the general expression for moment due to gyroscopic is given in Goraj and Chichoka [6]:

$$\mathbf{M}_{\mathrm{Gyro}} = \begin{bmatrix} M_x \\ M_y \\ M_z \end{bmatrix} = \frac{\partial \mathbf{L}_{\mathrm{p}}}{\partial t} + \boldsymbol{\omega}_0 \times \mathbf{L}_{\mathrm{p}} \tag{3.5}$$

Where $\mathbf{L}_{\mathrm{p}} = I \times \boldsymbol{\omega}_{\mathbf{p}}$ is the angular momentum of the propeller around its center of mass and $\boldsymbol{\omega}$ is the angular velocity vector of the aircraft.

3.4. Modelling of Powertrain

As part of the investigation is to observe the role of the torque delivery behaviors of different powertrain types on the impact of propeller gyroscopic effects on the flight dynamics of the aircraft. This section intends to present some mathematical models found in literature for modelling the three types of powertrain intended to be compared in the investigation.

3.4.1. Propeller Inertia Model

Common to all three types of powertrain is the propeller inertia model. For the purpose of this study, the propeller can be modelled as a single rotational mass with a single degree of freedom, whilst being rigidly mounted on the airframe. The engine torque (as discussed below) and the propeller aerodynamic torque loading (as discussed in Section 4.3) are assumed to the only torque source and sink acting on the rotating mass. It is also worth noting that whilst all of the following descriptions on the powertrain/torque source responses tries to identify the propeller-engine system as a whole, it would be necessary to isolate the engine part of those models during the implementation stage such that a common propeller inertia/aerodynamic model is used.

3.4.2. Electric

Pavel's research[15] provides an insight into electric motor models of suitable fidelity for the flight dynamics and control characteristics for eVTOL aircraft, which is also applicable in this research. In this case, a brushless-direct current(BLDC) motor can be assumed for the aircraft, and the finding by Hendricks et al.[16] indicate that the self-inductance within the motor is of a small magnitude and therefore can be ignored. As such, the change in electric current in the motor can be assumed to be instantaneous. Note that as constructions are similar, the behavior established here is also applicable to the AC synchronous motors with is widely used in the field of electrified aircraft.

Derived from Malpica and Withrow-Maser's analysis[17], the model for the torque response of an high-speed electric motor coupled with a rotor through a fixed-ratio reduction gearbox is:

$$(I_{\mathrm{p}}+Jr^2)\frac{d\Omega}{dt} = K_m r i_a + \tau_{\mathrm{A}} - Br^2 Q \tag{3.6}$$

Where I_{p} is the rotor/propeller inertia, J the high-speed rotating mass such as the motor and connected transmission gears, r the drive gear ratio, K_m the motor torque constant, i_a the motor armature current, τ_A the aerodynamic loading torque from the rotor/propeller, and B the linear representation of frictional losses in the drive system.

In the meantime, the simplified motor electrical circuit equation is:

$$L_a\frac{di_a}{dt} = -R_a i_a - K_e r\Omega + V_a \tag{3.7}$$

Where L_a is the armature inductance, R_a the equivalent resistance, $K_e = K_m$ the back-EMF constant, and V_a the voltage applied at the armature.

As such, assuming zero inductance based on state-of-art motors[17], the coupled response of the electrical and mechanical system is then:

$$\frac{d\Omega}{dt} = \left[-\frac{K_e^2 r^2}{R_a}\Omega + \tau_A - Br^2\Omega + \frac{K_e r}{R_a}V_a\right]\frac{1}{I_{\mathrm{p}}+Jr^2} \tag{3.8}$$

The time constant of this response is then:

$$T_c = -\frac{1}{\frac{\partial}{\partial\Omega}\left(\frac{d\Omega}{dt}\right)} = \frac{I_{\mathrm{p}}+Jr^2}{\frac{K_e^2 r^2}{R_a} - \frac{\partial Q_A}{\partial\Omega} + Br^2 - \frac{K_e r}{R_a}\frac{\partial V_a}{\partial\Omega}} \tag{3.9}$$

Whilst methods for estimating the motor parameters, such as K_e and R_a, were mentioned by Malpica and Withrow-Maser's study[17], the exact specification for a representative electric motor, the EMRAX 348, is already available[18]. This particular axial-flux permanent-magnet synchronous motor (PMSM), shown in is chosen as it has a version with similar power rating ($125kW/170hp$) as the reference aircraft's engine and it has already been used for conversion of similarly powered piston engine aircraft to electric power[19].

3.4.3. Piston

Piston engines are still very commonly utilized amongst the light GA aircraft thanks to their lower cost in the low power application. Richard's study in 1995[21] utilized knowledge on the piston engine models from automotive industry and presented a low-order, nonlinear time-dependent dynamic model of an internal combustion engine coupled with a variable-pitch propeller. The model itself is suitable for a representation of the propulsive system up to 10 Hz[21], which is also within the frequency range this flight simulation is expected to be in.

In this model, the engine is modelled macroscopically to be a supplier of torque to the propeller with the following state variables:

- Ω: Engine speed

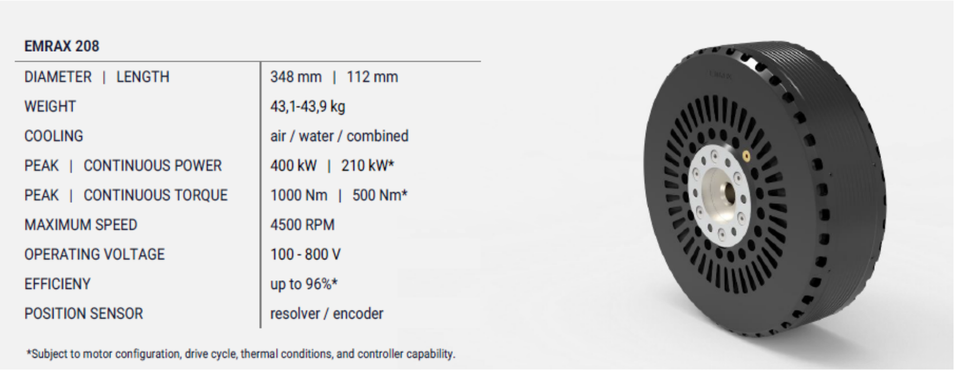

EMRAX 208

DIAMETER | LENGTH	348 mm | 112 mm
WEIGHT	43,1-43,9 kg
COOLING	air / water / combined
PEAK | CONTINUOUS POWER	400 kW | 210 kW*
PEAK | CONTINUOUS TORQUE	1000 Nm | 500 Nm*
MAXIMUM SPEED	4500 RPM
OPERATING VOLTAGE	100 - 800 V
EFFICIENY	up to 96%*
POSITION SENSOR	resolver / encoder

*Subject to motor configuration, drive cycle, thermal conditions, and controller capability.

Figure 3.1: Picture and Specification of the EMRAX 348[20] (Note that the 208 instead of 348 is an typo in the specsheet)

- Q_e: Engine torque
- p_{man}: Manifold pressure
- $\dot{m}_{man}$: Manifold air mass flow
- $\dot{m}_f$: Fuel mass flow

The model relies on a engine-specific map of the brake specific fuel consumption $BSFC$ to calculate the expected torque production:

$$Q_{e,map}(\dot{m}_f, \Omega, Q_e) = \frac{1}{\left|BSFC(\Omega, P_e)\right|} \frac{\dot{m}_f}{\Omega} \tag{3.10}$$

Due to the delay, the actual torque development is also modelled as a first-order delay:

$$\dot{Q}_e = \frac{1}{\tau_e}\left[Q_{r,map}(\dot{m}_f, \Omega, Q_e) - Q_e\right] \tag{3.11}$$

With the time constant τ_e generally being $\frac{2\pi}{\Omega}$.

3.4.4. Turboprop

Whilst purely physics-based simulations of turboprop engines were investigated in literatures such as the one documented in [22], for the purpose of this flight dynamics study, an empirical model generated using the system identification approach, such as the one by [23], could significantly reduce the amount of physical simulation required and thereby reducing the complexity of the simulation as a whole.

The experimental results indicate that approximating the engine-propeller combination as a linearly represented first-order system is accurate to around 10% of the steady-state values[23]. This can then be adapted using gain scheduling techniques to simulate the engine envelope rather than needing to perform a physics-based simulation.

The speed response of the turboprop engine with a disturbed fuel flow and propeller blade angle is:

$$\Delta\Omega = \left(\frac{\partial\Omega}{\partial\dot{m}_f}\right)_{\beta_{\text{blade}}} \left(\frac{1}{1+Ts}\right)\Delta\dot{m}_f + \left(\frac{\partial\Omega}{\partial\beta_{\text{blade}}}\right)_{\dot{m}_f} \left(\frac{1}{1+Ts}\right)\Delta\beta_{\text{blade}} \tag{3.12}$$

Where $\dot{m}_f$ is the fuel mass flow, T the time constant, Ω the propeller RPM, and β_{blade} the blade pitch.

Along with the speed, torque and other dependent variables, denoted as χ in equation 3.13, can be identified as:

$$\Delta\chi = \left(\frac{\partial\chi}{\partial\dot{m}_f}\right)_{\beta_{\text{blade}}} \left(\frac{1+aTs}{1+Ts}\right)\Delta\dot{m}_f + \left(\frac{\partial\chi}{\partial\beta_{\text{blade}}}\right)_{\dot{m}_f} \left(\frac{1+bTs}{1+Ts}\right)\Delta\beta_{\text{blade}} \tag{3.13}$$

Where the time constant T and rise ratios a and b are calculated as:

$$\begin{cases} T = \frac{I_e + I_p}{\left(\frac{\partial Q}{\partial \Omega}\right)_{\beta_\mathrm{p}} + \left(\frac{\partial Q}{\partial \Omega}\right)_{\dot{m}_f}} \\ a = 1 - \frac{\left(\frac{\partial \Omega}{\partial \dot{m}_f}\right)_{\beta_\mathrm{p}} \left(\frac{\partial \chi}{\delta \Omega}\right)_{\dot{m}_f, \beta_\mathrm{p}}}{\left(\frac{\partial \chi}{\partial \dot{m}_f}\right)_{\beta_\mathrm{p}}} \\ b = 1 - \frac{\left(\frac{\partial \Omega}{\partial \beta_\mathrm{p}}\right)_{\dot{m}_f} \left(\frac{\partial \chi}{\delta \Omega}\right)_{\dot{m}_f, \beta_\mathrm{p}}}{\left(\frac{\partial \chi}{\partial \beta_\mathrm{p}}\right)_{\dot{m}_f}} \end{cases} \tag{3.14}$$

Where I_e and I_p are the moment of inertia of the engine and propeller.

3.5. Modelling of Inertia and Moments of Inertia

To enable flight dynamics analysis for an aircraft, its mass moment of inertia(MoI), in addition to its weight, must also be obtained. As precise manufacturer data is not available to this study and estimating the MoI through flight test data and system identification method is also not viable, such values would have to be empirically estimated. As the reference aircraft is of an conventional layout, novel approaches such as the one proposed in Mutluay's thesis [24] is not required, as an empirical method such as one suggested in an US Air Force report[25] in 1979 for preliminary design flying qualities evaluation would be sufficient for the predictions in this study.

The basic equation for calculating an object with a mass of m, at a distance of R from the rotating axis, with a MoI of I_0 about its own centroid parallel to the rotating axis is:

$$I = I_0 + mR^2 \tag{3.15}$$

For a complex object consisting of many components/objects such as an aircraft, the total MoI of the object is then the simple sum of the MoI of its individual components.

With that in mind, this particular method[25] first allocates the total aircraft weight into separate groups:

1. Wing group
2. Horizontal tail group
3. Vertical tail group
4. Fuselage group
5. Propulsion group
6. Additional items

Then, the moment of inertia of each group are estimated about its own centroid, with major components such as the fuselage and the main wing modeled as shells and minor components such as landing gear, avionics and control actuators modelled as point masses. Finally, the group of inertias are translated using equation 3.15 to be about the center of gravity of the aircraft, which is what is required for flight dynamics simulation. For detailed equations and validation results, reader can refer to the text[25]. Sensitivity studies would also be done to explore how sensitive the results are to the value of MoI.

3.6. Implementation

Given the simulation fidelity and availability of resources in the faculty, two ways of implementing this flight simulation is being considered. To avoid "re-inventing the wheel", the TU Delft in-house built *PHALANX flight simulation toolbox*, as developed in-house and first introduced by Voskuijl et al. [26], is determined to be the primary choice used for the flight mechanics simulation of this experiment. It is a MATLAB/Simulink toolbox and is modular, as it combines numerous disciplines such as aerodynamics, multi-body inertia, propulsion and flight control systems. It allows for nonlinear, full six degrees-of-freedom flight simulation and also contains models for turbulence simulation. The toolbox was used for several past researches on control configurations and controllability studies such as [27] and [28]. The multi-body capability of the toolbox also allows the usage of MATLAB's built-in multi-body library for the implementation of the propeller inertia model. Being a MATLAB suite also means that it is relatively easy to extend upon given the vast amount of available libraries.

On the other hand, a second choice is implementing a new suite of flight dynamics simulation using *the Modelica Language*[29]. The language is an a-causal modelling language for physical simulations, being used widely in the automotive industry for system modelling[30]. This allows for faster implementation of physical simulations as equations can be applied verbatim as differential-algebraic equations(DAE) using the Modelica language without needing to worry about the numerical side of the implementation. A number of commercial and open-source libraries[31, 32], built for multi-body simulation and aircraft simulation, among other items, are readily available for Modelica. The language also has built-in linearization functionalities that would facilitate part of the research for the classical frequency domain handling qualities analysis. On the other hand, Modelica, along with its standard library, is still an ecosystem that is being actively developed. Because of this, there are still quite a few important utilities that are missing or only available as non-standard or commercial, proprietary implementations For example, the table interpolation tool included in the Standard Library only allows for 2 dimensions of interpolation, which is not enough for use in aerodynamic data interpolation, as 3 or more dimensions of independent variables are often required.

Finally, the possibility of using Julia[33] and its physical modelling toolbox[34] was also briefly explored. On one hand, Julia is said to be designed as a scientific language from the ground up and have performance advantage over traditional interpreted languages such as MATLAB. However, being also a language in active development, the existing libraries, such as the physical simulation toolbox mentioned above, is still lacking. Whilst acausal modelling is available just like Modelica, the said toolbox only supports modelling through pure text-based programming and does not currently have an graphical interface. Moreover, the toolbox currently does not have multi-body simulation nor any dynamics/mechanics simulation in general. Having to build such things from the ground up would post significant strain on the timeline of the research project.

In conclusion, given the availability of mature toolboxes, the PHALANX toolbox and its underlying MATLAB and Simulink framework is *tentatively chosen* as the foundation for simulations of this research project.

4

Aerodynamic Modelling

4.1. Introduction

To obtain an adequate flight simulation of the aircraft for the purpose of the study, suitable aerodynamic and propulsion models are required. As the main focus of this research is on propeller-driven aircraft, the various interaction effects between the propeller and the airframe must also be taken into account. As such, this chapter is dedicated presenting the aero-propulsive modelling part of the flight simulation.

4.2. Aircraft Aerodynamic Modelling

In this context, the aerodynamic model of an aircraft refers the model of aerodynamic forces experienced by the aircraft as a function of aircraft states such as attitude, speed, control deflections, and power settings. While there are various ways of generating an aerodynamic model for an aircraft, much consideration have to be made to balance the fidelity, cost of obtaining, and the ability to quickly manipulate the geometry. This section intends to provide a brief overview of available methods for generating aerodynamics model. The selected method is then presented and justified.

4.2.1. Overview of Approaches

Empirical Methods Empirical methods such as the one introduced by Smetana et al. [35] can be used to crudely estimate the stability derivatives of the aircraft at a very preliminary stage of the design process or when a reasonable 3D model for computational analysis is not attainable. The method uses a database approaches when it comes to estimating aerodynamic coefficients, leveraging the aerodynamic data of known shapes, such as fuselage, landing gear, empennage, etc., and combines the components' contribution. An example of which is shown in the table for various empennage drag numbers in figure

Low-Fidelity Solvers Low-fidelity aerodynamic solvers usually uses vortex-lattice method (VLM) and panel methods for surface flow solving. The former is an extension of the lifting line method, which itself is based on the Prandtl lifting line theory. The method approximates the lifting surfaces of the aircraft as a sheet of horseshoe vortices. Since no flow crosses the surface, the normal component of the induced velocity must be zero on the lifting surfaces. Thanks to the assumption on infinitely thin surface and inviscid conditions, the method is computationally inexpensive but also has low fidelity. Drela's AVL[36] being a widely used example of the former. The issue, however, is that due to the assumption of zero-thickness, the fuselage and other non-lifting surfaces cannot be represented very well in VLM solvers, with AVL providing options to only approximate non-lifting bodies as ellipsoids.

The *panel method* is a more sophisticated method that also employs the potential-flow model[37]. Compared to VLM, it takes into account the thickness of the aircraft surfaces and can have a numerical

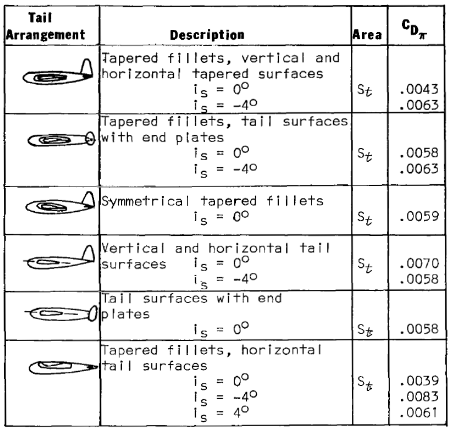

Tail Arrangement	Description	Area	C_{D_π}
	Tapered fillets, vertical and horizontal tapered surfaces $i_s = 0^\circ$ $i_s = -4^\circ$	S_t	.0043 .0063
	Tapered fillets, tail surfaces with end plates $i_s = 0^\circ$ $i_s = -4^\circ$	S_t	.0058 .0063
	Symmetrical tapered fillets $i_s = 0^\circ$	S_t	.0059
	Vertical and horizontal tail surfaces $i_s = 0^\circ$ $i_s = -4^\circ$	S_t	.0070 .0058
	Tail surfaces with end plates $i_s = 0^\circ$	S_t	.0058
	Tapered fillets, horizontal tail surfaces $i_s = 0^\circ$ $i_s = -4^\circ$ $i_s = 4^\circ$	S_t	.0039 .0083 .0061

Figure 4.1: A table for estimating the drag of various empennage shapes[35]

solution for any problem where the velocity potential satisfies the Laplace equation [38]. It can therefore also provide solutions

In Oosterom's study[39], the TU Delft-developed Q3D solver[40] was also considered. The Q3D solver extends AVL by augmenting the 3D but inviscid solution with the 2D viscid solution of airfoils of arbitrary shapes provided by XFOIL[41]. This means that along with the inviscid finite-wing lift and moment force estimation provided by AVL, the drag force of the aerodynamic configuration can also be measured at a sufficient fidelity for preliminary design iterations, thanks to the availability of XFOIL's viscid airfoil aerodynamic solutions. However, this tool, due its AVL based nature, is also only applicable for lifting surfaces, and thus is not suitable for the evaluation of the entire airframe.

High-fidelity Computational Fluid Dynamics The Reynolds-Averaged Navier-Stokes (RANS) method is a turbulence model used for computational fluid dynamic computation. It is commonly used for civil aircraft unsteady aerodynamic analysis thanks to its lower computational cost compared to more advanced methods such as LES and DNS [42], as shown in the pyramid in figure 4.2, adapted from Saguat et al. [43]. However, for the scope of this investigation, considering the number of data points required and the desire to be modular with the ability to change the aircraft mesh/geometry quickly, it is evident that high-fidelity CFD is not the suitable method due to its relatively much higher computational cost and complex mesh generation/validation process.

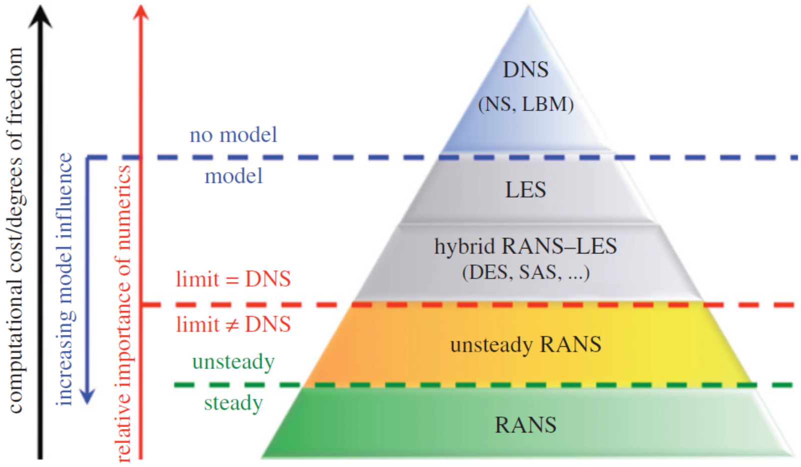

Figure 4.2: Classification of (unsteady) CFD methods based on computational cost and model influence, adapted from Saguat et al. [43]

Wind Tunnel Test / Subscale Model Test / Flight Test Scaled wind tunnel test such as [44] and real-world aircraft flight test[45, 46] were often done to establish the aerodynamic coefficients of an aircraft. In the wind tunnels, as variables such as α and β can be mostly independently controlled, a clear model can be generate by running through the set points. In the meantime, obtaining the aerodynamic model from real-world flight tests requires parameter estimations and system identifications as real-world conditions are highly complex and variables can often not be as easily independently manipulated. Moreover, as wind tunnel and flight tests require physical models to be produced, options are little when it comes to investigating the effect of different geometries.

Existing comparisons Whilst most professional flight simulators and training devices use flight test and/or wind tunnel test data, NASA conducted a study on the application of CFD data for pilot-in-the-loop simulation, especially in the domain of flight departure and aerodynamic fault tolerance study[47]. However, such data involves the highly-nonlinear region of the flight envelope and requires careful simulation setups as well as validations. It is therefore deemed to be beyond the scope of this thesis study. In other relevant literatures on flight simulation studies of rapid maneuvers and/or gust and turbulence encounters, a variety of types of aerodynamics methods were used for such purpose. Although static full-scale wind-tunnel data[48] seems like a more obvious choice, actually used datasets range from existing data that is deemed to resemble the real aircraft from subjective feedbacks[49], to FlightStream generated models[7].

As a verification study, Goraj and Chichoka, in their study on gyroscopic effects, also investigated different ways of obtaining the stability and control derivatives[6] The results of the comparison is partially shown in figure 4.3. One can see that the data from empirical methods as well as low-fidelity solvers (3D Panel Method) holds up well to the wind tunnel data

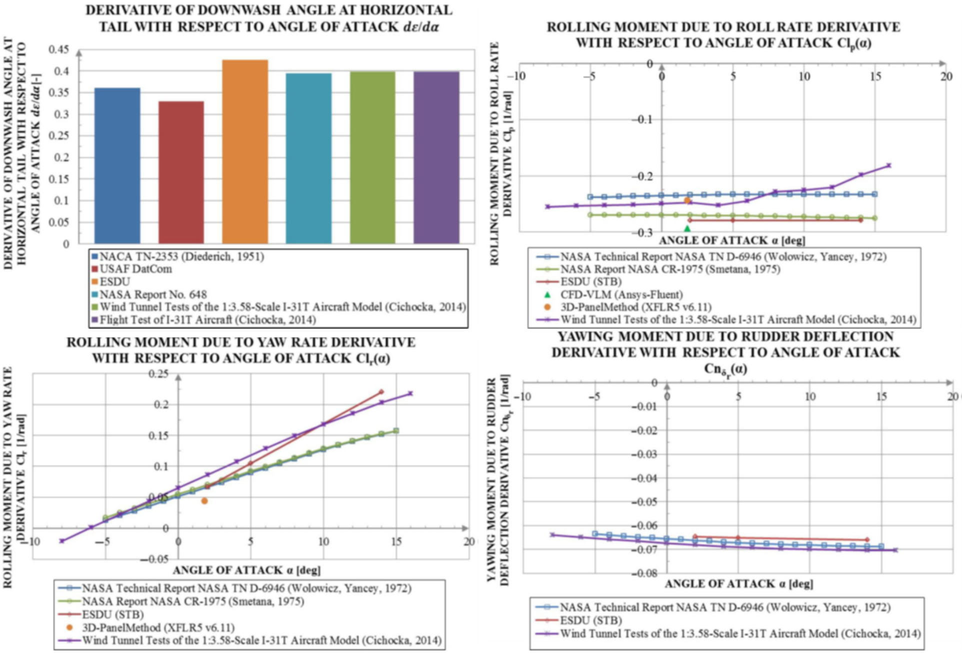

Figure 4.3: Comparison of various stability derivatives as generated by methods of different fidelity[6]

4.2.2. NASA Full-Scale Windtunnel Investigation

Thanks to the smaller sizes of light GA aircraft, real-size wind tunnel tests can be performed, as the one done by NASA in 1969[50] in the Piper PA-30 Twin Comanche aircraft, as shown in figure 4.4. The investigation includes a comprehensive study of the static longitudinal and lateral-directional stability, with the aerodynamic data obtained at a wide-sweep range of α and β and covers a large number of combinations of possible configurations, such as power settings, flap settings, contrl deflections, landing gear positions, etc. Moreover, hinge moments were also measured in the experiment, making this an optimal aerodynamic model for flight dynamics simulations.

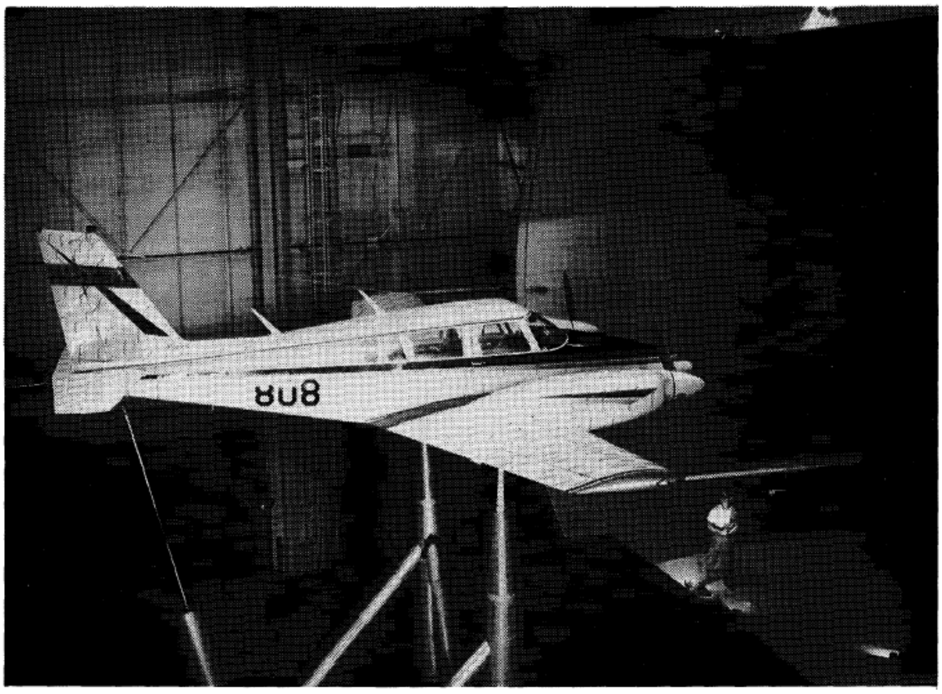

Figure 4.4: Picture of a Piper PA-30 Twin Comanche in a wind tunnel test[50]

4.2.3. Athena Vortex Lattice(AVL)

The Athena Vortex Lattice(AVL) is a vortex lattice method solver developed by Mark Drela and others at MIT[36]. Whilst lifting surfaces are approximated using infinitely thin vortex sheets, non-lifting bodies can only be approximated using ellipsoids with very limited accuracy. As such, the model would require external data sources for correction for the profile drag of the object.

The software offers a command-line based interface with a text-based input and output system. The tool has been used frequently for preliminary design studies and optimizations due to its simple text interface and fast computational speed. As such, it serves as a good example of low-fidelity aerodynamic solver that can be compared against others.

4.2.4. Selection: OpenVSP and FlightStream

Whilst the NASA model introduced in section 4.2.2 is fairly suitable for flight dynamics simulation, it lacks the flexibility that digital methods can provide, as this study also intends to investigate the effect of engine placement, size and number can have on the results. As such, the tentatively selection approach for generating the aerodynamics model is *FlightStream* is a mid-level-fidelity surface-vorticity aerodynamic solver published by Research in Flight. It allows for solving 3D geometries and includes models for skin friction and flow separation. Whilst the solver is still limited to subsonic regimes, it is more than enough for a light GA aircraft. The solver also allows the analysis for powered flight, which propellers modelled as actuator disks. For the interested readers, the algorithm used by FlightStream is presented in [51].

This solver would be coupled with the OpenVSP open-source software developed by NASA[52] for mesh generation, which is a parametric aircraft modelling and analysis software with the capability to estimate both inertial properties and aerodynamic coefficients. OpenVSP also integrates well with FlightStream by exporting the computational mesh directly to the latter. This selection is also based on the experience provided by Soikkeli's thesis[7] which also employs this aerodynamic tool stack for

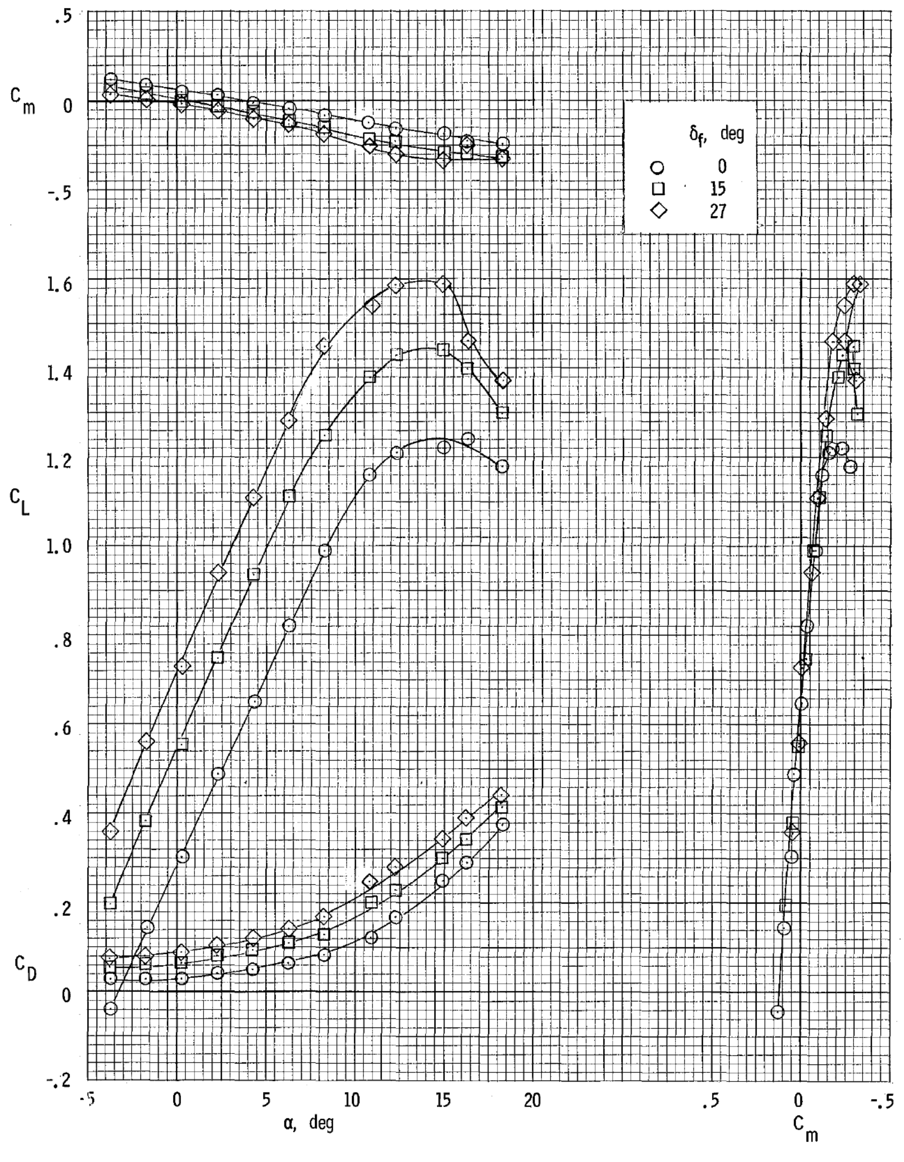

Figure 4.5: The lift coefficient vs α curve of the PA-30 with propellers removed and at several flap deflections as obtained from full-scale wind tunnel tests[50]

studying propeller thrust as a mean of directional control.

Preliminary trials of this toolchain were fairly satisfactory. Figure 4.6 shows the open-source DA-42 OpenVSP model[12] first examined in OpenVSP and then exported as a mesh to the FlightStream solver. An α and β sweep was then performed on the model with the sample results for the lift vs α curve shown in figure 4.7. The lift curve of the DA-42, obtained from a preliminary investigation on the tool, is shown in figure 4.7.

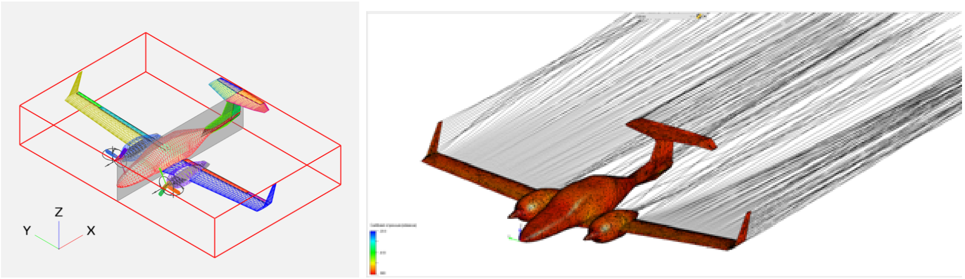

Figure 4.6: Screen Captures of the DA-42 aircraft geometry in OpenVSP(Left) and FlightStream(Right)

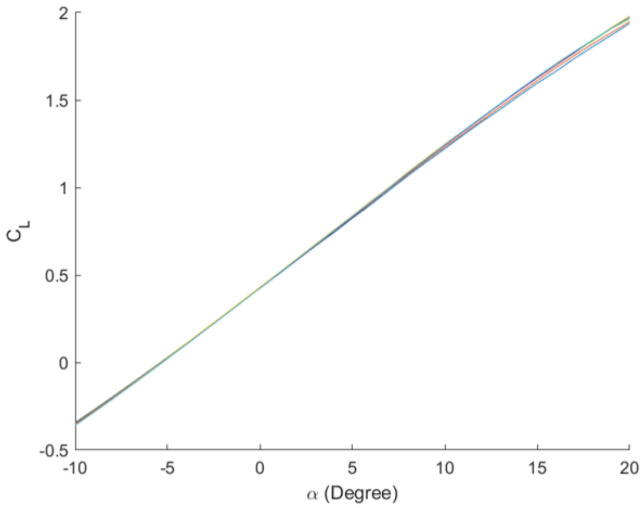

Figure 4.7: Lift vs α curve of the DA-42(propeller off) generated by FlightStream

FlightStream is a well-validated solver in general, with validation cases already provided by the developer. In his thesis, Soikkeli[7] performed a comprehensive set of validation on the FlightStream solver. Firstly, the external aero forces and moments of the unpowered, propeller-removed reference aircraft (the NASA X-57) generated by FlightStream was cross-compared with the solutions from two RANS solvers. Then, the validation of control derivatives were performed by comparing the elevator coeffients against the wind-tunnel measurement of a scaled model[53]. Finally, the aero-propulsion interaction was validated against a wind-tunnel investigation by van Arnhem et al. [54].

4.3. Propeller Performance Modelling

In simple terms, the goal of a propeller performance model is to provide value of thrust T_p and torque Q_p as a function of operating conditions such as rotational speed ω_p, inflow velocity V_∞, blade pitch angle β_p, etc. The first two parameter can also be non-dimensionalized into the advance ratio J:

$$J = \frac{V_\infty}{\omega_\mathrm{p} R} \tag{4.1}$$

4.3.1. Empirical Method

One generic and empirical method of modelling a variable-pitch propeller was provided in [55] and used as a part of the generic GA internal-combustion powertrain model proposed by [21].

$$
\begin{aligned}
T_\mathrm{p}(\beta_\mathrm{p}-\alpha,\omega_\mathrm{p},\rho,R_\mathrm{p}) &= \left[C_{L,\mathrm{p}}\cos(\beta_\mathrm{p}-\alpha)-C_{D,\mathrm{p}}\sin(\beta_\mathrm{p}-\alpha)\right]\frac{1}{2}\rho A_\mathrm{p}\left(\frac{R_\mathrm{p}\omega_\mathrm{p}}{\cos(\beta_\mathrm{p}-\alpha)}\right)^2 \\
Q_\mathrm{p}(\beta_\mathrm{p}-\alpha,\omega_\mathrm{p},\rho,R_\mathrm{p}) &= \left[C_{L,\mathrm{p}}\sin(\beta_\mathrm{p}-\alpha)+C_{D,\mathrm{p}}\cos(\beta_\mathrm{p}-\alpha)\right]\frac{1}{2}\rho A_\mathrm{p}\left(\frac{R_\mathrm{p}\omega_\mathrm{p}}{\cos(\beta_\mathrm{p}-\alpha)}\right)^2 R
\end{aligned}
\tag{4.2}
$$

Where $A_\mathrm{p} = \pi R_\mathrm{p}^2$ is the propeller disk area whilst the lift and drag coefficients ($C_{L,\mathrm{p}}$ and $C_{D,\mathrm{p}}$) are empirically determined using the following equation:

$$
\begin{cases}
C_\mathrm{L,p} = 0.1(\beta_\mathrm{p}-\alpha) \\
C_\mathrm{D,p} = 0.02(\beta_\mathrm{p}-\alpha)+0.002(\beta_\mathrm{p}-\alpha)^2
\end{cases}
\tag{4.3}
$$

4.3.2. Wind Tunnel Experiments

Wind tunnel experiments are also available as a way of determining the thrust and power coefficients of a propeller. A sample curve of propeller thrust-coefficient vs advance ratio for a typical general aviation aircraft propeller is shown in figure 4.8. Whilst this is the most accurate way of determining the performance curves for a particular propeller, there is no available data for the MTV propeller used by the reference aircraft. As a result, wind tunnel results can only serve more secondary rules such as being used to validate the computational results.

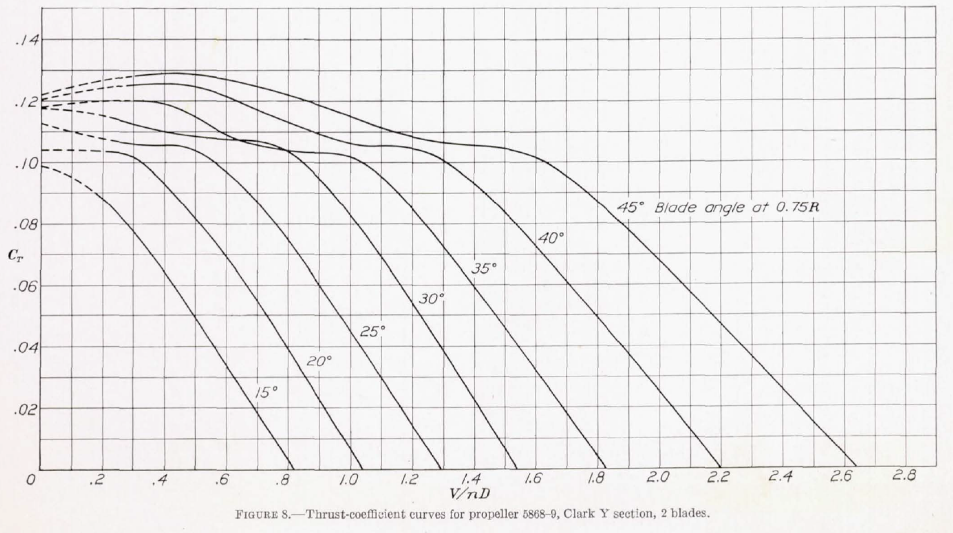

FIGURE 8.—Thrust-coefficient curves for propeller 5868-9, Clark Y section, 2 blades.

Figure 4.8: An example of propeller thrust-coefficient vs advance ratio curve for a 2-bladed propeller[56]

4.3.3. Computational Tools

In the meantime, both high and low fidelity computational/numerical solvers are available for generating the propeller performance maps. In his thesis on parametric propeller optimization, Klein[57] reviewed both high-fidelity propeller performance analysis using CFD as well as low-fidelity propeller performance solvers such as JavaProp and XROTOR.

JavaProp JavaProp is a low-fidelity propeller analysis tool by Martin Hepperle[58], written in Java. It allows for both the design and analysis of propellers and windmills and is based on the blade element theory, where the propeller blades are divided into individual small sections and handled independently.

Each sections are then analyzed independently like a small piece of wing with a chord, blade angle (analogous to angle of attack), and associated airfoil characteristics, which can be customized. The resultant forces from each sections are then summed together to result in the overall thrust and torque of the propeller. As the overall forces and torque are a simple summation of that of the spanwise sections, *no three-dimensional effects* such as sweep angle and cross-flow effects. However, the lack of three-dimensional effects is deemed to be acceptable for most aircraft propellers thanks to their relatively low thrust and power loading.

While simplistic, the program features only a limited set of airfoil and does not allow the possibility of custom airfoil polar. The program offers a native Java programming API along with MATlAB and Python bindings, allowing automation and an easy interface with the MATLAB/Simulink toolchain. A full graphical interface is also available.

XROTOR XROTOR is another low-fidelity propeller analysis and design tool developed by Drela et al.[59] at MIT, written in FORTRAN. It uses the same underlying theoretical foundation as QPROP and QMIL[60], its sister program: an extension of blade-element/vortex formulation through radially-varying self–induction velocity, enforced consistency between the analysis and design formulations, as well as a global Newton method for the overall system solution. Interested readers can refer to [60] for detailed formulation for the theoretical foundations of the program. Similar to AVL and as opposed to JavaProp, XROTOR employs a command line interface and text-based input and output methods. XROTOR allows the utilization of custom airfoil through the coupling with XFOIL[41], a 2D airfoil analysis tool also by Drela.

JavaProp vs XROTOR In the detailed comparison between XROTOR and JavaProp against high-fidelity CFD offered by Klein[57], the accuracy of JavaProp is much worse than XROTOR, crossing from over-estimation to under-estimation as the blade angle of a reference propeller increases. This could be due to the simplicity of the underlying theory used by JavaProp. On the other hand, whilst XROTOR has better accuracy overall, it still tends to over-predict the performance at high-load regions and vice versa for every blade angle, albeit to a more acceptable level. The inherent limitation of using only a low-fidelity solver should therefore be kept in mind. As a result, *XROTOR* is a more suitable tool for generating the desired propeller performance.

It is worth noting that both tools does not support the adjustment of inflows angle for the performance analysis. However, researches[61, 62] has shown that the an off-center inflow angle towards a propeller, which could be caused by both the angle of attack and sideslip of the aircraft, does not significantly contribute in any changes in propeller thrust and power coefficients within the range of α and β of normal flight regimes.

High-fidelity CFD Whilst CFD methods allows for higher fidelity, the accuracy relies heavily on the grid size of the CFD mesh[62], which means an exponentially increasing computational resource requirement. Considering the overall intended aerodynamic model fidelity is pegged at mid-level with the utilization of FlightStream, the extra accuracy brought by high-fidelity RANS CFD on the propulsion model alone is not necessary.

4.4. Propeller-Airframe Interaction Effects Modelling

Besides the gyroscopic procession effect, aircraft propellers interact in additional ways such as the slipstream, P-factor, as well as asymmetric thrust at increased AoA. As such, means must be introduced to account for such interaction effects.

FlightStream FlightStream is able to investigate propeller-fuselage interaction effect by modelling the propeller as an actuator disk, with results validated by Soikkeli[7] in his thesis by building a representative model in FlightStream and comparing the simulation results with the wind tunnel experiment results by van Arnhem et al.[54].

Schroijen and Slinglerland Method On the other hand, Propeller slipstream model by Schroijen and Slingerland[63] takes a more theoretical approach by combining various models on propeller, slipstream, lifting surfaces, fuselage, and empennage models to provide a fast prediction of the impact of propeller slipstream on aircraft stability derivatives using a small amount of available geometric data for the purpose of preliminary design and sizing. A brief description of the method is given below and interested readers can refer to [63] for the detailed theoretical description.

The induced axial velocity a and swirl a' are calculating using the propeller vortex theory, and the wing model is based on the Prandtl lifting line theory by the means of a horseshow vortex on the quarter chord and a collocation point at 3/4 chord position. The trailing vortices are then mirrored in the fuselage to include its effect. The fuselage blockage upwash is then included using the Multhopp's method[64]. The engine nacelle induced yaw moment is calculated again by translating it into an equivalent vortex.

Then, the wing trailing vortex sheet is calculated from the effect of wing trailing vortex sheet itself, propeller slipstream, and the mirror vortices that represent the fuselage using a time stepping method. The empennage, being similar to the wing model, has a corrected ”freestream velocity” based on the freestream velocity as well as induced velocity from propeller, fuselage, and wing trailing vortex sheet.

Propeller slipstream contributes to roll moment as well as yaw moment. The slipstream shearing over the wing is modelled by two concentric slipstream surfaces, which are then divided into panels of constant strength. The induced speed can then be calculated from slipstream surface itself, wing and wing trailing vortex sheet, as well as the fuselage. In the meantime, control surfaces can be modelled by including a secondary horseshoe vortex at the control surface's quarter chord. Through this way, the lift increment can be approximated by a lumped vortex model. Finally, the non-zero side force on the fuselage during OEI conditions can be approximated from the pressure distribution by assuming that propeller slipstream does not coincide with the fuselage itself.

The model was validated against wind tunnel data as well as flight test data. Whilst the validation against wind tunnel data shows some good correlations when the propeller slipstream shearing feature is turned off, the comparison against flight test data showed some inconsistency between the prediction for outboard and inboard engine. As a result, this method is deemed to be a less preferred method over the direct simulation provided by FlightStream as a way of generating propeller-airframe interaction effects.

4.5. Validation and Verification

Due to the lack of publicly available wind tunnel data and flight test data of the DA-42 aircraft, alternative means of validating and verifying the computationally generated aerodynamics would have to be devised.

Due to its comprehensiveness, the results of the windtunnel investigation by NASA[50] as previously introduced in can be used to both validate the bare-airframe aerodynamics model as well as the interaction effect between the propeller and the airframe.

The aero-propulsive performance of the computationally generated model can be further verified by recreating the steady-state flight conditions for which performance numbers are available in the AFM, such as all-engine climbing, cruising, and OEI climbing.

Last but not least, a comparison study between the aerodynamic models generated from FlightStream and from the lower fidelity AVL[36] will be done to grant an insight into the sensitivity of the simulation outcome to the fidelity of aerodynamic modelling.

5

Handling Qualities and Stability

5.1. Introduction

With the flight simulation model established in place, analysis can then be done to investigate how propeller gyroscopic effects can affect the handling qualities and the motion of a light twin-engine aircraft. Taking inspiration from Goraj and Chichoka's work[65] which distinguishes between weak and gyroscopic effect, the analysis methods discussed in this chapter would also be divided into frequency domain analysis in section 5.2 as well as time domain simulation in section 5.3.

It is important to note here that Cooper and Harper had defined *handling qualities* in their 1969 NASA report as ”those qualities or characteristics of an aircraft that govern the ease and precision with which a pilot is able to perform the tasks required in support of an aircraft role.” [66] This means that the so-called handling qualities are subjective evaluations in nature. In the meantime, *flying qualities* refer to ”objective metrics based on aircraft response and dynamic parameters”[67]. In the context of this research, however, the terms *”handling qualities”* and *”flying qualities”* will be used interchangeably to convey the meaning of the latter.

5.2. Classic Handling Quality Analysis

As civilian airworthiness standards such as the CS-23 [14] does not define any quantitative standards for handling quality of an aircraft, the military standard MIL-F-8785C[68] is widely adapted as the *de facto* standard for handling assessment of civil aviation as well. Within the scope of this standard, light twin-engine aircraft are categorized as *Class I* aircraft which include light utility and primary trainer aircraft. In the meantime, the flight phases that are applicable to the aircraft in question are *phase B*, the nonterminal flight phases that are accomplished using gradual maneuvers such as climbing, cruising, descent, etc., as well as *phase C* which is the terminal flight phases that require gradual maneuver and accurate flight-path tracking, such as take-off, approach, and landing. The specified requirements for a Class I aircraft in phase B and C are summarized in Table 5.1.

It is expected that the aircraft numerical simulation would be linearized at numerous points within the flight envelope of the aircraft, and the eigen modes at those points would be compared to see if handling qualities has deteriorated due to the presence of propeller gyroscopic precession.

5.3. Time-domain Handling Quality Analysis

5.3.1. Certification Standards and Test Flight Maneuvers

As discovered by Goraj and Chichoka[6], the maneuvers that most excites the gyroscopic effect are the pitch and yaw ”pull-up” maneuvers. For this study, such study can be performed with both engine operative, one-engine-inoperative, as well as with one or two engine changing speed as a result of

Table 5.1: Level 1 Flying Quality Requirements for Class I Aircraft, as Summarized from MIL-8785-C[68]

Test Case	Flight Phase	Level 1 Requirements
	Longitudinal	
Short Period Mode Frequency	B	Figure 5.1
	C	Figure 5.1
Short Period Mode Damping Ratio	B	$0.30 \leq \zeta_s \leq 2.00$
	C	$0.50 \leq \zeta_s \leq 1.30$
Phugoid Mode Damping Ratio	All	$\zeta_p \geq 0.04$
	Lateral-Directional	
Roll Mode Time Constant	B	$T_r < 1.0s$
	C	$T_r < 1.0s$
Spiral Mode Time Constant	B	$T_2 < 20s$
	C	$T_2 < 12s$
Dutch Roll Mode	B	$\zeta_d \leq 0.08, \zeta_d\omega_d \leq 0.15, \omega_d \leq 1.0$
	C	$\zeta_d \leq 0.08, \zeta_d\omega_d \leq 0.15, \omega_d \leq 0.5$

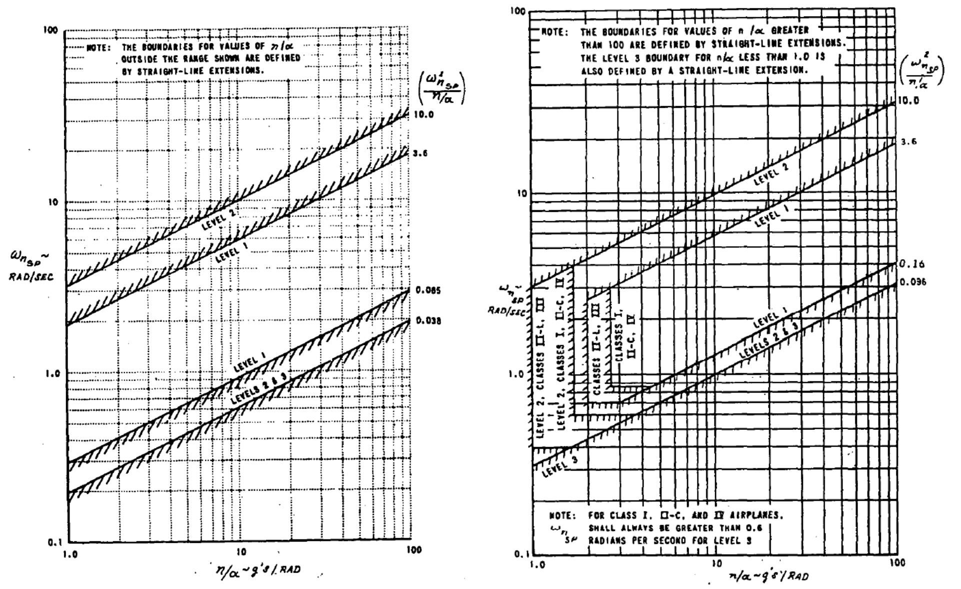

Figure 5.1: MIL-F-8785C[68] Short-period frequency requirement for Category B(left) and C(right) flight phases

failure or power demand from the pilot.

On the other hand, inspirations can be drawn from the required flight test demonstrations as listed in the certification standard[14]. CS23.147(b) dictates that the aircraft must remain controllable after a sudden engine failure. For an aircraft to be certified, controllability during the en-route climb phase after an sudden engine failure must be demonstrated in flight tests. The maneuver shall be performed as follows[14]:

> In complying with the testing required by 23.147(b), from an initial climb condition of straight flight with wings level, zero sideslip and in trim simulate a sudden and complete failure of the critical engine. In order to allow for an appropriate delay no action should be taken to recover the aeroplane for two seconds following first indication of engine failure. The recovery action should not involve movement of the engine, propeller or trimming controls.
>
> At no time until the completion of the manoeuvre should the bank angle exceed 45° or excessive yaw be developed. The evaluation of dangerous attitudes and characteristics should be based on each particular aeroplane characteristics and the flight test pilots evaluation.
>
> The method used to simulate engine failure should be:
>
> 1. for a reciprocating engine, closure of the mixture control; or
> 2. for a turbine engine, termination of the fuel supply by the means which results in the fastest loss of engine power or thrust. Engine shut-off procedures would normally be sufficient.

The different failure modes of the powertrain could also be worth exploring, as an engine slowly winding down due to fuel system issues could cause a different impact on flight dynamics than a powertrain that suddenly seizes due to a mechanical issue.

In the meantime, other dynamic stability testing maneuvers, such as doublet and pulse input for longitudinal short-period and phugoid behavior, as well as rudder pulsing for exciting the Dutch roll modes. For more in-depth description, readers can refer to the flight test guide section of the CS-23 standard[14].

5.3.2. Other Representative Maneuvers

Other maneuvers can also be performed for evaluating the handling qualities of a light-twin aircraft during an engine failure. Particularly, the take-off and initial climbing maneuver, as well as the approach and landing phase of the flight, is where light GA airplanes are most vulnerable to OEI-related accidents due to the low airspeed and the resulting low vertical fin effectiveness.

The NASA study on piloted simulation for the evaluation of an automatic trimming system for OEI conditions[48], for example, used the following maneuvers:

1. A take-off and initial climb maneuver with a sudden engine failure at 200ft above ground level, with some artificial delays for pilot action to simulate the initial confusion
2. An approach and landing maneuver with one engine already failed and secured (i.e. feathered), and with two abrupt power changes to simulate a misjudged approach (first a power chop due to being higher than expected then a sudden power increase to correct the higher than expected sink rate)

Both are equally applicable to the purpose of this research as they both contains sudden and asymmetric thrust changes and thereby elicits abrupt attitude change commensurate with the aforementioned rapid maneuvers.

5.4. Modelling of Pilot

Lone and Cooke[69], amongst other literature reviews on this subject[70, 71] provided a good overview of the pilot models, split into three categories:

- *Control-theoretic*, which as the name suggests models the pilot as a classical controller
- *Bio-mechanical*, which models the pilot from a physiological perspective such as taking into account kinesthetic cues, muscle movement rates and other biodynamics parameters
- *Sensory*, which models vision and other senses of the pilot

The complete breakdown of components in the pilot-vehicle system is shown in figure 5.2. Given the scope of this study, focus would only be placed on the control-theoretic model, which is still being used for the purposes of understanding aircraft handling qualities and aircraft-pilot coupling behaviors[70].

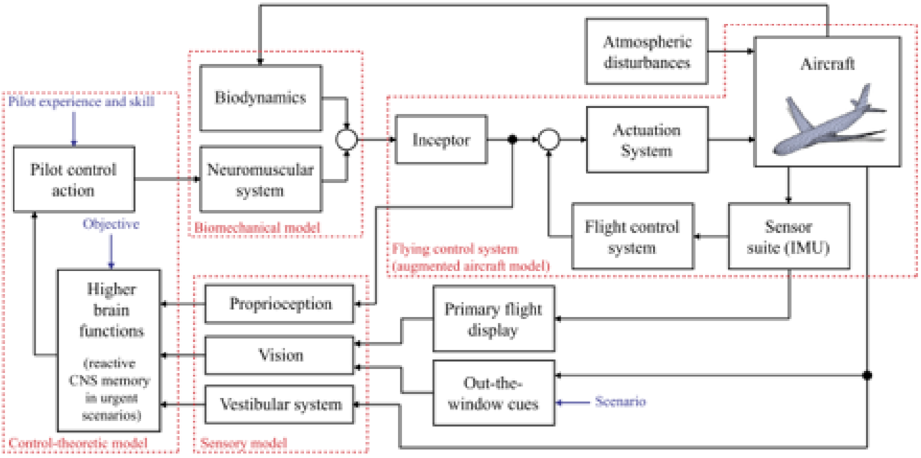
Atmospheric disturbances
Aircraft
Pilot experience and skill
Biodynamics
Pilot control action
Neuromuscular system
Inceptor
Actuation System
Objective
Biomechanical model
Flying control system (augmented aircraft model)
Flight control system
Sensor suite (IMU)
Higher brain functions
(reactive CNS memory in urgent scenarios)
Proprioception
Primary flight display
Vision
Out-the-window cues
Scenario
Vestibular system
Control-theoretic model
Sensory model

Figure 5.2: A block diagram of pilot-vehicle system under manual control[69]

For control theoretic models, two major types are available: quasi-linear model and optimal control models. The optimal control model are mainly used for detailed time delayed effect studies, such as the human factor investigation of flight instrument displays and crew workload[69]. As such, only quasi-linear model, being an mature and established model, is reviewed here as the selected model for the research.

Quasi-linear Model The quasi-linear model is first introduced by McRuer[72]. A block diagram of this model is shown in figure 5.3.

It is a crossover model which proposes that human pilot will provide lead or lag compensation, with an associated penalty. This means that the combined pilot-aircraft transfer function is proportional to an integrator at the crossover frequencyω_c with a time delay τ_e[72]. The said model is in the form:

$$Y_p Y_c(j\omega) = \frac{\omega_c e^{-\tau_e j\omega}}{j\omega} \tag{5.1}$$

Where Y_c is the describing function of the aircraft and Y_p the describing function of the pilot, typically in the form:

$$Y_p(s) = K_p \frac{T_L(j\omega) + 1}{T_l(j\omega) + 1} e^{-j\omega\tau} \tag{5.2}$$

Where K_p is the pilot's gain, T_L and T_l the lead and lag time constant, and τ the pilot's physical reaction time delay. One can select the parameters using the adjustment rules as reviewed in [72].

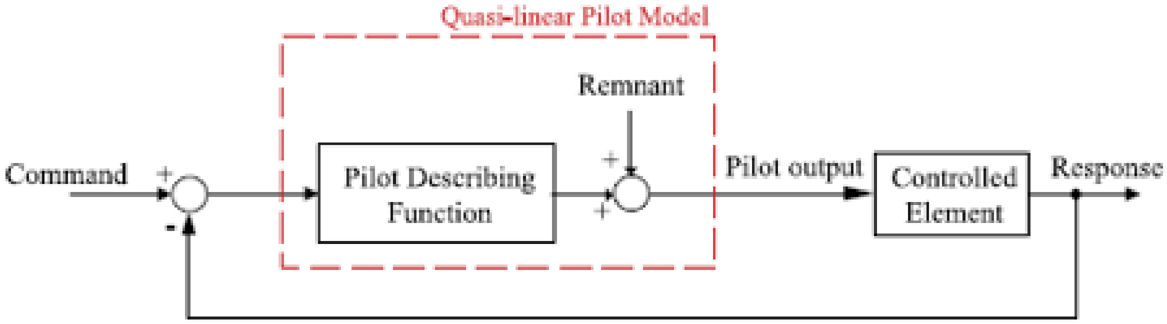
Quasi-linear Pilot Model
Remnant
Command
+
-
Pilot Describing Function
+
+
Pilot output
Controlled Element
Response

Fig. 14. Quasi-linear pilot model.

Figure 5.3: A block diagram overview of the quasi-linear pilot model[72], as adapted from Lone and Cooke[69]

6

Methodology

6.1. Introduction

This section intends to summarize the previously presented options of each components that will constitute the flight simulation study and indicate the tentative choices. It then provides a preliminary plan of simulations and validations to be perform for each parts of the study in order to answer the research questions.

6.2. Experiment Setup Overview

An overview of the tentative experimental setup is shown in figure 6.1, with the colors used for identifying the type of the components, such as input/output, off-the-shelf tools, and programs to be implemented.

It is worth noting that, as previously mentioned, while some of the components has already been chosen, some other ones are still undecided, such as the propeller analysis tools (JavaProp or XROTOR), as well as the flight simulation toolset (PHALANX, Julia, or Modelica).

6.3. Aerodynamic, Propulsion, and Inertia Model Generation

The aerodynamic, propulsion, and inertia model of the aircraft would be generated in the methodologies mentioned in chapter 4 and chapter 3, namely in the following sequence:

1. The aircraft parameter (primarily the engine placement) is inputted
2. The propeller performance model is generated through XROTOR
3. A parametrically mesh of the aircraft is generated through OpenVSP
4. The mesh is solved in FlightStream in through sweeping through the α and β as well as control surface deflections
5. The inertia model is also generated using the empirical method described in 3.5
6. The aero-propulsive model is then blended using either the FlightStream analysis or the method described in

6.4. Baseline Configuration

As comparison studies will be performed, it is essential at this point of the discussion that a baseline configuration of the aircraft simulation to be studied is established. Within the context of this research, the *baseline configuration* or *baseline simulation* refers to:

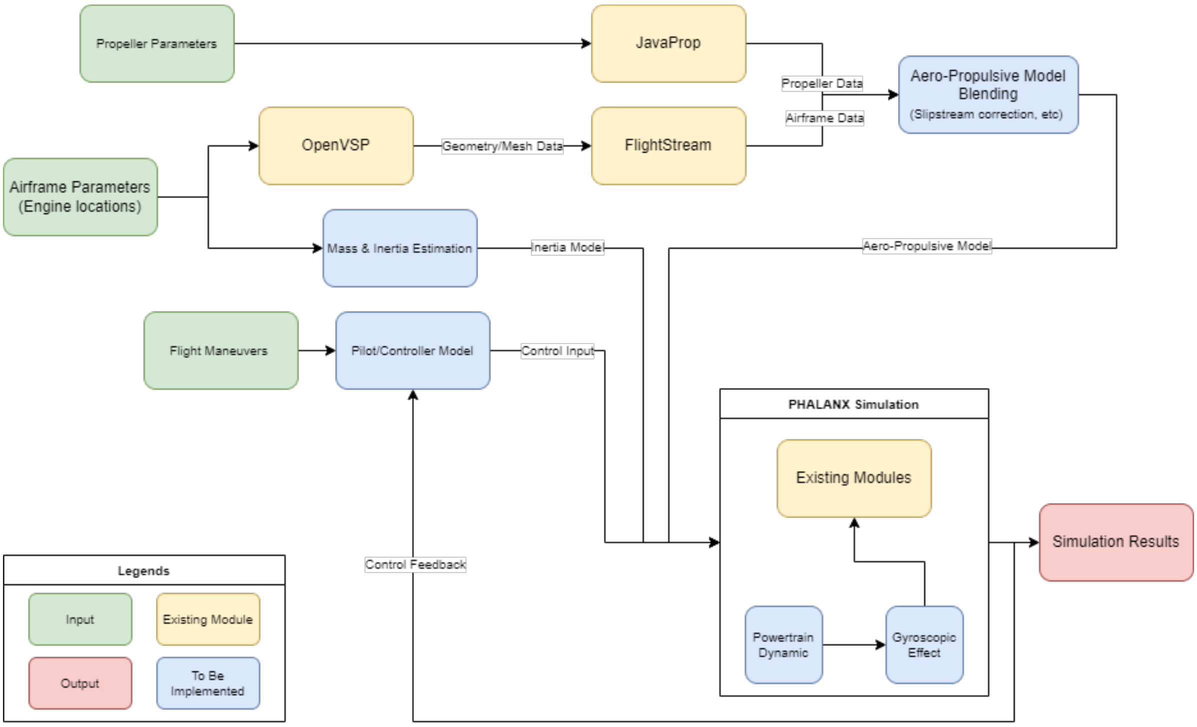
Propeller Parameters
JavaProp
Propeller Data
Airframe Data
Aero-Propulsive Model Blending
(Slipstream correction, etc)
OpenVSP
Geometry/Mesh Data
FlightStream
Airframe Parameters
(Engine locations)
Mass & Inertia Estimation
Inertia Model
Aero-Propulsive Model
Flight Maneuvers
Pilot/Controller Model
Control Input
PHALANX Simulation
Existing Modules
Simulation Results
Control Feedback
Powertrain Dynamic
Gyroscopic Effect
Legends
Input
Existing Module
Output
To Be Implemented

Figure 6.1: Tentative Flowchart of the Experimental Setup, with colored blocks indicating the origins of each components

- An FlightStream-generated aerodynamic model of the stock DA-42 aircraft as depicted in the open-source OpenVSP model[12]
- An piston engine model that is tuned to the best ability to replicate the performance of the AE300 engine used by DA-42
- A propeller model that is designed using XROTOR to be designed at the maximum cruising power settings (power and RPM) of the DA-42, since a reasonably accurate 3D model of the MTV propeller is not publicly available.

6.5. Validation and Verification Studies

In order to proceed with the research activity, validation and verification studies have to performed to establish the validity of the study. For this research, validation and verification activities would be focused on the implementation of the gyroscopic effect as well as the accuracy of the aerodynamic and propulsion model.

6.5.1. Flight Dynamics Model Validation

The general behavior of the aircraft simulation with and without gyroscopic effect would also be observed and compared against existing literature such as [6] and [5] to confirm that the flight dynamics model is exhibiting the correct gyroscopic cross-coupling behavior. This can be done by using performing the same all-engine-operative rapid maneuvers in Goraj and Chichoka's experiment[6]: pitch and yaw pull-up maneuvers, using the baseline simulation.

6.5.2. Aerodynamic and Propulsion Model Validation

The accuracy of the aerodynamic model generated by FlightStream would require validation against existing data. In this study, this can be done by recreating a parametric model of the PA-30 Twin Comanche aircraft and comparing the FlightStream solution of this model against the wind tunnel investigation results mentioned in subsection 4.2.2[50].

The propulsion model generated by the low-fidelity computational tools such as JavaProp and XROTOR would be first validated against wind tunnel experiments such as the NASA experiment[73].

Additionally, the propeller-interaction effects generated by the solvers can also be validated using the same set of wind-tunnel data as mentioned in subsection 4.2.2[50] by using the comparison between prop-off data and propeller-on data.

The combined aerodynamic and propulsion data would be further verified by performing maneuvers on the baseline simulation against numbers as listed in the performance tables in the AFM of the aircraft[10]. A non-exhaustive list of validation maneuvers that can be performed is shown in table 6.1.

Table 6.1: Summary of Flight Performance Validation from the AFM[10]

Item	Power L/R	Flaps	Gear	IAS	Altitude	To Observe	AFM Section
All Engine Climb	92%/92%	UP	UP	92kt	0ft	Climb rate	5.3.7
	92%/92%	APP	UP	85kt	0ft	Climb rate	5.3.7
OEI Climb	Feathered/92%[1]	UP	UP	85kt	0ft	Climb rate	5.3.8
Level Cruise	92%/92% 75%/75% 60%/60% 35%/35%	UP	UP	N/A	2000ft	TAS	5.3.10

6.6. Main Test

The main test matrix involves first performing the classical modal analysis with the *baseline simulation*, as outlined in section 5.2. The eigenvalue analysis of the system would be performed for aircraft model linearized across different flight conditions, such as climbing, cruising, and approach. The outcome of the eigenvalue analysis for both simulation with and without gyroscopic effects would then be compared as well as time-domain-simulated rapid maneuvers, both all-engine-operating and one-engine-inoperative, as outlined in section 5.3. The aforementioned tests would be performed with the aircraft being flown by a pseudo-autopilot controller that is setup to mimic the response of a typical pilot, as described in section 5.4 and maintain a required flight path. Artificial delay such as the one used in [48] to simulate initial confusion can also be implemented to further enhance the fidelity of the simulation. The tracking performance of the controller such as rise time, peak overshoot, as well as peak deflection, could then be used as parameters to be compared between the different cases.

6.7. Comparison Studies

The following comparison studies are to be done for the purpose of this research:

1. *Comparison between Different Types of Powertrain Responses*: compare the simulation results from using three different types of typical propeller prime movers (piston, turboprop, and electric) of the same maneuvers as those types of engine each have distinct torque responses to power commands

2. *Comparison between Aerodynamic Model Fidelity*: compare the results of using different aerodynamic fidelity levels: wind tunnel, FlightStream, AVL

3. *Comparison between Varying Spanwise Engine Position on the Wing*: compare the results of using variations of the reference aircraft with engine placed at different locations along the span of the wing

On the other hand, the following comparison studies can optionally be performed to enhance the understanding of the topic, ranked in the matter of priority:

1. *Comparison between Different Numbers of Engines*: study the effect of dividing the engine into smaller devices with the same amount of total power, as this would grant some more insight into the impact of distributed propulsion on light aircraft flight dynamics
2. *Comparison between Fixed-Pitch Propeller and Constant-Speed Propellers*: although almost all multi-engine airplanes use constant-speed propellers due to the need to feather propellers after engine failure, it would be interesting to see how gyroscopic precession plays its role when the constant-speed assumption is no longer valid

The specific maneuvers to be performed for the comparison studies above would be chosen based on the results of the main test, specifically the ones that exhibit the most prominent evidence of gyroscopic procession coupling.

7

Conclusion

The increased probability of a fatal accident caused by the failure of an engine of a multi-engine light aircraft, as compared with a single-engine one, can be attributed to the handling difficulty introduced by the asymmetric situation. A substantial part of a multi-engine aircraft's sizing and design is therefore dedicated to addressing this situation. In the meantime, aircraft propellers, being fast rotating masses, exert gyroscopic precession effect on the aircraft in flight, especially during rapid maneuvering. As a sudden engine loss on one side of a multi-engined aircraft resembles rapid maneuvering, with pilot having to quickly regain the flight path of the aircraft, it would be worthwhile to explore the role propeller gyroscopic effect could play on the handling qualities of the aircraft during such a scenario.

A literature review on the topic of investigating the effect of propeller gyroscopic effect on the flight dynamics of light multi-engine General Aviation aircraft was therefore conducted and the results was presented in this report.

The equation of motion for a rigid aircraft along with a simplified 1DoF propeller procession model was first presented as the basis of the study. The torque/speed response models of the three types of propeller powertrain (electric, piston, and turbine) are then introduced for the study of the effects different powertrain types can have on the prominence of gyroscopic procession. An inertia estimation model for preliminary design evaluation was then introduced as a way to obtain the inertial properties of the aircraft. Then, the choice of two simulation platforms, PHALANX (through MATLAB/Simulink) and Modelica, were presented as two potential ways to implement the simulation.

Next, the method for obtaining aero-propulsive model of the aircraft was then discussed, with the combination FlightStream and OpenVSP being chosen based on previous experiences in the faculty. Whilst the advantage of the former is its mid-level fidelity that combines computational speed with suitable accuracy as well as the ability to investigate propeller interaction effects, the latter possess parametric capabilities, a good open-source library of aircraft models, as well as a good interface with the former. Several propeller performance models were also presented with XPROP and JavaProp being the prime choice for proceeding, again thanks to their good combination of fidelity and computational efficiency. Along with the FlightStream's aforementioned ability to investigate propeller-airframe interaction effects, analytical methods were also presented as an alternative way of modelling such effects.

Consequently, methodologies for evaluating the effects of gyroscopic procession on handling qualities of the aircraft was presented, both with the classical frequency domain evaluations as well as time-domain simulations of rapid maneuvers. A series of maneuvers, drawn from both the Certification Standard's Accepted Means of Compliance as well as typical One-Engine-Inoperative procedures, was then discussed. To aid in the performance of such maneuvers, a control-theoretic model was presented as a human-aircraft interaction model.

Last but not least, the setup of the study as well as the brief overview of the experiments and comparisons to be performed were also provided. Methodologies for generating the relevant models as well as methods of validation, if required, is also proposed.

In summary, the aim of this research is to grant additional insight on the role propeller gyroscopic effects play on the handling qualities by extending the existing flight simulation study on single-engine propeller aircraft to multi-engine aircraft. Being able to quantify such effects using flight simulations as well as computationally generated aerodynamic and propulsive models allows the adverse and proverse aspects of the gyroscopic procession to be evaluated early in the design process and thus allows for more precise sizing in during the preliminary design phases.

IV

Conclusions, Recommendations and Appendices

8

Conclusions and Recommendations

8.1. Conclusion

In conclusion, this research has presented an investigation on the impact of propeller gyroscopic effects on the handling qualities of a twin-engine light general aviation aircraft. Traditional handling qualities assessments using modal analysis as well as time simulation of rapid maneuvers were performed using an augmented flight mechanics simulation suite which incorporates a multi-body physics based simulation of propeller gyroscopic phenomena, a non-linear wind tunnel aerodynamic model, and propeller-governor-engine dynamics.

The answer to research (sub-)questions are presented as follows:

- *What are the relevant parameters that can be used to quantify the impact of the gyroscopic effect on the flying qualities?*

  Traditional modal analysis shows very little difference between the linearized models with and without the presence of gyroscopic effects. This is because the linearized models are obtained based on small flight parameter perturbations whereas the gyroscopic effect is nonlinear in nature and only manifest itself at considerable rotation rates. Peculiarity in the trend of modes vs airspeed is the same for all amplitudes of propeller angular momentum, and therefore is more likely due to the non-linear aerodynamics model.

  Next, open-loop simulations of various flight maneuvers at different flight phases shows that rapid pitch and yaw maneuvers does excite a coupled reaction of the yaw and pitch axis, respectively, as evident from the time history of the angles of attack and sideslip angles. The stronger the angular rate that the maneuver generates, the larger the induced response from the excited axis is. As such, the impact of gyroscopic effect in the short-term aircraft motions can be measured well by the initial α and β excursions.

  The phugoid motion was also evidently affected by the presence of gyroscopic effect, though the question of which maneuver(s) are more significantly affected by the gyroscopic moments remains inconclusive when measured by minimum airspeed and altitude reached. This is because the open-loop nature of the simulation and the non-linear aerodynamics model means that undesired roll motion is also introduced, which further restricts the ability to draw more conclusions from the flight trajectory.

  Maneuvers performed with a simple wing leveling controller allows a slightly better insight into the long-term motion. With the aileron in closed-loop control, the pure pitch input cases such as elevator impulses no longer show any deviation in phugoid path with strong GE. On the other hand, the yaw-input cases show phugoid motion modified in the presence of strong GE. In this case, the long-term impact of gyroscopic effect can be observed by the max deviation from the non-GE cases in airspeed and altitude for the duration of the simulation, where the maneuvers with the largest magnitude of difference are all high-rate yaw maneuvers.

- During which maneuvers is the effect of propeller gyroscopic procession more prominent?

  As mentioned above, pitch-dominant maneuvers showed prominent coupling yaw moments whereas yaw-dominant maneuvers showed noticeable pitch variations as well. The exact degree to which the maneuvers of gyroscopic moment on the excited axis is highly dependent on the rotation rate of the exciting axis.

- How do different powertrain torque responses impact the results?

  The comparison between different powertrain lag shows that in an sudden one-engine-failure situation, the powertrain lag plays almost no role in the short-term motion of the aircraft and also very little role in the long-term phugoid motion. On the other hand, during a dual engine go around, the powertrain lag plays a major role in changing the phugoid mode as well as the short term dynamics, mainly through reducing the initial peak alpha value.

- How sensitive is the result of this study to the unsteady aerodynamic derivatives?

  The sensitivity study on unsteady aerodynamic coefficients shows that whilst the peak amplitude of the gyroscopic moment induced motion changes with the varying damping coefficients on the related axis, the coupling between the pitch and yaw axis is still evident for all cases. One can then reasonably conclude that the relatively low fidelity of the unsteady aerodynamic coefficients do not detract from the comparison between cases with or without the presence of gyroscopic effects.

8.2. Future Recommendations

Further research could consider first enhancing the aerodynamics with higher fidelity model by including the aero-propulsion interaction effects and combine such increase in aerodynamics accuracy by also incorporating force-based controls rather than the existing deflection-based controls. Aerodynamics models for alternative configurations such as flaps down and gear down could also be useful for more accurately studying maneuvers such as engine failure during final approach and missed approach, where twin-engine aircraft are the most vulnerable to the adverse effect of flight upset.

Even though a closed-loop wing leveler was included, the incorporation of a well-designed three-axis autopilot or human pilot model could also be useful for studying how the propeller gyroscopic effect affects closed-loop behavior of the aircraft as well as adding the capability to fly maneuvers how they are actually flown in real life.

Last but not least, the research can be further parameterized to include higher number of propulsors on the aircraft, similar to the distributed propulsion concerts currently in study for future electric aviation. This, in combination with a parameterized aerodynamics model, would contribute immensely to the research of the effect the emergent distributed propulsion technology can have on aircraft handling quality from a gyroscopic effect perspective.

Bibliography

[1] *Light Twin-Engine Aircraft Accidents Following Engine Failures, 1972-1976*, resreport (National Transportation Safety Board, 1979).

[2] R. H. SCANLAN and J. C. TRUMAN, *The gyroscopic effect of a rigid rotating propeller on engine and wing vibration modes,* Journal of the Aeronautical Sciences **17**, 653 (1950).

[3] V. Liu, *Propeller-Wing Whirl Flutter - An Analytical Study*, Master's thesis, Delft University of Technology (2020).

[4] P. C. Teixeira and C. E. S. Cesnik, *Propeller effects on the response of high-altitude long-endurance aircraft,* AIAA Journal **57**, 4328 (2019).

[5] C. C. Smith, Jr, *Hovering and Transition Flight Tests of a 1/5-Scale Model of a Jet-Powered Vertical-Attitude VTOL Research Airplane*, techreport (Langley Field, Va., 1958).

[6] Z. J. Goraj and E. Cichocka, *Influence of weak and strong gyroscopic effects on light aircraft dynamics,* Aircraft Engineering and Aerospace Technology **88**, 613 (2016).

[7] J. Soikkeli, *Vertical Tail Reduction Through Differential Thrust*, Master's thesis, Delft University of Technology (2020).

[8] G. Bock, *Airscrew Gyroscopic Moments*, Tech. Rep. (1941).

[9] Jane's, *Jane's All the World's Aircraft : Development & Production : 2021/2022* (Jane's, 2021).

[10] Diamond Aircraft Industries GmbH, *Aircraft Flight Manual DA 42 NG*, Wiener Neustadt, Austria (2012).

[11] Diamond Aircraft Industries GmbH, *DA 42 NG Airplane Maintenance Manual*, Wiener Neustadt, Austria (2021).

[12] zakharov, *Diamond da-42,* (2020).

[13] B. Etkin and L. D. Reid, *Dynamics of Flight* (Wiley) p. 400.

[14] European Union Aviation Safety Agency, *Easy access rules for normal, utility, aerobatic and commuter category aeroplanes (cs-23) (amendment 4),* (2018).

[15] M. D. Pavel, *Understanding the control characteristics of electric vertical take-off and landing (eVTOL) aircraft for urban air mobility,* Aerospace Science and Technology **125**, 107143 (2022).

[16] E. S. Hendricks, E. Aretskin-Hariton, D. Ingraham, J. S. Gray, S. L. Schnulo, J. Chin, R. Falck, and D. Hall, *Multidisciplinary optimization of an electric quadrotor urban air mobility aircraft,* in *AIAA AVIATION 2020 FORUM* (American Institute of Aeronautics and Astronautics, 2020).

[17] C. Malpica and S. Withrow-Maser, *Handling qualities analysis of blade pitch and rotor speed controlled evtol quadrotor concepts for urban air mobility,* in *VFS International Powered Lift Conference* (2020) pp. 21–23.

[18] EMRAX d.o.o., *EMRAX Motor Installation and Maintenance Manual* (2022).

[19] F. Rasimarzabadi, A. Crain, P. Canteenwalla, P. Zdunich, and E. Gibney, *Performance improvement of heat exchangers used in a hybrid electric aircraft,* in *Volume 6B: Heat Transfer - General Interest/Additive Manufacturing Impacts on Heat Transfer; Internal Air Systems; Internal Cooling* (American Society of Mechanical Engineers, 2022).

[20] EMRAX d.o.o., *EMRAX 348 Axial Flux Permanent Magnet Synchronous Electric Motor* (2022).

[21] J. C. Richard, *Low-Order Nonlinear Dynamic Model of IC Engine-Variable Pitch Propeller System for General Aviation Aircraft*, Tech. Rep. (1995).

[22] A. Filippone and Z. Mohamed-Kassim, *Multi-disciplinary simulation of propeller-turboprop aircraft flight,* The Aeronautical Journal **116**, 985 (2012).

[23] R. Craig, S. Nakanishi, and D. B. Wile, *Analytical and Experimental Study of Transient-Response Characteristics of a Turboprop Engine*, Tech. Rep. (1955).

[24] T. Mutluay, *The Development of an Inertia Estimation Method to Support Handling Quality Assessment*, Master's thesis, Delft University of Technology (2015).

[25] C. Lanham, *Inertia Calculation Procedure for Preliminary Design*, Tech. Rep. (1979).

[26] M. Voskuijl, G. La Rocca, and F. Dircken, *Controllability of blended wing body aircraft,* in *Proceedings of the 26th International Congress of the Aeronautical Sciences, ICAS 2008, including the 8th AIAA Aviation Technology, Integration and Operations (AIO) Conference, Anchorage, Alaska, September 14-19,(2008)* (Optimage Ltd., 2008).

[27] C. Varriale, K. Hameeteman, M. Voskuijl, and L. L. Veldhuis, *A thrust-elevator interaction criterion for aircraft optimal longitudinal control,* in *AIAA Aviation 2019 Forum* (American Institute of Aeronautics and Astronautics, 2019).

[28] C. Varriale, A. Raju Kulkarni, G. La Rocca, and M. Voskuijl, *A hybrid, configuration-agnostic approach to aircraft control surface sizing,* in *Proceedings of the 25th International Congress of the Italian Association of Aeronautics and Astronautics (AIDAA), Rome, Italy* (2019) pp. 9–13.

[29] Modelica Association, *Modelica language,* (2021).

[30] Modelica Association, *Modelica, A Unified Object-Oriented Language for Systems Modeling - Language Specification Version 3.5* (2021).

[31] Modelica Association, *Modelica standard library,* (2022).

[32] G. Looye, *An integrated approach to aircraft modelling and flight control law design*, Ph.D. thesis, S.l (2007).

[33] J. Bezanson, A. Edelman, S. Karpinski, and V. B. Shah, *Julia: A fresh approach to numerical computing,* SIAM Review **59**, 65 (2017).

[34] Y. Ma, S. Gowda, R. Anantharaman, C. Laughman, V. Shah, and C. Rackauckas, *Modelingtoolkit: A composable graph transformation system for equation-based modeling,* (2021), arXiv:2103.05244 [cs.MS] .

[35] F. O. Smetana, D. Summery, and W. D. Johnson, *Riding and handling qualities of light aircraft: A review and analysis,* (1972).

[36] M. Drela and H. Youngren, *AVL Aerodynamic Analysis, Trim, Calculation, Dynamic Stability Analysis, Aircraft Configuration Development*, MIT ().

[37] J. L. Hess, *Panel methods in computational fluid dynamics,* Annual Review of Fluid Mechanics **22**, 255 (1990).

[38] J. M. Ezquerro, V. Lapuerta, A. Laveron-Simavilla, J. M. Garcia, and T. Aviles, *Panel method for mixed configurations with finite thickness and zero thickness,* Engineering Analysis with Boundary Elements **44**, 28 (2014).

[39] W. J. Oosterom, *Flying-V Family Design*, Master's thesis, Delft University of Technology (2021).

[40] J. Mariens, A. Elham, and M. J. L. van Tooren, *Quasi-three-dimensional aerodynamic solver for multidisciplinary design optimization of lifting surfaces,* Journal of Aircraft **51**, 547 (2014).

[41] M. Drela and H. Youngren, *XFOIL: Subsonic Airfoil Development System*, Massachusetts Institute of Technology ().

[42] S. Deck, F. Gand, V. Brunet, and S. B. Khelil, *High-fidelity simulations of unsteady civil aircraft aerodynamics: stakes and perspectives. application of zonal detached eddy simulation,* Philosophical Transactions of the Royal Society A: Mathematical, Physical and Engineering Sciences **372**, 20130325 (2014).

[43] P. Sagaut, S. Deck, and M. Terracol, *Multiscale and Multiresolution Approaches in Turbulence* (IMPERIAL COLLEGE PRESS, 2012).

[44] F. Nicolosi, S. Corcione, and P. D. Vecchia, *Commuter aircraft aerodynamic characteristics through wind tunnel tests,* Aircraft Engineering and Aerospace Technology **88**, 523 (2016).

[45] F. Nicolosi, A. D. Marco, and P. D. Vecchia, *Flight tests, performances, and flight certification of a twin-engine light aircraft,* Journal of Aircraft **48**, 177 (2011).

[46] F. Nicolosi, A. De Marco, and P. D. Vecchia, *Stability, flying qualities and longitudinal parameter estimation of a twin-engine CS-23 certified light aircraft,* Aerospace Science and Technology **24**, 226 (2013).

[47] N. T. Frink, P. C. Murphy, H. L. Atkins, S. A. Viken, J. L. Petrilli, A. Gopalarathnam, and R. C. Paul, *Computational aerodynamic modeling tools for aircraft loss of control,* Journal of Guidance, Control, and Dynamics **40**, 789 (2017).

[48] E. C. Stewart, P. W. Brown, and K. R. Yenni, *Piloted simulation study of the effects of an automated trim system on flight characteristics of a light twin-engine airplane with one engine inoperative*, Tech. Rep. (1986).

[49] C. Varriale, A. D. Marco, E. Daniele, J. Schmidt, and B. Stoevesandt, *Flight load assessment for light aircraft landing trajectories in windy atmosphere and near wind farms,* Aerospace **5**, 42 (2018).

[50] M. P. Fink and D. C. F. Jr, *Full-Scale Wind-Tunnel Investigation of Static Longitudinal and Lateral Characteristics of a Light Twin-Engine Airplane*, Tech. Rep. (1969).

[51] V. Ahuja and R. J. Hartfield, *Aerodynamic loads over arbitrary bodies by method of integrated circulation,* Journal of Aircraft **53**, 1719 (2016).

[52] R. A. McDonald and J. R. Gloudemans, *Open Vehicle Sketch Pad: An Open Source Parametric Geometry and Analysis Tool for Conceptual Aircraft Design,* in *AIAA SCITECH 2022 Forum* (American Institute of Aeronautics and Astronautics, 2022).

[53] A. Raju Kulkarni, G. La Rocca, and L. L. Veldhuis, *Degree of similitude estimation for sub-scale flight testing,* in *AIAA Scitech 2019 Forum* (American Institute of Aeronautics and Astronautics, 2019).

[54] N. v. Arnhem, T. Sinnige, T. C. Stokkermans, G. Eitelberg, and L. L. Veldhuis, *Aerodynamic interaction effects of tip-mounted propellers installed on the horizontal tailplane,* in *2018 AIAA Aerospace Sciences Meeting* (American Institute of Aeronautics and Astronautics, 2018).

[55] R. von Mises, *Theory of Flight* (1959).

[56] E. P. Hartman and D. Biermann, *The Aerodynamics Characteristics of Full-Scale Propellers Having 2, 3, and 4 Blades of Clark Y and R. A. F. 6 Airfoil Sections*, techreport (1938).

[57] P. C. Klein, *Parametric Modeling and Optimization of Advanced Propellers for Next-Generation Aircraft*, Master's thesis, Delft University of Technology (2017).

[58] M. Hepperle, *Javaprop - users guide,* (2018).

[59] M. Drela and H. Youngren, *XROTOR Design and Analysis of Ducted and Free-tip Propellers and Windmills*, MIT (2022).

[60] M. Drela, *QPROP Formulation* (2006).

[61] C. E. Hughes and J. A. Gazzaniga, *Low-Speed Wind Tunnel Performance of High-Speed Counterrotation Propellers at Angle-of-Attack*, Tech. Rep. (1989).

[62] B. Ortun, R. Boisard, and I. Gonzalez-Martino, *In-plane airloads of a propeller with inflow angle: Prediction vs. experiment,* in *30th AIAA Applied Aerodynamics Conference* (American Institute of Aeronautics and Astronautics, 2012).

[63] M. Schroijen and R. Slingerland, *Propeller slipstream effects on directional aircraft control with one engine inoperative,* in *45th AIAA Aerospace Sciences Meeting and Exhibit* (American Institute of Aeronautics and Astronautics, 2007).

[64] M. Renooij and R. Slingerland, *Propeller slipstream and wing-fuselage interference effects on three-axis stability and control,* in *42nd AIAA Aerospace Sciences Meeting and Exhibit* (American Institute of Aeronautics and Astronautics, 2004).

[65] Z. Goraj, A. Baron, and J. Kacprzyk, *Dynamics of a light aircraft in spin,* Aircraft Engineering and Aerospace Technology **74**, 237 (2002).

[66] G. E. Cooper and R. P. Harper Jr., *The use of pilot rating in the evaluation of aircraft handling qualities*, Tech. Rep. (1969).

[67] P. M. Callaghan and D. L. Kunz, *Evaluation of unmanned aircraft flying/handling qualities using a stitched learjet model,* Journal of Guidance, Control, and Dynamics **44**, 842 (2021).

[68] Department of Defence, *Military specification flying qualities of piloted airplanes,* Standard (1969).

[69] M. Lone and A. Cooke, *Review of pilot models used in aircraft flight dynamics,* Aerospace Science and Technology **34**, 55 (2014).

[70] S. Xu, W. Tan, A. V. Efremov, L. Sun, and X. Qu, *Review of control models for human pilot behavior,* Annual Reviews in Control **44**, 274 (2017).

[71] M. C. Cotting, *Evolution of flying qualities analysis: Problems for a new generation of aircraft,* (2010).

[72] D. T. McRuer and E. S. Krendel, *Mathematical models of human pilot behavior*, Tech. Rep. (1974).

[73] P. F. Yaggy and V. L. Rogallo, *A wind-tunnel investigation of three propellers through an angle-of-attack range of 0 deg to 85 deg,* (1960).

[74] C. Varriale, *Flight Mechanics and Performance of Direct Lift Control: Applying Control Allocation Methods to a Staggered Box-Wing Aircraft Configuration*, Ph.D. thesis, Delft University of Technology (2022).

A

Appendix

A.1. Flight Mechanics Model

This section intends to describe the flight mechanics system of equations used for the simulation. The simulation setup is based on the PHALANX toolbox developed in-house at TU Delft, with an overview shown in Figure A.1. The definitions for body, wind, and aerodynamics axes as well as the relevant angles are shown in Figure A.2 The 6 DoF non-linear equation of motion used by the simulation [74] is shown in equation A.1 and A.2. The last term in the angular equations (A.2) are the gyroscopic terms, with the actual implementation being done through SimScape MultiBody library as described in the academic paper.

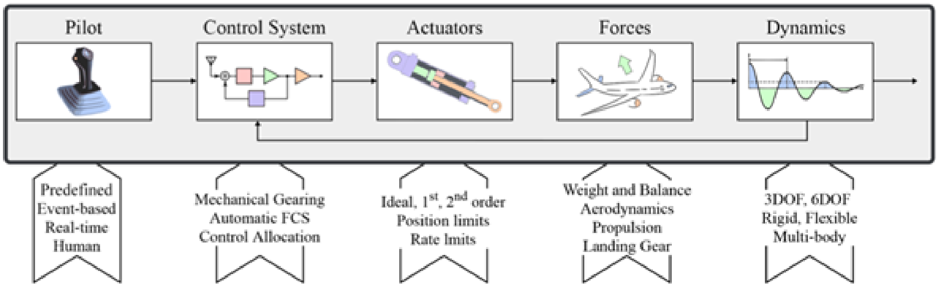
Pilot
Control System
Actuators
Forces
Dynamics
Predefined
Event-based
Real-time
Human
Mechanical Gearing
Automatic FCS
Control Allocation
Ideal, 1st, 2nd order
Position limits
Rate lmits
Weight and Balance
Aerodynamics
Propulsion
Landing Gear
3DOF, 6DOF
Rigid, Flexible
Multi-body

Figure A.1: Overview of the PHALANX toolbox [74]

$$m\begin{bmatrix}\dot{u}\\ \dot{v}\\ \dot{w}\end{bmatrix} + m\begin{bmatrix}p\\ q\\ r\end{bmatrix} \times \begin{bmatrix}u\\ v\\ w\end{bmatrix} = q_\infty S\begin{bmatrix}C_{fx}(a,\beta,p,q,r,\delta_{\mathrm{CS}})\\ C_{fy}(a,\beta,p,q,r,\delta_{\mathrm{CS}})\\ C_{fz}(a,\beta,p,q,r,\delta_{\mathrm{CS}})\end{bmatrix} + g\begin{bmatrix}-\sin\theta\\ \cos\theta\sin\psi\\ \cos\theta\cos\psi\end{bmatrix} \tag{A.1}$$

$$\mathbf{I}\begin{bmatrix}\dot{p}\\ \dot{w}\\ \dot{r}\end{bmatrix} + \begin{bmatrix}p\\ q\\ r\end{bmatrix} \times \mathbf{I}\begin{bmatrix}p\\ q\\ r\end{bmatrix} = q_\infty Sc\frac{q_\infty S}{m}\begin{bmatrix}C_{Mx}(a,\beta,p,q,r,\delta_{\mathrm{CS}})\\ C_{My}(a,\beta,p,q,r,\delta_{\mathrm{CS}})\\ C_{Mz}(a,\beta,p,q,r,\delta_{\mathrm{CS}})\end{bmatrix} + g\begin{bmatrix}-\sin\theta\\ \cos\theta\sin\psi\\ \cos\theta\cos\psi\end{bmatrix} + 2\left[\frac{\mathrm{d}\mathbf{L}_p}{\mathrm{d}t} + \begin{bmatrix}p\\ q\\ r\end{bmatrix} \times \mathbf{L}_p\right] \tag{A.2}$$

Where $\mathbf{L}_p(t)$ is the angular momentum of the propeller.

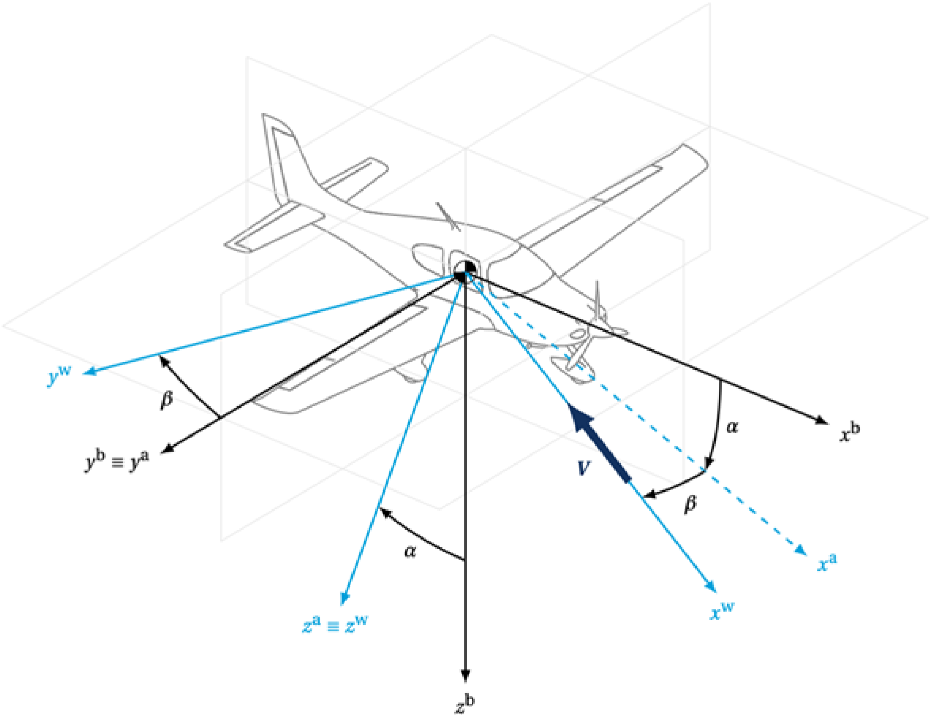
y^{w}
β
$y^{\mathrm{b}} \equiv y^{\mathrm{a}}$
α
x^{b}
V
β
x^{a}
α
x^{w}
$z^{\mathrm{a}} \equiv z^{\mathrm{w}}$
z^{b}

Figure A.2: Illustration of body(b), wind(w), and aerodynamic(a) axis definition used in PHALANX [74]

A.2. Simulink Models

This appendix intends to present diagrams of additional Simulink models not presented in the main academic paper.

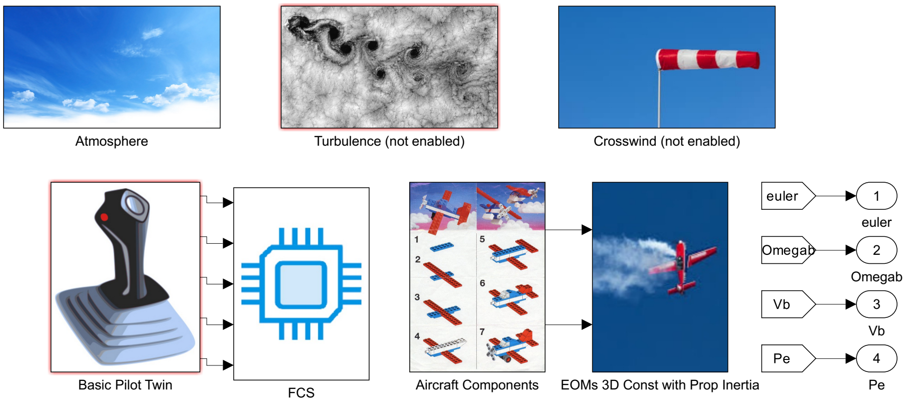
Atmosphere
Turbulence (not enabled)
Crosswind (not enabled)
Basic Pilot Twin
FCS
Aircraft Components
EOMs 3D Const with Prop Inertia
euler
1
euler
Omegab
2
Omegab
Vb
3
Vb
Pe
4
Pe

Figure A.3: Simulink Diagram of the overall view of the PHALANX simulation

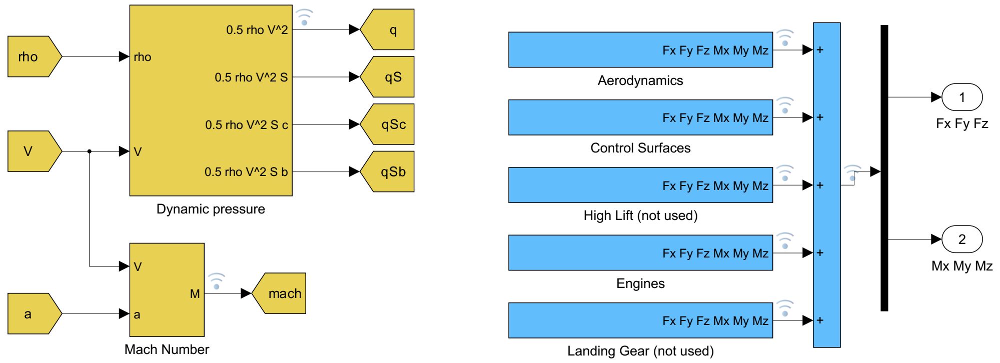
rho
V
a
rho
V
0.5 rho V^2
0.5 rho V^2 S
0.5 rho V^2 S c
0.5 rho V^2 S b
Dynamic pressure
q
qS
qSc
qSb
V
a
M
Mach Number
mach
Fx Fy Fz Mx My Mz
Aerodynamics
Fx Fy Fz Mx My Mz
Control Surfaces
Fx Fy Fz Mx My Mz
High Lift (not used)
Fx Fy Fz Mx My Mz
Engines
Fx Fy Fz Mx My Mz
Landing Gear (not used)
1
Fx Fy Fz
2
Mx My Mz

Figure A.4: Simulink Diagram of the components of the aircraft

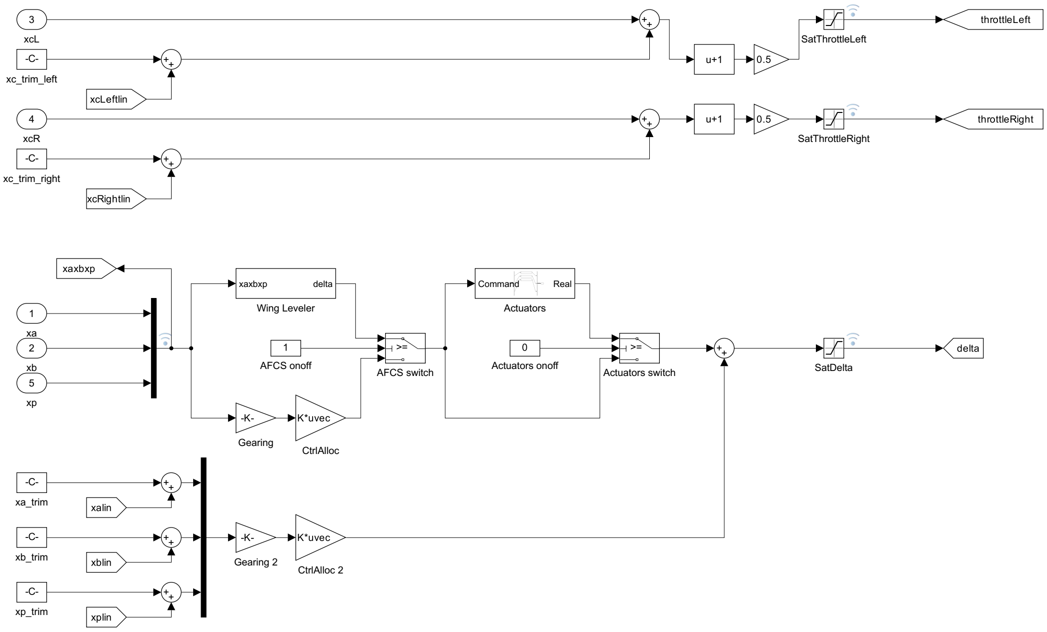
3
xcL
-C-
xc_trim_left
xcLeftlin
u+1
0.5
SatThrottleLeft
throttleLeft
4
xcR
-C-
xc_trim_right
xcRightlin
u+1
0.5
SatThrottleRight
throttleRight
xaxbxp
1
xa
2
xb
5
xp
xaxbxp
delta
Wing Leveler
1
AFCS onoff
AFCS switch
-K-
Gearing
K*uvec
CtrlAlloc
Command
Real
Actuators
0
Actuators onoff
Actuators switch
SatDelta
delta
-C-
xa_trim
xalin
-C-
xb_trim
xblin
-C-
xp_trim
xplin
-K-
Gearing 2
K*uvec
CtrlAlloc 2

Figure A.5: Simulink Diagram of the flight control system model

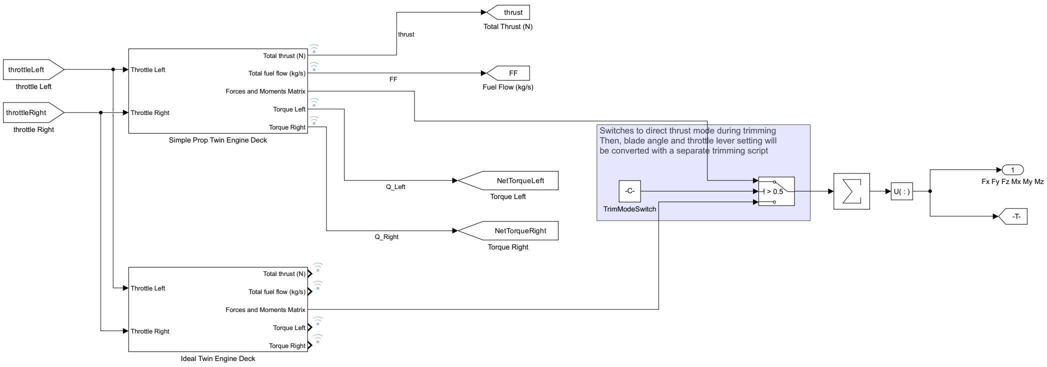
throttleLeft
throttle Left
throttleRight
throttle Right
Throttle Left
Throttle Right
Total thrust (N)
Total fuel flow (kg/s)
Forces and Moments Matrix
Torque Left
Torque Right
Simple Prop Twin Engine Deck
thrust
thrust
Total Thrust (N)
FF
FF
Fuel Flow (kg/s)
Q_Left
NetTorqueLeft
Torque Left
Q_Right
NetTorqueRight
Torque Right
Switches to direct thrust mode during trimming
Then, blade angle and throttle lever setting will
be converted with a separate trimming script
-C-
TrimModeSwitch
> 0.5
U(:)
1
Fx Fy Fz Mx My Mz
-T-
Throttle Left
Throttle Right
Total thrust (N)
Total fuel flow (kg/s)
Forces and Moments Matrix
Torque Left
Torque Right
Ideal Twin Engine Deck

Figure A.6: Simulink Diagram of the Engine model

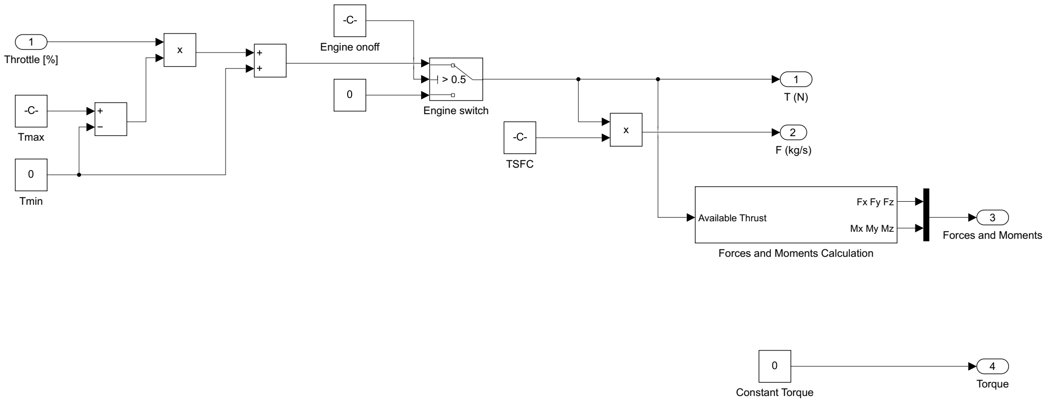
1
Throttle [%]
-C-
Tmax
0
Tmin
+
–
x
+
+
-C-
Engine onoff
0
> 0.5
Engine switch
-C-
TSFC
x
1
T (N)
2
F (kg/s)
Available Thrust
Fx Fy Fz
Mx My Mz
Forces and Moments Calculation
3
Forces and Moments
0
Constant Torque
4
Torque

Figure A.7: Simulink Diagram of the Ideal Powertrain

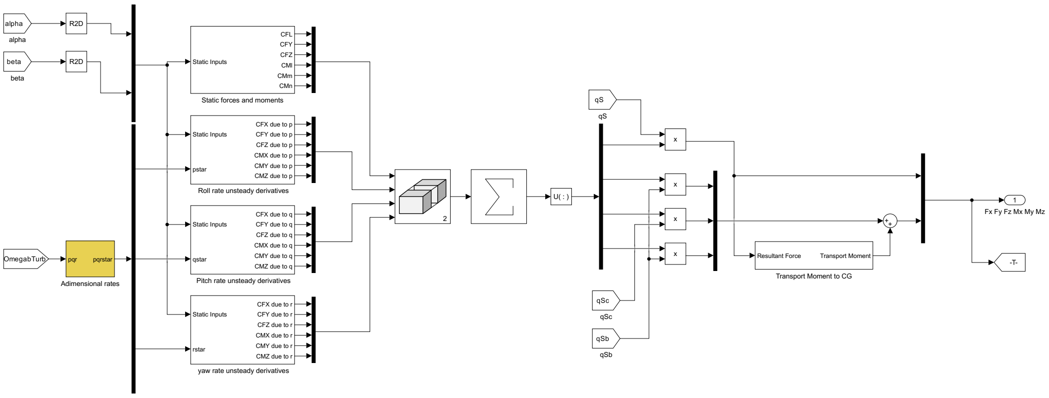
alpha
alpha
R2D
beta
beta
R2D
Static Inputs
CFL
CFY
CFZ
CMl
CMm
CMn
Static forces and moments
Static Inputs
pstar
CFX due to p
CFY due to p
CFZ due to p
CMX due to p
CMY due to p
CMZ due to p
Roll rate unsteady derivatives
OmegabTurb
pqr
pqrstar
Adimensional rates
Static Inputs
qstar
CFX due to q
CFY due to q
CFZ due to q
CMX due to q
CMY due to q
CMZ due to q
Pitch rate unsteady derivatives
Static Inputs
rstar
CFX due to r
CFY due to r
CFZ due to r
CMX due to r
CMY due to r
CMZ due to r
yaw rate unsteady derivatives
2
U(:)
qS
qS
x
x
x
x
qSc
qSc
qSb
qSb
Resultant Force
Transport Moment
Transport Moment to CG
1
Fx Fy Fz Mx My Mz
-T-

Figure A.8: Simulink Diagram of the table-based aerodynamicsforce and moment interpolation model

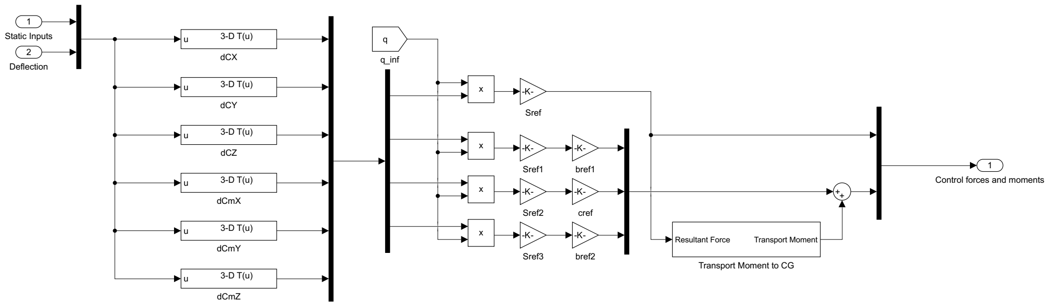
1
Static Inputs
2
Deflection
u
3-D T(u)
dCX
u
3-D T(u)
dCY
u
3-D T(u)
dCZ
u
3-D T(u)
dCmX
u
3-D T(u)
dCmY
u
3-D T(u)
dCmZ
q
q_inf
x
-K-
Sref
x
-K-
Sref1
-K-
bref1
x
-K-
Sref2
-K-
cref
x
-K-
Sref3
-K-
bref2
Resultant Force
Transport Moment
Transport Moment to CG
1
Control forces and moments

Figure A.9: Simulink Diagram of one of the table-based CS force and moment interpolation model

A.3. Static Windtunnel data

This section intends to present the rest of the complete aerodynamic dataset [50] used in this simulation study not shown in the academic paper.

Table A.1: Wind Tunnel Testing Parameters

Test Conditions [50]			
Data reference point	Center of Gravity	**Configuration**	Flap and Gear Up
Tunnel Speed	$28.35 m/s$	**Reynolds number**	2.96×10^6
α **Range**	$-14° - 4°$	β **Range**	$\pm 8°$

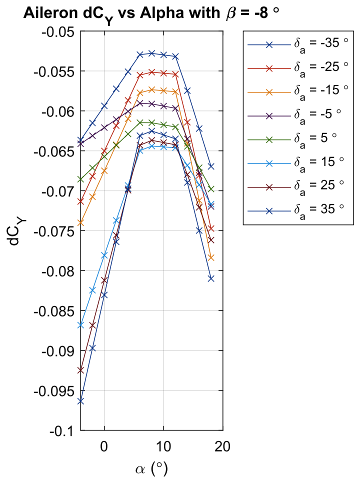

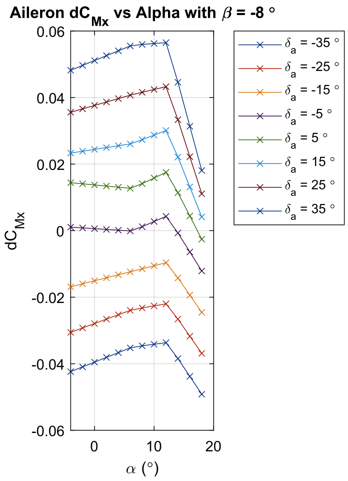

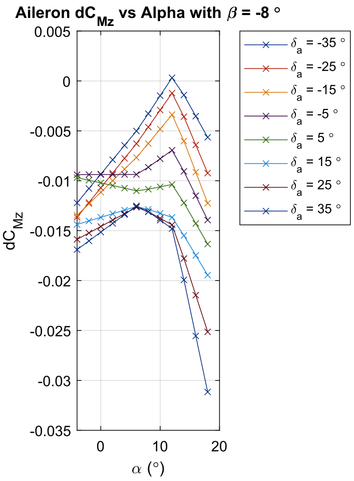

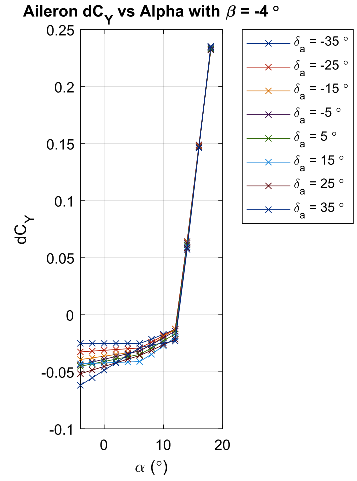

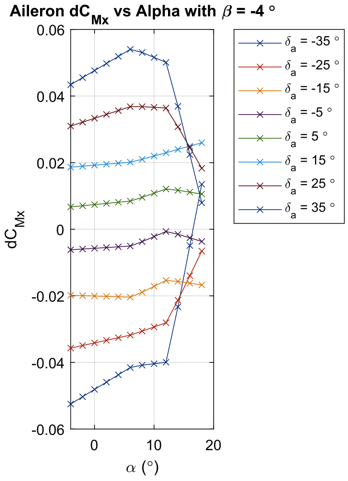

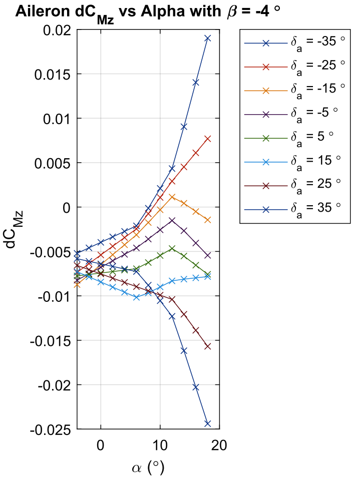

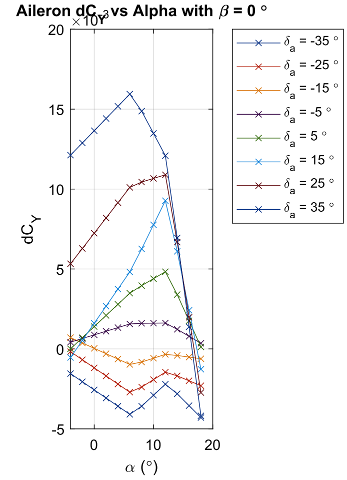
Aileron dC_Y vs Alpha with β = 0 °
$\times 10^{-3}$
20
15
10
5
0
-5
dC_Y
0
10
20
α (°)
δ_a = -35 °
δ_a = -25 °
δ_a = -15 °
δ_a = -5 °
δ_a = 5 °
δ_a = 15 °
δ_a = 25 °
δ_a = 35 °

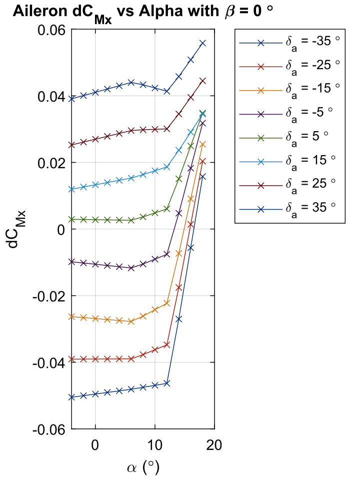
Aileron dC_{Mx} vs Alpha with β = 0 °
0.06
0.04
0.02
0
-0.02
-0.04
-0.06
dC_{Mx}
0
10
20
α (°)
δ_a = -35 °
δ_a = -25 °
δ_a = -15 °
δ_a = -5 °
δ_a = 5 °
δ_a = 15 °
δ_a = 25 °
δ_a = 35 °

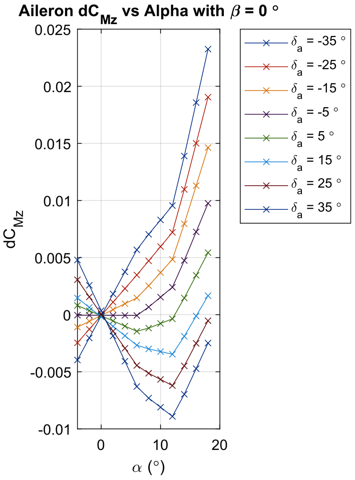
Aileron dC_{Mz} vs Alpha with β = 0 °
0.025
0.02
0.015
0.01
0.005
0
-0.005
-0.01
dC_{Mz}
0
10
20
α (°)
δ_a = -35 °
δ_a = -25 °
δ_a = -15 °
δ_a = -5 °
δ_a = 5 °
δ_a = 15 °
δ_a = 25 °
δ_a = 35 °

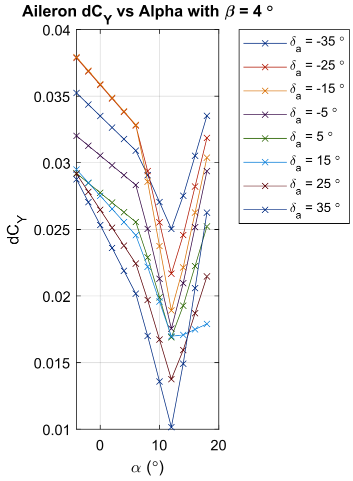
Aileron dC_Y vs Alpha with β = 4 °
0.04
0.035
0.03
0.025
0.02
0.015
0.01
dC_Y
0
10
20
α (°)
δ_a = -35 °
δ_a = -25 °
δ_a = -15 °
δ_a = -5 °
δ_a = 5 °
δ_a = 15 °
δ_a = 25 °
δ_a = 35 °

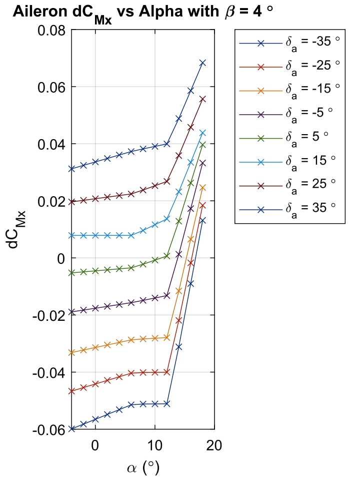
Aileron dC_{Mx} vs Alpha with β = 4 °
0.08
0.06
0.04
0.02
0
-0.02
-0.04
-0.06
dC_{Mx}
0
10
20
α (°)
δ_a = -35 °
δ_a = -25 °
δ_a = -15 °
δ_a = -5 °
δ_a = 5 °
δ_a = 15 °
δ_a = 25 °
δ_a = 35 °

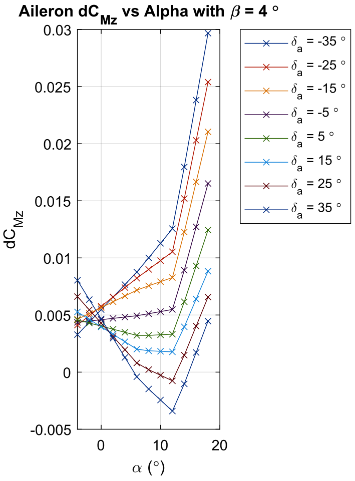
Aileron dC_{Mz} vs Alpha with β = 4 °
0.03
0.025
0.02
0.015
0.01
0.005
0
-0.005
dC_{Mz}
0
10
20
α (°)
δ_a = -35 °
δ_a = -25 °
δ_a = -15 °
δ_a = -5 °
δ_a = 5 °
δ_a = 15 °
δ_a = 25 °
δ_a = 35 °

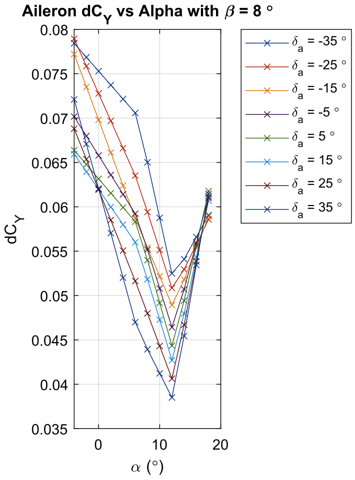
Aileron dC_Y vs Alpha with β = 8 °
0.08
0.075
0.07
0.065
0.06
0.055
0.05
0.045
0.04
0.035
dC_Y
0
10
20
α (°)
δ_a = -35 °
δ_a = -25 °
δ_a = -15 °
δ_a = -5 °
δ_a = 5 °
δ_a = 15 °
δ_a = 25 °
δ_a = 35 °

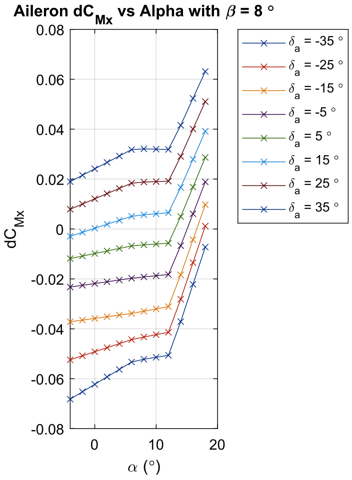
Aileron dC_{Mx} vs Alpha with β = 8 °
0.08
0.06
0.04
0.02
0
-0.02
-0.04
-0.06
-0.08
dC_{Mx}
0
10
20
α (°)
δ_a = -35 °
δ_a = -25 °
δ_a = -15 °
δ_a = -5 °
δ_a = 5 °
δ_a = 15 °
δ_a = 25 °
δ_a = 35 °

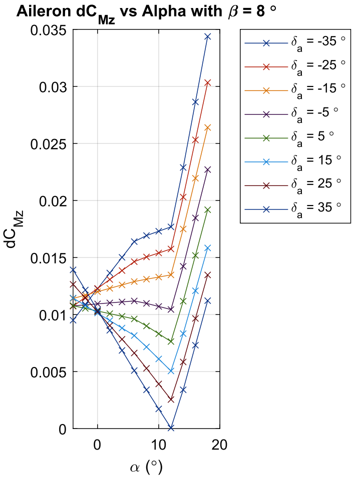
Aileron dC_{Mz} vs Alpha with β = 8 °
0.035
0.03
0.025
0.02
0.015
0.01
0.005
0
dC_{Mz}
0
10
20
α (°)
δ_a = -35 °
δ_a = -25 °
δ_a = -15 °
δ_a = -5 °
δ_a = 5 °
δ_a = 15 °
δ_a = 25 °
δ_a = 35 °

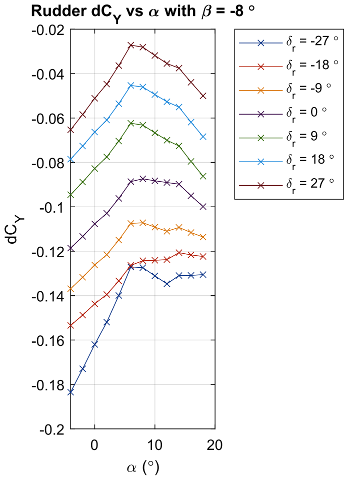
Rudder dC_Y vs α with β = -8 °
dC_Y
-0.02
-0.04
-0.06
-0.08
-0.1
-0.12
-0.14
-0.16
-0.18
-0.2
0
10
20
α (°)
δ_r = -27 °
δ_r = -18 °
δ_r = -9 °
δ_r = 0 °
δ_r = 9 °
δ_r = 18 °
δ_r = 27 °

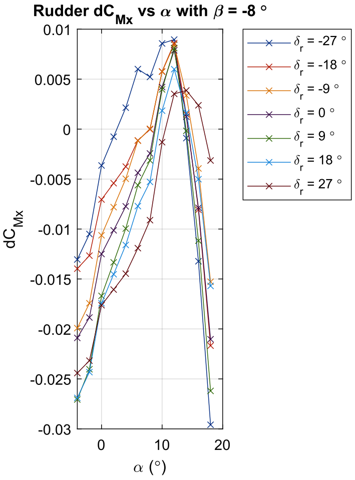
Rudder dC_{Mx} vs α with β = -8 °
dC_{Mx}
0.01
0.005
0
-0.005
-0.01
-0.015
-0.02
-0.025
-0.03
0
10
20
α (°)
δ_r = -27 °
δ_r = -18 °
δ_r = -9 °
δ_r = 0 °
δ_r = 9 °
δ_r = 18 °
δ_r = 27 °

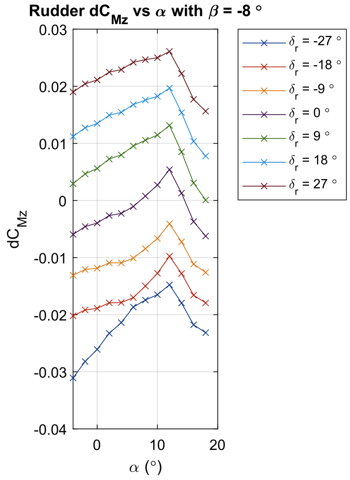
Rudder dC_{Mz} vs α with β = -8 °
dC_{Mz}
0.03
0.02
0.01
0
-0.01
-0.02
-0.03
-0.04
0
10
20
α (°)
δ_r = -27 °
δ_r = -18 °
δ_r = -9 °
δ_r = 0 °
δ_r = 9 °
δ_r = 18 °
δ_r = 27 °

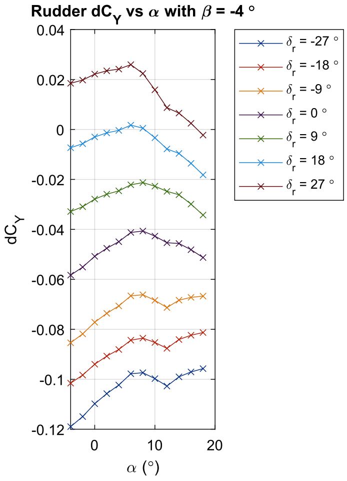
Rudder dC_Y vs α with β = -4 °
dC_Y
0.04
0.02
0
-0.02
-0.04
-0.06
-0.08
-0.1
-0.12
0
10
20
α (°)
δ_r = -27 °
δ_r = -18 °
δ_r = -9 °
δ_r = 0 °
δ_r = 9 °
δ_r = 18 °
δ_r = 27 °

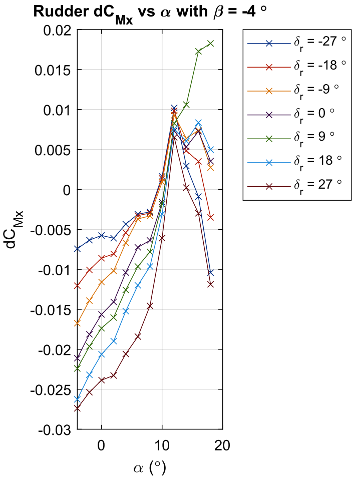
Rudder dC_{Mx} vs α with β = -4 °
dC_{Mx}
0.02
0.015
0.01
0.005
0
-0.005
-0.01
-0.015
-0.02
-0.025
-0.03
0
10
20
α (°)
δ_r = -27 °
δ_r = -18 °
δ_r = -9 °
δ_r = 0 °
δ_r = 9 °
δ_r = 18 °
δ_r = 27 °

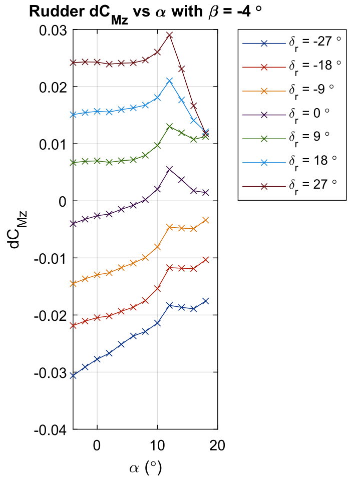
Rudder dC_{Mz} vs α with β = -4 °
dC_{Mz}
0.03
0.02
0.01
0
-0.01
-0.02
-0.03
-0.04
0
10
20
α (°)
δ_r = -27 °
δ_r = -18 °
δ_r = -9 °
δ_r = 0 °
δ_r = 9 °
δ_r = 18 °
δ_r = 27 °

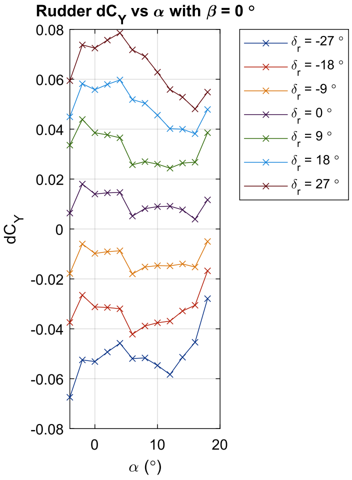
Rudder dC_Y vs α with β = 0 °
dC_Y
0.08
0.06
0.04
0.02
0
-0.02
-0.04
-0.06
-0.08
0
10
20
α (°)
δ_r = -27 °
δ_r = -18 °
δ_r = -9 °
δ_r = 0 °
δ_r = 9 °
δ_r = 18 °
δ_r = 27 °

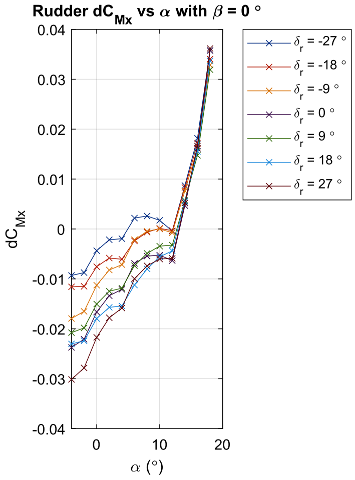
Rudder dC_{Mx} vs α with β = 0 °
dC_{Mx}
0.04
0.03
0.02
0.01
0
-0.01
-0.02
-0.03
-0.04
0
10
20
α (°)
δ_r = -27 °
δ_r = -18 °
δ_r = -9 °
δ_r = 0 °
δ_r = 9 °
δ_r = 18 °
δ_r = 27 °

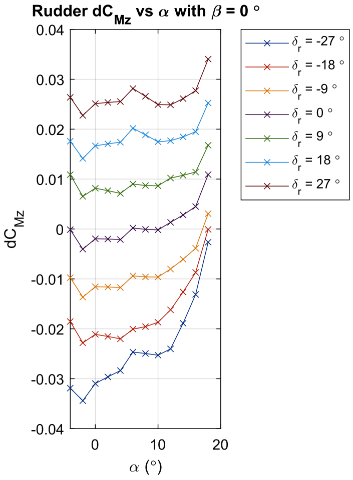
Rudder dC_{Mz} vs α with β = 0 °
dC_{Mz}
0.04
0.03
0.02
0.01
0
-0.01
-0.02
-0.03
-0.04
0
10
20
α (°)
δ_r = -27 °
δ_r = -18 °
δ_r = -9 °
δ_r = 0 °
δ_r = 9 °
δ_r = 18 °
δ_r = 27 °

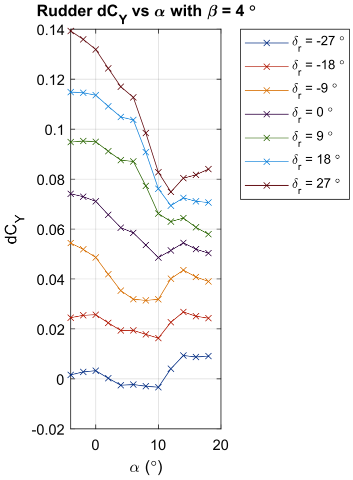
Rudder dC_Y vs α with β = 4 °

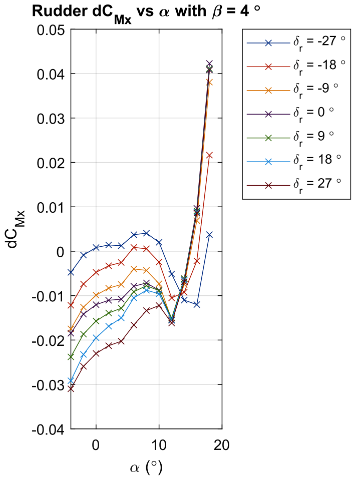
Rudder dC_{Mx} vs α with β = 4 °

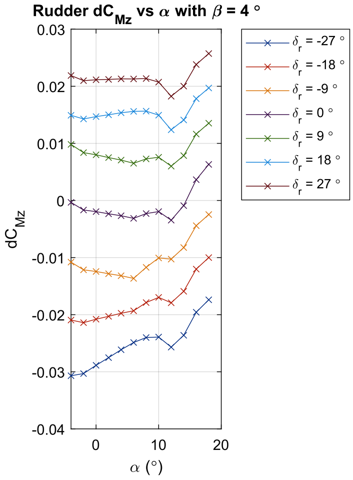
Rudder dC_{Mz} vs α with β = 4 °

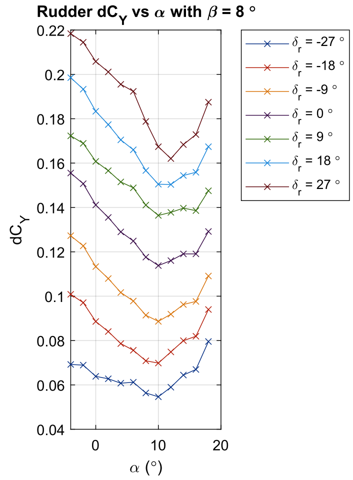
Rudder dC_Y vs α with β = 8 °

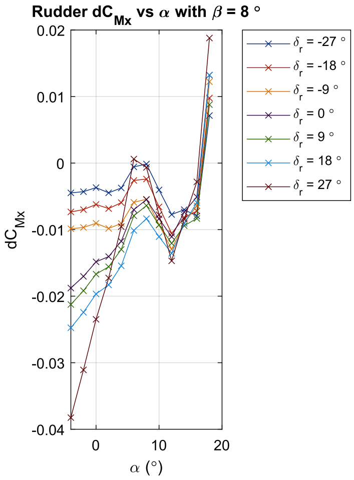
Rudder dC_{Mx} vs α with β = 8 °

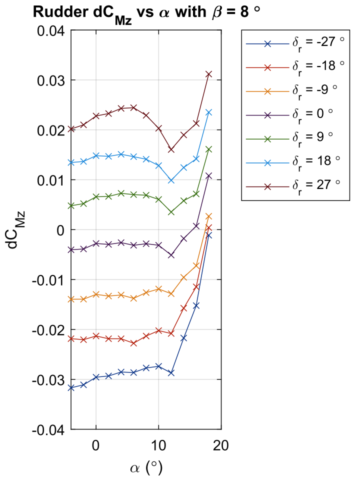
Rudder dC_{Mz} vs α with β = 8 °

A.4. Complete Time Simulation Summarized Results

A.4.1. Result Summary for All-Engine-Operative Open-Loop Maneuvers

Table A.2: Percentage Difference in α excursion between cases with and without GE for all-engine-operating scenario

Difference in Initial α Excursion (Degrees)			
Maneuver	**Initial Climb (AEO)**	**Cruise**	**Approach**
Impulse Elevator	-0.21 (-4.5%)	-0.06 (-0.9%)	-0.14 (-3.1%)
Impulse Rudder	-0.81 (-81341.4%)	-1.04 (-190.4%)	-0.53 (1833.3%)
Sudden Left Fail	-0.32 (-92.5%)	-0.08 (-67.4%)	0.01 (10.8%)
Dual Engine Increase	N/A	-0.03 (10.6%)	0.13 (-10.6%)
Go Around	N/A	N/A	-0.11 (-3.2%)

Table A.3: Difference in β excursion between cases with and without GE for all-engine-operating scenario

Difference in Initial β Excursion (Degrees)			
Maneuver	**Initial Climb (AEO)**	**Cruise**	**Approach**
Impulse Elevator	-1.61 (-5590.0%)	-2.62 (-115.1%)	-1.06 (143.2%)
Impulse Rudder	0.31 (-4.1%)	0.13 (-2.1%)	0.18 (-2.5%)
Sudden Left Fail	0.05 (-4.1%)	-0.00 (0.2%)	0.01 (-2.4%)
Dual Engine Increase	N/A	0.03 (47.0%)	-0.05 (148.4%)
Go Around	N/A	N/A	-1.08 (177.4%)

Table A.4: Max difference in airspeed between cases with and without GE for all-engine-operating scenario

Max Difference in Airspeed (m/s)			
Maneuver	**Initial Climb (AEO)**	**Cruise**	**Approach**
Impulse Elevator	-0.79m/s	3.05m/s	-1.29m/s
Impulse Rudder	-1.41m/s	-1.62m/s	-2.88m/s
Sudden Left Fail	2.33m/s	1.38m/s	0.33m/s
Dual Engine Increase	N/A	0.70m/s	-9.82m/s
Go Around	N/A	N/A	2.81m/s

Table A.5: Max difference in altitude between cases with and without GE for all-engine-operating scenario

Max Difference in Altitude (m)			
Maneuver	**Initial Climb (AEO)**	**Cruise**	**Approach**
Impulse Elevator	4.93	-35.98	7.49
Impulse Rudder	-5.61m	-37.71m	14.33
Sudden Left Fail	-13.83m	-15.63m	-1.47
Dual Engine Increase	N/A	-7.31m	64.65m
Go Around	N/A	N/A	-8.79m

A.4.2. Result Summary for One-Engine-Inoperative Open-Loop Maneuvers

Table A.6: Difference in initial α excursion between cases with and without GE for one engine inoperative scenario

Difference in Initial α Excursion (Degrees)		
Maneuver	**Initial Climb (OEI)**	**Approach**
Impulse Elevator	-0.05 (-1.0%)	-0.06 (-1.3%)
Impulse Rudder	-0.24 (-19787.4%)	-0.16 (-1503.9%)
Dual Engine Increase	N/A	-0.22 (-44.2%)
Go Around	N/A	-0.19 (-4.6%)

Table A.7: Difference in initial β excursion between cases with and without GE for one engine inoperative scenario

Difference in Initial β Excursion (Degrees)		
Maneuver	**Initial Climb (OEI)**	**Approach**
Impulse Elevator	-1.04 (-663.7%)	-0.47 (-49.9%)
Impulse Rudder	0.04 (0.9%)	0.05 (1.2%)
Dual Engine Increase	N/A	0.11 (2.1%)
Go Around	N/A	-0.30 (-4.7%)

Table A.8: Max difference in airspeed between cases with and without GE for one engine inoperative scenario

Max Difference in Airspeed (m/s)		
Maneuver	**Initial Climb (OEI)**	**Approach**
Impulse Elevator	-1.09m/s	-0.20m/s
Impulse Rudder	-2.49m/s	-1.44m/s
Dual Engine Increase	N/A	0.95m/s
Go Around	N/A	4.78m/s

Table A.9: Max difference in altitude between cases with and without GE for one engine inoperative scenario

Max Difference in Altitude (m)		
Maneuver	**Initial Climb (OEI)**	**Approach**
Impulse Elevator	7.37m	0.94m
Impulse Rudder	14.09m	7.21m
Dual Engine Increase	N/A	-4.72m
Go Around	N/A	-38.54m

A.4.3. Result Summary for All-Engine-Operative Closed-Loop Maneuvers

Table A.10: Percentage Difference in α excursion between cases with and without GE for all-engine-operating scenario with wing leveler enabled

Difference in Initial α Excursion (Degrees)			
Maneuver	**Initial Climb (AEO)**	**Cruise**	**Approach**
Impulse Elevator	-0.27 (-5.7%)	-0.11 (-1.9%)	-0.23 (-5.0%)
Impulse Rudder	-1.16 (-17138.0%)	-1.01 (-470.2%)	-0.81 (81509.5%)
Sudden Left Fail	-0.52 (-95.6%)	-0.07 (-63.1%)	-0.12 (-97.4%)
Dual Engine Increase	N/A	-0.02 (6.3%)	0.04 (-3.6%)
Go Around	N/A	N/A	-0.05 (-3.5%)

Table A.11: Difference in β excursion between cases with and without GE for all-engine-operating scenario with wing leveler enabled

Difference in Initial β Excursion (Degrees)			
Maneuver	**Initial Climb (AEO)**	**Cruise**	**Approach**
Impulse Elevator	-3.68 (-27331.3%)	-2.45 (-219.5%)	-3.78 (-50036.0%)
Impulse Rudder	0.67 (-7.2%)	0.33 (-4.3%)	0.50 (-5.3%)
Sudden Left Fail	-0.01 (0.5%)	-0.01 (0.8%)	-0.00 (-22.0%)
Dual Engine Increase	N/A	0.03 (37.8%)	0.39 (271.7%)
Go Around	N/A	N/A	-1.07 (-7328.0%)

Table A.12: Max difference in airspeed between cases with and without GE for all-engine-operating scenario with wing leveler enabled

Max Difference in Airspeed (m/s)			
Maneuver	**Initial Climb (AEO)**	**Cruise**	**Approach**
Impulse Elevator	0.23	0.03	0.15
Impulse Rudder	0.28	0.53	0.21
Sudden Left Fail	-0.68	-0.40	-0.10
Dual Engine Increase	N/A	-0.13	0.07
Go Around	N/A	N/A	-0.09

Table A.13: Max difference in altitude between cases with and without GE for all-engine-operating scenario with wing leveler enabled

Max Difference in Altitude (m)			
Maneuver	**Initial Climb (AEO)**	**Cruise**	**Approach**
Impulse Elevator	1.36	0.46	0.89
Impulse Rudder	-4.42	-14.11	-2.64
Sudden Left Fail	3.42	3.50	0.51
Dual Engine Increase	N/A	1.33	-0.33
Go Around	N/A	N/A	0.30